SPATIOTEMPORAL PATTERNS IN POPULATIONS OF DICTYOSTELIUM DISCOIDEUM

A Dissertation

Presented to the Faculty of the Graduate School

of Cornell University

in Partial Fulfillment of the Requirements for the Degree of

Doctor of Philosophy

by

Kaumudi Hassan Prabhakara

December 2017

SPATIOTEMPORAL PATTERNS IN POPULATIONS OF DICTYOSTELIUM DISCOIDEUM

Kaumudi Hassan Prabhakara, Ph.D.

Cornell University 2017

Pattern formation is widely observed in nature. One organism that shows spectacular patterns is *Dictyostelium discoideum (D.d.)*. When nutrients are available in plenty, *D.d.* lead solitary lives - they feed and divide. However, when a population of *D.d.* begins to starve, the cells become social. Each cell emits a chemical called cyclic adenosine monophosphate (cAMP), which diffuses in the medium. When neighboring cells detect cAMP, they also secrete cAMP. An enzyme phosphodiesterase, secreted by the cells, degrades cAMP. The system is therefore a reaction-diffusion system. After a few hours of signaling, the response of the cells to cAMP is seen either as large scale spiral waves or target patterns. The waves persist for about 2h. Towards the end, the cells aggregate towards the centers of the spirals and targets through chemotaxis and form mounds. These mounds can form multi-cellular slugs which move around looking for food. Failing to find food, the slug transforms into a fruiting body with spores on the top. *D.d.* is thus a unique organism that exhibits unicellular and multicellular behavior.

In this thesis, I analyze the effect of various parameters on the patterns formed by *D.d.*. As *D.d.* starves, its internal biochemistry changes. This developmental changes drastically affect the patterns. I will present results of a systematic analysis of the effects of the developmental path on pattern formation. Next, I considered the effects of variability in parameters in a population

on the patterns. By mixing two populations at different developmental stages, I introduced developmental variability in the population and found that the patterns depend on the heterogeneity in the biochemical parameters and in spatial distribution of cells. By modifying an existing model, by introducing temporal variations of certain biochemical parameters, I was able to simulate the experimental results. Further, using the simulations I was able to determine that the dynamics of the starving populations changes from being excitable to oscillatory. This work proved that a systematic analysis of patterns can provide information about the developmental pathways in a system. Using the idea that populations at different developmental stages form different patterns, I performed experiments to check for the existence of "memory." Indeed, I found that populations have a memory of starvation for about 1 h. These results indicate that the biochemical parameters do not deregulate at the same time. Simulations of the model that I modified confirmed this analysis.

In a population, the amount of cAMP produced by cells varies. Despite this variation, the signaling mechanism is robust. Experiments to understand this robustness revealed that signaling can occur at very low amounts of cAMP. In fact, when a low density population of wild type cells that could not aggregate on its own was mixed with a high density population of mutants that could not produce cAMP, the resulting mixture aggregates. Counterintuitively, rather than a lack of cAMP, this effect was because of insufficient amount of the enzyme, phosphodiesterase, which degrades cAMP. Estimates of the degradation rates confirm that phosphodiesterase is necessary for wave propagation.

In nature, the cells have to survive on various kinds of substrates. To understand the importance of substrates for pattern formation, I performed experiments to observe their effects. I used agar gels of various densities as the

substrate and found that as the density of the agar substrate increased the patterns needed more time to form, and a transition from spirals to targets was observed. However, if the cells are immersed in larger amounts of buffer, the effect vanishes. I hypothesize that this could mean that the thin layer of buffer over the cells is very important.

In all the simulations, I have varied the parameters by hand. To establish a mathematically rigorous method to estimate the parameters, I have worked with different methods of coupling data to models to optimize the parameters.

BIOGRAPHICAL SKETCH

My hometown is Bangalore. I did my schooling and undergraduate studies there. I completed my Masters in Physics at Indian Institute of technology, Madras, in Chennai. After that I got admitted to Cornell University for a PhD program in Physics. During the course of my PhD, I conducted my doctoral research at the Max-Planck Institute for Dynamics and Self-Organization in Göttingen, Germany for four years, where my advisor, Prof. Bodenschatz has his laboratories.

To my parents.

ACKNOWLEDGEMENTS

First and foremost, I convey my heartfelt gratitude to my advisor Prof. Eberhard Bodenschatz. He has always been very encouraging and supportive of my research. He allowed me to explore various research ideas, and has always provided valuable insights that have helped me progress. There was a well-balanced amount of freedom and supervision in his group. He has done everything possible to ensure my professional success and personal well-being. Working under his guidance has helped me be a better scientist, thinker, and communicator.

I thank my parents for always being supportive of my work. Their constant encouragement has been invaluable in my graduate life. Their unwavering belief in me, through the highs and lows of my research, has been critical to my successful completion of my PhD.

I thank Dr. Aazm Gholami and Dr. Vladimir Zykov, with whom I closely worked during my research. Without their guidance, I would not have been able to conduct my research successfully. Apart from helping me with the experiments and simulations, discussing my research with them regularly taught me to thoroughly analyze my results. In particular, I thank Azam for being a pillar of strength in times of despair. I will always fondly remember the wonderful time I spent with her family, when she invited our group members to her house.

I thank Dr. Albert Bae for his vital help in performing various experiments. He taught me new techniques in experiments and data analysis. Working with him has substantially broadened my experience as a physicist, and enabled me to be a better scientist. He has been a good friend and has always cheered me up with anecdotes when the pressures of academia were dragging me down.

I thank Dr. Christian Westendorf for his support throughout my PhD. He was always willing to help me with any aspect of research – setting up microscopes, debugging programs in MATLAB, scientific discussions, and general talk about life. I thank Dr. Isabella Guido for all the useful discussions about our experiments. These discussions helped me to look at my results from new perspectives. Further, I thank her for setting up another dark field microscope, which enabled me and others to make more measurements. Her persistence and cheerful optimism has been inspirational. I also thank Dr. Marco Tarantola for useful discussions and for teaching me to use the AFM.

I thank the present and past members of my group, Laura, Prasanth, Holly, Nadine, Jenny, Michael, Fabio, Christoph, Hsin-Fang, Jose, Smrithika, Lukas, Jan, Christian, Estefania and Torsten for their support. I have immensely enjoyed the various dinners, hikes, games and trips we took together.

I thank the administrative assistants, Kacey Acquilano and Debra Hatfield at Cornell and Angela Meister at MPIDS for their extraordinary support to facilitate my move from Ithaca to Göttingen and back, in terms of paperwork, travel documents etc. Their help greatly reduced the stress of moving.

I convey a deep gratitude to the technical staff at MPIDS. In particular, Maren Müller, Katharina Gunkel, Tina Althaus and Marion Kunze have always cheerfully provided the support I needed to conduct experiments. Whether I wanted to work at dawn, late in the evenings or over weekends, they always ensured that I had the cells I needed. Their friendliness will always make me remember the times I spent in lab with great fondness. I also thank our lunch group for great German conversations, which provided a pleasant break from work. I also thank all the other people I interacted with, whose names I haven't mentioned here.

TABLE OF CONTENTS

LIST OF FIGURES

CHAPTER 1

INTRODUCTION

Patterns are ubiquitous in nature; be it sea shells, sand dunes, or snowflakes, they never cease to amaze us. Living organisms in particular, display a huge array of patterns - stripes on tigers, spots on leopards, complex patterns on the scales of snakes etc. [38] Alan Turing's seminal paper revolutionized our thinking about these patterns. [53] He proposed that the same basic mechanism underlies diverse patterns such as sea shell patterns and spots on leopards. The mechanism, now called the Turing mechanism, has since been shown to apply to an even wider range of phenomena like morphology and spread of diseases. The basic premise of the mechanism is that an interplay between a global inhibitor and a local activator can produce the observed patterns. While these patterns are exciting, visually similar, but fascinating dynamic patterns that change over space and time are more complex. These are observed in fluid phenomena - like Rayleigh-Benard convection [37, 2], chemical reactions - like the Belusouv-Zhabotinsky reaction [61], populations of micro-organisms - like *E. coli* [5] etc. These patterns evolve with time, can be spatially heterogeneous and may reach steady state eventually. However, although these patterns resemble each other, the mechanism of formation is very different.

Patterns in chemical reactions are formed by a reaction-diffusion mechanism when the system is far from equilibrium. These systems can be thought of as a group of local oscillators - each of which follow the governing equations without diffusion - that are coupled by diffusion. The global behavior can be qualitatively predicted by the local behavior. In this respect, these systems are similar to the classical thermodynamic fields that are composed of smaller subunits like

magnetic spins, atoms etc. However, the similarity ends there. Classical thermodynamic systems cannot display such a rich variety of behavior because they are equilibrium systems.

The astonishing aspect of these patterns is the ability of the individual local oscillators, numbering millions, to self-organize to form a large scale global pattern. Apart from the patterns on animal coats and in chemical reactions, some common examples of self-organization are flocking of birds [56], insects [43], embryo morphogenesis, etc. To understand the phenomenon of self-organization, it is not sufficient (and sometimes, necessary) to know the details of how the individual entity functions. Interactions between entities and long range couplings are of paramount importance.

Patterns like spiral waves or circular waves are seen in a wide range of systems including the cardiac dynamics [4], oxidation of CO on platinum [25], retina [21] etc. This widespread occurrence led physicists and mathematicians to formulate general sets of equations that can produce spirals and circular waves. [7] However, it would be incorrect to group all spirals and circular waves as being solutions of the same set of equations. This is because, some systems are inherently different from each other. Certain systems are excitable and some are oscillatory. Similar patterns can be seen in both kinds of systems. Section 1.1 deals with the description of the two kinds of systems. It should be noted here that in the field of fluid dynamics, spirals and targets are observed in Rayleigh-Benard convection. These patterns have a different origin - neither excitable nor oscillatory [37, 2].

Although these patterns have been observed for decades, it has not been easy to deduce information about the systems through a systematic study of

patterns. In this work, I focus on patterns formed by populations of amoebae, *Dictyostelium discoideum* (D.d) to uncover more information about the system. D.d is ideally suited for studies on pattern formation, self-organization, chemotaxis, response to stimuli, etc. [32] Section 1.3 provides an introduction to world of D.d and it's mysteries.

1.1 Excitable and Oscillatory dynamics

In this section, I will describe two kinds of dynamical systems - excitable and oscillatory, by following the arguments presented in [8]. To begin with, let us consider a general reaction diffusion system - the FitzHugh-Nagumo model. The equations of this model two variable model are given by equations 1.1 - 1.4.

$$\frac{\partial u}{\partial t} = f(u, v) + \nabla^2 u \tag{1.1}$$

$$\frac{\partial v}{\partial t} = g(u, v) + d\nabla^2 v \tag{1.2}$$

$$f(u, v) = \eta^{-1}(3u - u^3 - v) \tag{1.3}$$

$$g(u, v) = u - a - bv \tag{1.4}$$

Let's first consider the dynamics without diffusion - the spatially homogeneous state. An important tool to understand the dynamics of such systems is the nullcline. The nullclines of a system are curves in the space of its variables, which describe its behavior at equilibrium. They are obtained by setting the time derivative and diffusion terms to zero (because this defines the equilibrium). So in equations 1.1 and 1.2, these conditions imply $f(u, v) = 0$ and $g(u, v) = 0$. All the points (u, v) that satisfy $3u - u^3 - v = 0$ form the u-nullcline and all the points that satisfy $u - a - bv = 0$ form the v-nullcline. The u-nullcine has no parameters. For the equations 1.1 - 1.4, the nullclines are shown in fig.

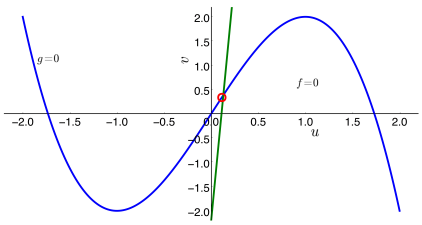

Figure 1.1: The nullclines of the FitzHugh-Nagumo model. The point of intersection is the equilibrium.

1.1. The point of intersection of the two nullclines is the point of equilibrium or the fixed point. Depending on the parameters of the model, the system can have multiple fixed points. Linear stability analysis determines whether a fixed point is stable or not. See Box 1.1 for the basics of linear stability analysis.

Nullclines are useful because they can predict the direction the dynamics of the system will take. On the u-nullcline, $\dot{u} = 0$. This means there is no flow in the u direction i.e., all the flow is long the vertical v axis. Similarly, along the v-nullcline, $\dot{v}$ is zero. So there is no motion along v axis, and all the motion is along the u axis, i.e. the flow is horizontal. The u and v nullclines separate the phase space into regions where $\dot{u} > 0$, $\dot{u} < 0$ and $\dot{v} > 0$, $\dot{v} < 0$. The signs can be found by evaluating the functions $f(u, v)$ and $g(u, v)$ at a point on one side of the nullclines (if the functions are positive at one point, they should be positive at all points on that side of the nullcline). The side of the nullcline on which they are positive, the system flows towards the positive side, and on the other side of the nullcline, the system flows in the negative direction. In fact, these flow field directions can also be used to determine the stability of the fixed points. If the flow on either side of the fixed point is towards the fixed point, the system is attracted to that fixed point, and therefore it must be stable. If the flow on either side of the fixed point points away from the fixed point, then the system tends to move away from the fixed point, so it must be unstable. If the flow

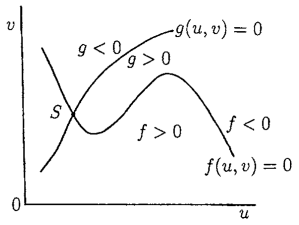

Figure 1.2: The nullclines divide the space of the variables into regions where $\dot{u} > 0$, $\dot{u} < 0$ and $\dot{v} > 0$, $\dot{v} < 0$. Figure reproduced with permission from [38].

points towards the fixed point on one side and away from it on the other, the fixed point is a saddle point. The figure shows the direction of the flow for the equations under consideration.

If the parameter η is small, the dynamics of the variable u is faster than the dynamics of variable v because the dynamics of u is proportional to η^{-1} whereas the dynamics of v is independent of η. So any small deviation of u from the $f(u, v) = 0$ nullcline will result in a rapid change in u, whereas v changes slowly. From the condition $f(u, v) = 0$, we get an expression for v in terms of u.

$$v = 3u - u^3 \tag{1.5}$$

Similarly, from the condition $g(u, v) = 0$, we get

$$v = \frac{u - a}{b} \tag{1.6}$$

The fixed points can be found by solving the above equations. Depending on the parameters a and b, the system can either have one or three fixed points. The stability of the fixed points can be found using the method described in Box 1.1. Three possibilities are considered here.

In fig. 1.3 there is one fixed point, which is unstable. The instability can be visualized in the following way. Suppose, a perturbation occurs, which in-

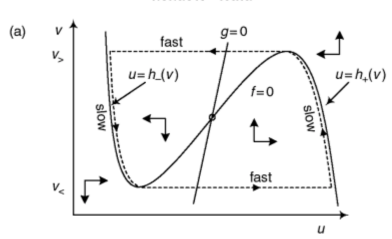

Figure 1.3: The nullclines of the Fitz-Hugh Nagumo model. The system has one unstable fixed point. Figure reproduced with permission from [8].

creased the value of v slightly. Then, due to the direction of the flow, u rapidly decreases until it reaches the slow arm of the u nullcline. During this decrease v is almost constant. Once it reaches the nullcline, u is almost constant and v decreases slowly. When v reaches the minimum of the u-nullcline, u increases rapidly until it satisfies the u-nullcline again. Now v increases until it reaches the maximum of the u nullcline. Then, v remains almost constant while u decreases rapidly until the system reaches the left branch of the u nullcline. The entire process then repeats, without the necessity of additional stimulations. Therefore this is an oscillatory system - a single perturbation results in repeated oscillations. The period of these oscillations mainly depends on the time spent in the slow portions. The trajectory of the system is called a limit cycle. The change in the dynamics from steady state to oscillatory behavior occurs through a Hopf bifurcation as the value of the bifurcation parameter passes through a critical value. See Box 1.2 for more details. Next, let's consider the case shown in fig. 1.4 where there is only one fixed point. This fixed point is stable i.e., when the perturbations are small, the system returns to the fixed point. However, for perturbations larger than a particular threshold, the system performs a large excursion in phase space. For instance, in the figure, if the system's v value is decreased to X, them due to the dynamics, the system will increase its u value

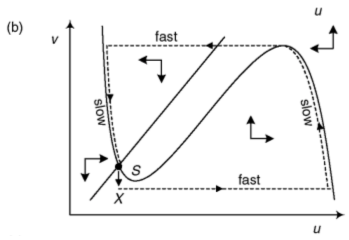

Figure 1.4: The nullclines of the Fitz-Hugh Nagumo model. The system has one stable fixed point. Figure reproduced with permission from [8].

until it reaches the right branch of the u-nullcline. From here, the system moves slowly along the right branch of the nullcline, where u is almost constant and v increases. As the system reaches the maximum of the nullcline, u value decreases rapidly and the system moves to the left branch of the u nullcline. Once it is reached, u value stays almost constant and the v decreases until the system is back to the stable fixed point. This describes an excitable system - perturbation above a threshold causes a large excursion in phase space, whereas a small perturbation does not. Further, unlike the oscillatory system, in the excitable regime, each excursion on the phase space needs a perturbation.

In fig. 1.5, the system has three fixed points. The fixed points on the right and left branches of the u-nullcline are stable whereas the fixed point on the central branch is unstable. Starting from one of the stable fixed points, one can make the same argument as in the previous case. However, in this case, instead of undergoing one complete loop in phase space, the system begins at one stable fixed point and ends up at the other stable fixed point. Such a system is bistable excitable.

Box 1.1: Linear Stability Analysis

Linear stability analysis is an important method to analyze the dynamics

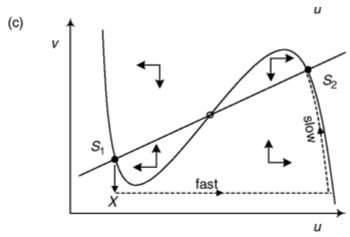

Figure 1.5: The nullclines of the Fitz-Hugh Nagumo model. The system has three fixed points, of which one is unstable and two are stable. Figure reproduced with permission from [8].

of a system without *actually* solving the model equations. This method has been extensively discussed in books dealing with non-linear dynamics and pattern formation such as [38, 51]. Consider a system governed by a two variable system of equations.

$$\dot{x} = f_1(x, y) \tag{1.7}$$

$$\dot{y} = f_2(x, y) \tag{1.8}$$

Let $(\bar{x}, \bar{y})$ represent the steady state i.e. it is the point of intersection of the curves obtained by setting the right hand sides of equations 1.7 and 1.8 to zero. Mathematically, $f_1(\bar{x}, \bar{y}) = 0$ and $f_2(\bar{x}, \bar{y}) = 0$. Linear stability analysis equips us with a way to determine the stability of the steady state(s). In other branches of physics, the stability of steady states or equilibria is determined by studying the reaction of the steady state to small perturbations. The same concept is applied in this case as well. If the applied perturbations die out, the steady state is stable. If the perturbations increase in time, the steady state is unstable. A lot more can be inferred about the steady states by a detailed mathematical analysis. We'll start by perturbing the steady state by a small amount. This is represented by $x = \bar{x} + u$ and

$y = \bar{y} + v$, where u and v are assumed to be small. Now, we analyze the temporal behavior of u and v to determine the stability of the steady states.

$$\dot{u} = \dot{x} + \dot{\bar{x}} = \dot{x}, \text{(because } \bar{x} \text{ is a constant)}$$

$$\dot{u} = f_1(x, y)$$

$$\dot{u} = f_1(\bar{x} + u, \bar{y} + v)$$

A Taylor series expansion gives

$$\dot{u} = f_1(\bar{x}, \bar{y}) + \frac{\partial f_1}{\partial x}(\bar{x}, \bar{y})u + \frac{\partial f_1}{\partial x}(\bar{x}, \bar{y})v + ...$$

By the definition of the steady state, $f_1(\bar{x}, \bar{y}) = 0$.

$$\dot{u} = \frac{\partial f_1}{\partial x}(\bar{x}, \bar{y})u + \frac{\partial f_1}{\partial y}(\bar{x}, \bar{y})v + ...$$

Similarly,

$$\dot{v} = \frac{\partial f_2}{\partial x}(\bar{x}, \bar{y})u + \frac{\partial f_2}{\partial y}(\bar{x}, \bar{y})v + ...$$

The higher order terms, which involve higher powers of u and v can be ignored because of our assumption that u and v are small. This linearizes the system about the steady state $(\bar{x}, \bar{y})$. The two equations can be reformulated in the matrix notation.

$$\begin{bmatrix} \dot{u} \\ \dot{v} \end{bmatrix} = \begin{bmatrix} \frac{\partial f_1}{\partial x}(\bar{x}, \bar{y}) & \frac{\partial f_1}{\partial y}(\bar{x}, \bar{y}) \\ \frac{\partial f_2}{\partial x}(\bar{x}, \bar{y}) & \frac{\partial f_2}{\partial y}(\bar{x}, \bar{y}) \end{bmatrix} \begin{bmatrix} u \\ v \end{bmatrix} \tag{1.9}$$

The 2 x 2 matrix is the Jacobian of the system. The solution to this linearized set of equations determines whether the perturbations grow or decay. In other words, the eigenvalues of this matrix determine the stability of the

steady states. Let's rewrite the Jacobian as

$$J = \begin{bmatrix} a & b \\ c & d \end{bmatrix}$$

Let λ_1 and λ_2 be the two eigenvalues of J. [51] provides a classification of the stabilities. If the eigenvalues are both real, but have opposite signs, the steady state is a saddle point. If both the eigenvalues are real and have the same sign, the fixed point is unstable if they're positive and stable if they're negative. If the eigenvalues are complex (they are necessarily complex conjugates), three cases arise: if the real part is zero, the fixed point is a centre; if the real part is negative, the fixed point is an inward spiral or a spiral sink; if the real part is positive, the fixed point is a spiral source. If the eigenvalues are equal to each other, the fixed point is a star node, if there are two eigenvectors and the fixed is a degenerate node, if there is only one eigenvector. With this knowledge of the behavior of the fixed point, it is possible to draw trajectories in the phase plane for any given initial point.

Now, we recall the diffusion term in the equations. So far we have considered the stability of the spatially homogeneous solutions of the system of equations. What is the effect of diffusion? To understand this, let us begin with the solutions for stability without diffusion.

$$u_t = f(u, v)$$

$$v_t = g(u, v)$$

The analysis proceeds along the lines of Box 1.1. Let the system be perturbed around the homogeneous steady state (u_0, v_0).

$$\boldsymbol{w} = \begin{bmatrix} u - u_0 \\ v - v_0 \end{bmatrix} \tag{1.10}$$

I will consider the conditions for which the perturbation will be stable in the absence of diffusion and then consider what happens when diffusion is turned on. As described in Box 1.1, the effect of the perturbation is determined by the determinant of the Jacobian evaluated at the steady state (u_0, v_0).

$$A = \begin{bmatrix} \frac{\partial f}{\partial u} & \frac{\partial f}{\partial v} \\ \frac{\partial g}{\partial u} & \frac{\partial g}{\partial v} \end{bmatrix}$$

where

$$\boldsymbol{w}_t = A\boldsymbol{w} \tag{1.11}$$

If the perturbation decays in time, the steady state is stable. To determine this, the decay rate has to be found. So we assume that the solution to the above equation is $\boldsymbol{w} \propto e^{\lambda t}$ and find the conditions for which λ is negative (because negative value implies decay and hence stability of steady state). λ is given by the eigenvalues of the Jacobian.

$$\lambda^2 - (f_u + g_v)\lambda + (f_u g_v - f_v g_u) = 0$$

Here, $f_u + g_v$ is the trace of A and $f_u g_v - f_v g_u$ is its determinant. So the value of λ are given by

$$\lambda_{1,2} = \frac{1}{2}[Tr(A) \pm \sqrt{Tr(A)^2 - 4det(A)}]$$

For stability, $\mathrm{Re}(\lambda) < 0$, i.e.,

$$Tr(A) < 0, det(A) > 0. \tag{1.12}$$

Now, we re-insert diffusion. Equation 1.11 becomes

$$\boldsymbol{w}_t = A\boldsymbol{w} + D\nabla^2\boldsymbol{w},\ D = \begin{bmatrix} 1 & 0 \\ 0 & d \end{bmatrix} \tag{1.13}$$

The equation 1.13 can be solved by separation of variables. The spatial component is given in terms of spatial waves with wave vector $\mathbf{k}$. Also, since equation

1.13 has been linearized, the general solution is the linear superposition of the solutions. So, the general solution is

$$\boldsymbol{w}(\boldsymbol{r}, t) = \sum_k c_k e^{\lambda t} e^{i\boldsymbol{k}\cdot\boldsymbol{r}} \tag{1.14}$$

Substituting equation 1.14 into equation 1.13 gives the condition

$$|\lambda I - A + Dk^2| = 0 \tag{1.15}$$

Evaluating this determinant gives

$$\lambda^2 + \lambda[k^2(1+d) - (f_u + g_v)] + h(k^2) = 0 \tag{1.16}$$

where

$$h(k^2) = dk^4 - k^2(df_u + g_v) + |A| \tag{1.17}$$

In this case, we are looking for traveling wave solutions i.e., the cases where the steady state obtained before becomes *unstable* to spatial disturbances, i.e. $Re(\lambda) > 0$ for some $k \neq 0$. From equation 1.16, this condition requires either the coefficient of λ to be negative, or $h(k^2) < 0$ for some $k \neq 0$. But from the conditions in equation 1.12, $f_u + g_v < 0$, and $k^2(1+d) > 0$ for all k. So the coefficient of λ cannot be negative. So, the only way the steady state can be unstable to spatial perturbations is for $h(k^2)$ to be negative. From equation 1.12, we know that $|A| > 0$, so the only way for $h(k^2) < 0$ is, from equation 1.6, $(df_u + g_v) > 0$. Further since from equation 1.12 $(f_u + g_v) < 0$, this implies $d \neq 1$. So the requirement for instability is

$$df_u + g_v > 0, \quad d \neq 1. \tag{1.18}$$

From the nullclines in fig. 1.3 we see that $f_u > 0$ and $g_v < 0$. This implies, $d > 1$ i.e., the inhibitor must diffuse faster than the activator. However, the condition

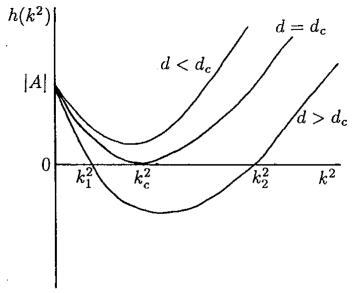

Figure 1.6: The variation of $h(k^2)$ as a function of k, for different values of the the diffusion coefficient, d. Figure reproduced with permission from [38].

in equation 1.18 is necessary, but not sufficient. For $h(k^2)$ to be negative, it's minimum value should be negative for some $k \neq 0$. The minimum is given by

$$h_{min} = \left[|A| - \frac{(df_u + g_v)^2}{4d}\right] \tag{1.19}$$

So, for $h(k^2) < 0$ for some $k \neq 0$, we need

$$\frac{(df_u + g_v)^2}{4d} > |A|. \tag{1.20}$$

This condition can be satisfied if the diffusion coefficient, d, is is above a critical value given by $\frac{(d_c f_u + g_v)^2}{4d} > |A|$. Fig. 1.6 shows the plots of $h(k^2)$ with respect to k^2, indicating the stable and unstable modes. So far, I have described the conditions for which the steady states become unstable in the presence of diffusion. It is this instability that leads to spatial patterns. In the next sections, I consider how traveling waves are produced in excitable and oscillatory systems.

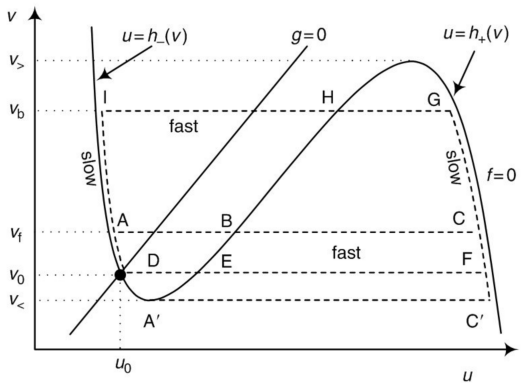

Figure 1.7: The nullclines of the Fitz-Hugh Nagumo model with one stable fixed point. Figure reproduced with permission from [8].

1.1.1 Waves in Excitable systems

Before describing wave propagation, I will describe wave fronts and pulses. I'll begin with the Fitz-Hugh Nagumo equations described above in equations 1.1 - 1.4. If the system allows traveling wave solutions, then the concentrations of u and v are functions of z=x-vt, assuming the wave travels along +x axis. The equations can be re-written in terms of derivatives of z as

$$u'' + cu' + \eta^{-1} f(u, v) = 0 \tag{1.21}$$

$$dv'' + cv' + g(u, v) = 0 \tag{1.22}$$

Here the prime denotes derivative with respect to z. First, let's look at the propagation fronts of u. From fig. 1.7, u takes the value $u = u_- = h_-(v_f)$ on the left branch of the nullcline, whereas on the right branch, $u = u_+ = h_+(v_f)$. The front connects these two regions of constant u, for some fixed $v = v_f$. We can assume v stays fixed because the change in u is rapid (see discussion above). The equation of the front is

$$u'' + cu' + \eta^{-1} f(u, v_f) = 0 \tag{1.23}$$

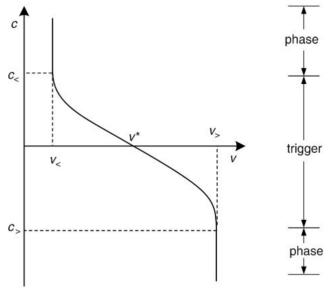

Figure 1.8: The dependence of the speed of the front on the concentration of the slow variable v. Figure reproduced with permission from [8].

Rescaling, $Z = \eta^{-1/2}z$ and $C = \eta^{1/2}c$, the above equation becomes

$$u'' + Cu' + F(u) = 0 \tag{1.24}$$

Here, the prime denotes differentiation with respect to Z. If Z corresponds to time, u to space, and $F(u) = -\partial\phi/\partial u$, where ϕ is a "potential" with two peaks, the equation 1.24 resembles the equation of motion of a particle with frictional damping in a potential. So, the wavefront can be thought of as connecting a high and a low peak of the potential. The width of this front is of the order of $\eta^{1/2}$ and its speed is of the order of $\eta^{-1/2}$. The concentration of the slow variable, v, sets the speed. As the concentration of the slow variable v changes, the speed changes sign, going through zero for some particular concentration. Fig. 1.8 shows the variation of the speed with respect to the concentration of v. $v_<$ and $v_>$ are values of v corresponding to the minimum and the maximum of the u nullcline in fig. 1.7. Between these two values of v, the speed is unique. The fronts characterized by this dynamics are called trigger fronts. However, it is possible that the system starts at the value of v corresponding to either $v_<$ or $v_>$. In such cases, one of the two peaks of the "potential" in equation 1.24 disappear, and the speed of the front can have any value. Such dynamics create a phase front.

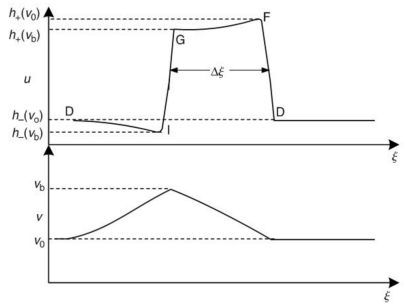

Figure 1.9: A pulse solution of the Fitz-Hugh Nagumo model. The letters correspond to the paths in fig. 1.7. Figure reproduced with permission from [8].

Next, let us consider a pulse traveling in a system described by the above equations, as shown in fig. 1.9. The front of the pulse connects the two regions of different values of u as described above, i.e., from the nullclines, it connects $u_0 = h_-(v_0)$ and $u = h_+(v_0)$. This is the fast region DF in fig. 1.7 and fig. 1.9. The slow region of the nullcline is represented by FG in the two figures, where v decreases from v_0 to v_b, but u is almost the same. Then, the dynamics is again rapid, corresponding to the back of the pulse, which connects $u = h_+(v_b)$ with $u_0 = h_-(v_b)$. Since this is the reverse of the front of the pulse, the concentration of v, v_b, should be such that the speed is same in magnitude but opposite in sign as in the wavefront, i.e. $c(v_b) = -c(v_0)$. As before, the speed of the pulse is of the order of $\eta^{-1/2}$, which makes the second term the most dominant in equation 1.22. So by dropping the first term, the equation can be written as:

$$cv' + g = 0 \tag{1.25}$$

This equation can be directly integrated to give the width of the pulse in terms of the variable Z. Keeping in mind that in this step, v is a constant and therefore $u = h_+(v)$, the pulse width is given by:

$$\Delta Z = c \int_{v_0}^{v_b} \frac{dv}{g(h_+(v), v)} \tag{1.26}$$

In the last step, the dynamics is slow again, with v decreasing from v_b to v_0, while u is almost constant.

Waves are a series of such pulses traveling through the medium. This can only be allowed if the trajectory does not pass through the steady state D in the fig. 1.7. The fast variable u begins to increase before the slow variable v can relax to its steady state value. The path ABCGHIA is one such trajectory. The wave speed is equal to the speed of the speed of the front and the back, i.e., $c(v_b) = -c(v_f) = c$. The speed cannot be greater than the speed of a single pulse. The speed of the pulse is the limiting value of the speed of waves of very long wavelengths. The wavelength of the wave, defined as the distance between two successive fronts, is determined by the two slow portions of the dynamics, i.e., an equation similar to equation 1.26 can be written. Since the wave period is the wavelength divided by the wave speed, we get

$$P = \frac{1}{c}(\Delta Z_1 + \Delta Z_2) = \int_{v_f}^{v_b} \frac{dv}{g(h_+(v), v)} + \int_{v_b}^{v_f} \frac{dv}{g(h_-(v), v)} \tag{1.27}$$

The above equation also gives the dispersion relation for the system. Smaller speeds correspond to the case where the loop in fig. 1.7 becomes smaller i.e., v_b and v_f approach each other decreasing the period. Since the wave front and the wave back have speeds of opposite signs, the v_b and v_f will settle around the value of v corresponding to zero wave speed. At these small values of the speed, diffusion cannot be ignored in equation 1.22, the approximation equation 1.25 is not valid, and therefore the above equation does not hold.

1.1.2 Waves in Oscillatory systems

As described before, oscillatory systems are characterized by limit cycle oscillations. To understand wave propagation in oscillatory systems, I will consider the example of the 1D $\lambda - \omega$ system as described in [38]. This system is characterized by the equations

$$\frac{\partial}{\partial t}\begin{bmatrix} u \\ v \end{bmatrix} = \begin{bmatrix} \lambda(r) & -\omega(r) \\ \omega(r) & \lambda(r) \end{bmatrix}\begin{bmatrix} u \\ v \end{bmatrix} + \frac{\partial^2}{\partial x^2}\begin{bmatrix} u \\ v \end{bmatrix}, \quad r^2 = u^2 + v^2 \tag{1.28}$$

$\omega(r)$ is a positive function of r. $\lambda(r)$ is positive for $0 \leq r \leq r_0$ and negative for $r \geq r_0$ i.e., it is zero at r_0. Converting the variables to polar variables,

$$u = rcos(\theta), \quad v = rsin(\theta) \tag{1.29}$$

Substituting these into the equation 1.28 gives

$$r_t = r\lambda(r) + r_{xx} - r\theta_x^2 \tag{1.30}$$

$$\theta_t = \omega(r) + \theta_{xx} + \frac{2}{r} r_x \theta_x \tag{1.31}$$

It can be seen immediately, that setting $r = r_0$ gives a limit cycle solution:

$$r = r_0, \quad \theta = \theta_0 + \omega(r_0)t \tag{1.32}$$

Substituting these into equations 1.29, the limit cycle solutions are

$$u = r_0 cos[w(r_0)t + \theta_0], \quad v = r_0 sin[w(r_0)t + \theta_0] \tag{1.33}$$

With diffusion, we can expect traveling wave solutions in this system. Consider a traveling wave in the polar form.

$$r = \alpha, \quad \theta = \sigma t - kx \tag{1.34}$$

Substituting into the equations 1.30,1.31 gives

$$\sigma = \omega(\alpha), \quad k = \sqrt{\lambda(\alpha)} \tag{1.35}$$

So the traveling wave solutions for this case are parametrized by α.

$$u = \alpha cos[\omega(\alpha)t - x\lambda^{1/2}(\alpha)], \quad v = \alpha sin[\omega(\alpha)t - x\lambda^{1/2}(\alpha)] \tag{1.36}$$

The speed of these waves is given by $c = \frac{\sigma}{k} = \frac{\omega(\alpha)}{\lambda^{1/2}(\alpha)}$. As α approaches r_0, the wave vector goes to zero (because $\lambda(r_0) = 0$). So, we expect plane waves near the limit cycle. To obtain the form of these waves, let's consider the specific form:

$$\omega(r) = 1, \quad \lambda(r) = \gamma - (u^2 + v^2). \tag{1.37}$$

With this form, the steady state is (0,0) for (u,v), as can be seen in

$$f(u,v) = \frac{\partial u}{\partial t} = (\gamma - u^2 - v^2)u - v = 0 \tag{1.38}$$

$$g(u,v) = \frac{\partial v}{\partial t} = u + (\gamma - u^2 - v^2)v = 0 \tag{1.39}$$

A linear stability analysis gives the Jacobian to be

$$\begin{bmatrix} \gamma - 3u^2 - v^2 & -2uv - 1 \\ 1 - 2uv & \gamma - u^2 - 3v^2 \end{bmatrix} \tag{1.40}$$

At the steady state values of (0,0), the eigenvalues of the above Jacobian are $\gamma \mp i$. Therefore, the steady state is stable for $\gamma < 0$ and unstable for $\gamma > 0$. At $\gamma_c = 0$, Hopf bifurcation occurs and the system become oscillatory. Just above the Hopf bifurcation, since $\lambda = 0$ (because $\gamma = 0$ and (u,v)=(0,0)), and $\gamma = \gamma_c + \epsilon$, with $0 < \epsilon << 1$, we can expect limit cycle solutions of the form

$$u(t) = \sqrt{\gamma} cos(t), \quad v(t) = \sqrt{\gamma} sin(t) \tag{1.41}$$

which in polar form becomes

$$r_0 = \sqrt{\gamma}, \quad \theta = t + \theta_0. \tag{1.42}$$

Therefore, in oscillatory systems, we have seen that diffusion can create traveling waves. This is a characteristic of problems with Hopf bifurcation. See Box 1.2 for more on Hopf bifurcations.

Box 1.2: Hopf bifurcation

The stability of the steady state of a two dimensional system is determined by the eigenvalues of its Jacobean. Suppose the eigenvalues are a complex conjugate pair. As described in Box 1.1, for the steady state to be stable, $Re(\lambda) < 0$. At steady state, for small perturbations, the system oscillates about the steady state with decaying amplitudes and settles back to the steady state. If the parameter of the system that controls this decay increases beyond a critical value, instead of decaying, small perturbations will grow in amplitude, making the steady state unstable and the system undergoes small amplitude limit-cycle oscillations. This bifurcation corresponds to a change phase-space flow from a stable spiral to an unstable spiral. The amplitude of the limit cycle is of the order of the square root of the difference between the bifurcation parameter and its critical value. The frequency is approximately equal to the imaginary part of the eigenvalue. This is a supercritical Hopf bifurcation.

In a subcritical Hopf bifurcation, the trajectory of the system typically jumps to a distant attractor, resulting in large amplitude oscillations. For example, consider a system has a stable fixed point surrounded by a stable limit cycle, with an unstable limit cycle in between. The change in the bifurcation parameter could decrease the radius of the unstable limit cycle, until it renders the fixed point unstable. Now any perturbation around the previously stable fixed point will send the system into the distant, large ampli-

tude limit cycle oscillations. If the bifurcation parameter was reversed, the system does not go back to the stable fixed point immediately – it shows hysteresis. Subcritical Hopf bifurcations are therefore very dangerous in practical applications.

1.2 All about spirals

The set equation such as the ones described above for excitable and oscillatory systems allow spiral wave solutions. This means at a given point of time, the concentration of a chemical or the density of a species looks like a spiral. With time, the profile of the concentration or the population density changes like a rotating clock spring. These waves are rigid rotors, rotating with a frequency Ω. It has been shown analytically that the frequency of the spiral wave is fixed for a given wave number. Unlike plane waves, these spiral waves have curved fronts. The curvature can be described by the eikonal equation that connects the normal velocity of the front c_n to its curvature K. The concentration profile can be described by the phase ϕ. So, a rotating spiral can be described by

$$\phi(r,t) = \Omega t \pm m\theta + \psi(r) \tag{1.43}$$

Here, m is the number of arms of the spiral, and the sign in front of it determines the direction of rotation. The function $\psi(r)$ determines the kind of spiral. For example, $\psi(r) = ar$ gives an Archimedian spiral while $\psi(r) = alnr$ gives a logarithmic spiral. The core a spiral is a defect or a singularity in phase. This means that if the phase of the oscillations were plotted, at the core, the phase would be undefined. In most cases, the core rotates along a circle creating the

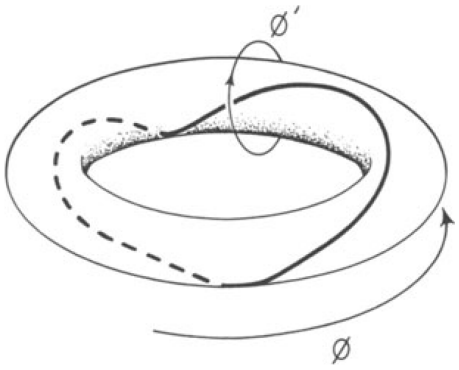

Figure 1.10: The mapping from a ring to a ring can be represented by a Torus. ϕ denotes the position of the point on the first ring, while ϕ' denotes the resultant angle. Figure reproduced with permission from [60].

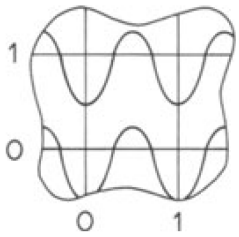

Figure 1.11: The mapping on a Torus can be represented by a two dimensional unit cell. The four vertices of the unit cell represent the same point. Figure reproduced with permission from [60].

waves. In some cases, the core tends to meander.

Box 1.3: Phase singularity

To understand the concept of phase singularities, I will follow the discussions by A. Winfree in [60]. First, I will consider the concept of winding number. Consider a mapping from a ring $\mathbb{S}^1$ to another ring: $\mathbb{S}^1 \mapsto \mathbb{S}^1$. This is the simplest mapping that introduces winding numbers. This map basically, takes a point on a ring and maps it to a point on another ring. As the point on the first ring completes one rotation and returns to its initial position, the mapped point on the the other ring should also reach its

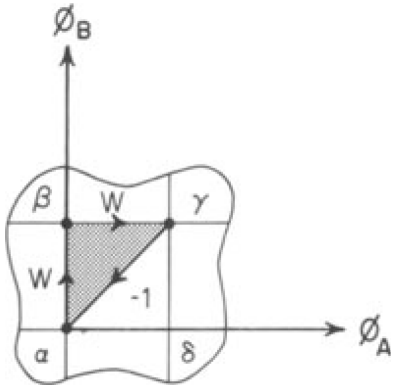

Figure 1.12: Variation of the input phases. One phase is maintained at zero, while the other completes an full rotation.Figure reproduced with permission from [60].

initial position; however, it may have completed more than one rotation around the ring. The number of rotations completed by the mapped point is the winding number. The mapping between two rings is represented by a torus: $\mathbb{T}^2$. As shown in fig. 1.10, even though there is a unique output ϕ' for every ϕ, and when ϕ returns to its initial position, so should ϕ', the curve that connects them can travel up and down the vertical axis of the torus many number of times. An easier way to describe the torus is by mapping its two axes on a plane, as shown in fig. 1.11. In such a representation, the winding number is the number of times the data climbs vertically in one cell.

Now, I will use such representations of maps to explain phase singularities. Suppose a system has two phases ϕ_A and ϕ_B. This gives a map from $\mathbb{S}^1 \times \mathbb{S}^1 \mapsto \mathbb{S}^1$ The resulting phase ϕ' follows these axioms

- Small changes in ϕ_A and ϕ_B result in small change in ϕ' for almost all cases.

- The two input phases are equivalent.
- If the two input phases are approximately equal, ϕ' is also approximately equal to them.

Consider fig. 1.12, which shows an example of the variation of the input phases. Here, one phase is kept constant, at zero, while the other phase completes a full cycle. As before, the points α, β, γ and δ represent the same point i.e., $\phi_A = \phi_B = \phi' = 0$. Along the paths $\alpha\beta$ and $\beta\gamma$, suppose ϕ' completes W rotations. Along the diagonal, the resultant phase goes back by one cycle. The resultant winding number is, therefore, 2W-1. According to the first axiom, if the path $\alpha\beta$ were changed slightly, it should not affect the resultant phase. We can make the loop as small as possible. This means that even though the input phases do not change, the resultant phase jumps by at least one winding number. So it is impossible for the resultant phase to depend smoothly on the input phases. This results in a singularity.

1.3 Dictyostelium discoideum

Dictyostelium discoideum (*D.d*) is a single celled amoeba that generally lives in the soil and feeds on bacteria. It belongs to the group of slime molds, which includes Physarum, the enormous single celled organism with thousands of nuclei. *D.d.* is an ancient organism studies have shown [14] that *D.d.* diverged from the animalfungal lineage after the plantanimal split, around 1.5 billion years ago. The ancientness of *D.d.* implies that it has a robust survival mechanism that has prevented its extinction despite the severity of the environmental conditions over the centuries. When conditions become unfavorable, *D.d.* (and

all the slime molds) forms spores that can be dispersed by wind or water. These spores can re-form cells if conditions become favorable.

Compared to other organisms, *D.d.* has retained more of the diversity of its ancient genome [14]. Thanks to this diversity, many genes in *D.d.* are related to genes involved in human diseases. Therefore a study of *D.d.* could help in the understanding of human diseases. Further, this diversity has allowed researchers to use *D.d.* to identify targets for drug delivery to cure diseases [59]. Another major feature of *D.d.* is that it is very similar to the human macrophage. This similarity enable these cells to be used instead of human cells to understand how the human macrophages function, and how to treat their diseases [58].

Another interesting behavior that is being studied in various labs is the phenomenon of chemotaxis showed by *D.d.* Chemotaxis is the movement of an organism along or against a chemical gradient. Its particularly relevant for humans because cancer cells show chemotaxis. Therefore understanding chemotaxis in D.d has a lot of practical applications.

Apart from these applications, the process by which *D.d.* forms spores is fascinating and insightful. As will be described later, populations of *D.d.* become social — they communicate with each other and form various large-scale patterns - when they starve. These patterns are similar to the patterns formed by heart tissues during arrhythmias. Not only are such patterns important from a medical viewpoint, they are also important in the industry because similar patterns are observed in industrial processes like electrodeposition of binary systems [20]. In fact, these patterns are ubiquitous — populations of predators and preys [35, 57], cell division [47], static patterns on seashells, skins of animals etc. [38] have the same basic mechanism as these patterns. A good understand-

ing of patterns in *D.d.* can help the understanding of patterns in other systems too.

Finally, *D.d.* has a unique ability it can live as a unicellular organism or millions of *D.d.* can synchronize together to form a multi-cellular organism. In fact, for *D.d.*, multicellularity is essential to form the spores discussed previously. This phenomenon has therefore been the subject of a lot of research, not only because it explains *D.d.*s robust survival strategy, but also because it could answer the questions about how multi-cellular life evolved.

Although *D.d.* has so many intriguing aspects, this work will focus on pattern formation in *D.d.* This is because although self-organized pattern formation is seen widely in nature, its origin and causes are not well understood. What are the fundamental properties that define pattern formation? Are these properties similar to other pattern forming systems? Are there parameters which are evolutionarily optimal for *D.d.*? While it is easy to observe patterns, it is not trivial to analyze them to get information about the underlying processes and answer these questions. In this work, I will analyze the two kinds of patterns formed by *D.d.* — spiral waves and target patterns.

When a large population (about 40 million cells) of *D.d.* starves, some cells secrete a chemical called cyclic Adenosine Monophosphate (cAMP) with the help of an enzyme called adenyl cyclase. cAMP then diffuses into the surrounding medium. Phophodiesterase (PDE) secreted in the medium by the cells, degrades cAMP. This degradation is necessary to create excitation pulses. Each pulse of cAMP lasts about 100s. cAMP binds to cAMP receptors that are present on the outer membranes of neighboring cells. When cAMP binds to these receptors, internal signaling pathways are triggered, which lead to the production of

more cAMP inside the cells. This cAMP is then released into the medium. Immediately after the release of cAMP the cells enter a refractory state a state where they cannot detect any new cAMP signals because their receptors are saturated. PDE breaks down cAMP in the medium outside the cells, creating a global inhibition of cAMP. This breakdown is necessary to re-sensitize the receptors on the cell membrane. The release of cAMP, its diffusion and breakdown forms a reaction-diffusion system. Such a repeated detection and release of cAMP synchronizes the cells after a few hours. In this context, synchronization refers to the release of cAMP at the same frequency by the cells. So, eventually a group of cells emit cAMP together. This cAMP moves outward from the group isotropically, in a large circle. It is possible that this wave of outward moving cAMP encounters some cells that are still in the refractory state. Such an encounter causes the wave to break and curl up around the cells. This leads to the formation of spirals. These patterns are typically about 1- 2 mm in size.

The patterns (spirals or circular waves) persist for about 2 - 3 h. Towards the end of the signaling phase, the cells begin to move chemotactically toward the center of the patterns. This is the streaming phase. Once all the cells reach the center, they form a mound. This mound transforms into a slug with about 105 individual cells. All these cells work together to move the slug to scourge for food. If no food is available, the slug transforms into a fruiting body with spores on the top. To achieve this, many cells voluntarily die to become a part of the stalk of the fruiting body. The rest of the cells form spores at the top of the fruiting body. These spores can be transported by wind or water to distant places. When food is available, the spores turn into cells and continue their life process.

How are the waves of cAMP detected experimentally? To see these waves, experimentalists use the change in morphology of the cells. When the cells first detect cAMP, they cringe and become rounded, for about 25 s. As the wave of cAMP passes by, the cells elongate or polarize their bodies. When light is shone on the cells, when they are cringed, they scatter a small amount of light, because their surface area is smaller. As the cAMP wave passes and the cells polarize their bodies, their surface area becomes larger and more light is scattered. So, by detecting the amount of light scattered by the cells, the progress of the wave can be monitored. The dark-field set-up performs this task. Such a set-up was first used by Gerisch to study waves and oscillations on a dish and in a continuously stirred suspension of cells.

As mentioned before, D.d shows two main types of wave patterns spiral and circular waves. Despite extensive research on D.d, the reason for the selection of one pattern over the other is still unclear. It has also not been easy to reconstruct the dynamics of D.d using information provided by the patterns. In this work, I will analyze patterns systematically to extract useful information from them.

1.3.1 Experimental results on spatiotemporal patterns in *D.d.*

Wave Characterization

Waves are characterized by three quantities velocity, wavelength and oscillation period. Consider the spirals waves in fig 1.13. The width of the white band corresponds to the distance travelled by cAMP during the time that the cells remain elongated. The distance between two successive white bands corresponds to the distance travelled by the wave between successive cAMP pulses. The

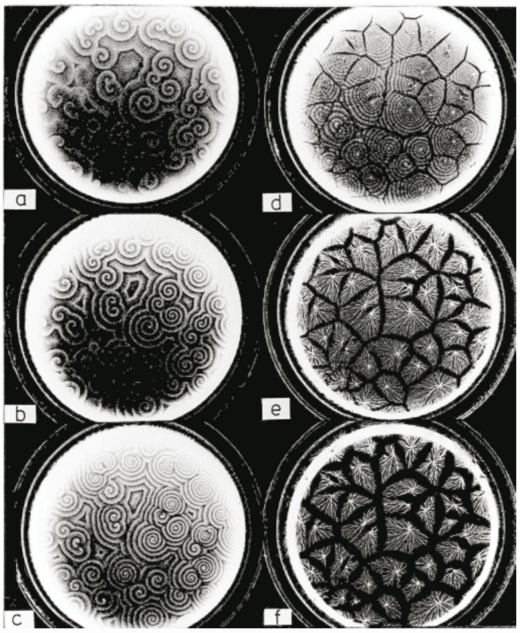

Figure 1.13: Waves formed by populations of *D.d.*. After a few hours of signaling, aggregation territories are formed. Figure reproduced with permission from [33].

latter distance depends on the frequency of cAMP emission [1]. The time period (T) of the wave is the time interval between movements of selected cells in response to successive signal fronts. The wavelength, λ is defined as the sum of the widths of the white and dark bands. Wave velocity, v, is obtained by combining the wave period and the wavelength i.e. $v = \lambda T$.

When a wave passes over a cell, the cell begins to move along the cAMP gradient, towards increasing concentrations of cAMP. However, during the back of the wave, the direction of the gradient is reversed. To ensure that the waves propagate outwards and the cells move towards the signaling center, it is required that the cells become refractory for some time immediately after being signaled, though the refractory periods for the two need not be the same. In [44], it was shown that the refractory period for relay of the signal decreases from 7 min to 2 min during aggregation. In [1] it is shown that the refractory period for

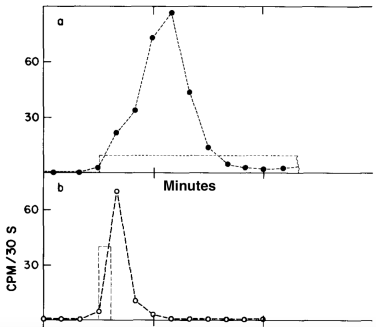

Figure 1.14: Waves formed by populations of *D.d.*. After a few hours of signaling, aggregation territories are formed. Figure reprinted with permission from [9].

cell movement is not more than 12 s. This was further proven by stimulating cells with cAMP pulses and measuring the production of intracellular cAMP [9]. In experiments with external cAMP pulses, it was seen that the cells adapt to the external cAMP pulses. (Fig. **??**) The production of intracellular cAMP pulses decreases with time, even if the external pulse is maintained. The rate of adaptation also depends on the stimulation history of the cells. [9] If the cells are pretreated with higher concentrations of cAMP, their response to test stimulus attenuates faster and for a given concentration of pretreatment, the attenuation rate of the production of intracellular cAMP decreases with increase in cAMP concentration of the test stimulus. [9]

Kymographs are space-time plots of specified regions in an image stack. Using kymographs, it was found that the wave travels with constant velocity, but velocity of later spiral arms decreases sigmoidally with time from 467μm/min to 240μm/min over about 50 mins [23]. This was confirmed by later experiments [50]. The decrease in wave speed means that the same cells which propagate the first wave at higher speeds, somehow propagate the successive waves slower. The cells thus evolve synchronously in time corresponding to the num-

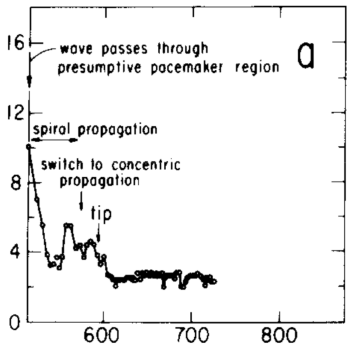

Figure 1.15: Time interval between successive waves. Figure reprinted with permission from [13].

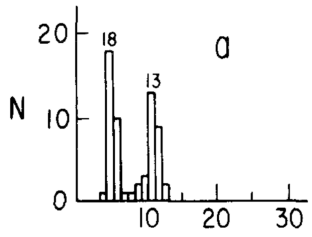

Figure 1.16: Histogram of the time interval between successive waves of target patterns showing a bimodal distribution. Figure reprinted with permission from [13].

ber of waves they have propagated, rather than laboratory time. The excitations change the cells properties through cAMP signals [23]. Further, the velocity ranges from 7μm/s to 4.7μm/s as cell density increases from 5x10^{4}cells/cm^2 to 5x10^{5}cells/cm^2 [1]. The period of the spiral waves was measured to be about 4min by extrapolating the kymographs [23]. However, later experiments revealed a slight decrease in the period viz. from 5.8min to 4.5min. [50] In another work, the period was defined as the time interval between two successive waves from a center crossing a fixed reference point. It was found that the spirals start out with a period of 10min, which decreases with time to about 2min [13] (Fig. 1.15). A spiral wave can be thought of as being formed by the propagation of signal around the central core. The period, therefore, is the time needed by all

the cells in the spiral core to fire once. The decreasing period implies that the size of the loop of cells that form the spiral core evolves with time, to a size in which the time taken for the excitation to complete one loop is equal to the time required for one cell to go back to being excitable after its refractory phase [23]. This was also hypothesized by Durston [12]. The cAMP waves can also take the form of target patterns. In fact, in many cases, the formation of spirals are preceded by targets, implying that spatial inhomogeneities due to refractory periods creates spirals. Sustaining spiral waves depends only on signal relay, whereas sustaining targets depends on autonomous firing of cells. Two kinds of target patterns were found: the bimodal targets start with a period of 10min, but after 3h their period decreases to 5min, either smoothly or abruptly; the unimodal targets, the period can either remain somewhere between 5-10min or decrease gradually. (Fig. 1.16) This has been explained by suggesting the presence of a gate that blocks the 5 min period during the early aggregation stage [13]. As mentioned earlier, by measuring response to artificial signals it was found that the refractory period of cells exceeds 6 min at the early stages and is about 2 min at the later stages [44]. This explains why the 5 min signal is gated in the early stages, but not in the later stages. In both spirals and target patterns, we have seen that the frequency of the waves increases while the velocity decreases. [23, 50] This dispersion relation is similar to the dispersion relation of the Belousouv-Zabotinsky reaction [10].

On varying temperature, it was found that the average velocity and rate of decrease in velocity with time increase from 160 to 400 μm/min with increase in temperature from 7C to 24C. [23] The period of the waves increases with decrease in temperature. When fit with an Arrhenius type equation, it yields a activation energy of 17kcal/mol. [23] This is similar to the values obtained for

cells in suspension [62] which indicates that the underlying processes are the same in both cases.

Information obtained from factors affecting pattern formation

Caffeine is known to decrease the production of cAMP [3, 55]. It was observed that treating cells with caffeine improves the visibility of the spirals and changes all their observed parameters. From kymographs it is possible to extract the light scattering response as a function of time at a given pixel. The amplitude of these oscillations indicates the degree of light scattering and the synchrony of cells. When treated with caffeine, this response curve showed drastic changes. The dark bands are much wider. The decay of the scattered light amplitude is twice as slow as the decay in untreated cells. This could either be because of a change in the shape of cAMP signal or because of the change in chemotactic response. The shape of the cAMP response depends on the adaptation of the cells as explained earlier. However, it was shown that caffeine does not influence the adaptation time [52]. So, the change in shape of the light scattering curve should be due to the change in chemotactic response. The amplitude of the light scattering does not change. This is surprising because it means that the light scattering does not depend on the strength of the cAMP signal. This could either mean that the chemotaxis must be proportional to the relative change in signal strength or that the receptors of cAMP on the cell are fully occupied even for extremely low signal strengths [50].

The aggregation territories increase in size as concentration of caffeine increases. This is consistent with the view that the spiral core evolves to a size where the signal relay takes a time equal to refractory period of a cell to com-

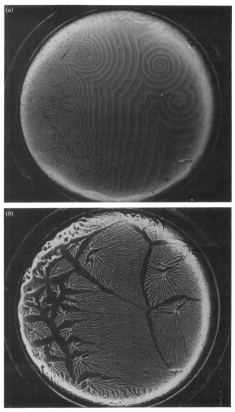

Figure 1.17: The agar substrate has a gradient of adenosine, which affects pattern formation. Figure reprinted with permission from [39].

plete a loop [12]. Since caffeine increases the period, the size of the spiral cores are larger. The wave propagation velocity decreases in the presence of caffeine. The decrease in velocity of propagation is sigmoidal [23] in the absence of caffeine, but linear in the presence of caffeine [50]. The period (measured by time intervals between successive wave) also shows an opposite trend; it increases with time as opposed to untreated samples where it decreases [13]. Power spectral analysis shows that caffeine treated cells have two harmonic frequencies as opposed to one in the untreated cells [50]. Also, increasing caffeine decreases the overall frequency. The addition of caffeine produces a dispersion relation different from the one described above; velocity decreases with frequency [50]. Similar experiments were performed by growing cells on a gradient of adenosine [39]. The aggregation territories were much larger on the side with more adenosine and had much fewer spirals. (Fig. 1.17) Alternatively, when adenosine was sprayed on a plate of starving cells which were just about to start forming centers, formation of new centers were inhibited and existing centers acquired larger territories. This is attributed to the effect of adenosine on the binding affinity of cAMP to the receptors [39]. 5mM adenosine inhibits bind-

ing of cAMP to the receptors by 90%. However, increase in concentration does not affect binding further. Also, the extent of inhibition is independent of the concentration on cAMP over the range 2-400nM. This indicates non-competitive inhibition by binding of adenosine to other receptors [39].

D.d. cells have at least four types of cAMP receptors (cAR1-cAR4). These are expressed at different times of starvation and have different affinities to cAMP [11]. cAR1 has the highest affinity and is expressed the earliest. Cells lacking in this receptor fail to aggregate. cAR3 is expressed next, but it has no obvious phenotype. cAR2 is expressed during the mound stage and has very low affinity to cAMP. Absence of cAR2 stops the development at the mound stage. cAR4 is expressed at the slug stage. Deletion of cAR4 causes defects during the spore formation [11]. A mutant cell line, which expresses only cAR1, showed waves from random positions and did not form clear centers. The wave velocity however, is not different from the parent cell line. Cell lines expressing only cAR2 did not form any waves and failed to aggregate. A cell line expressing only the cAR3 receptor showed large spiral waves (larger than the parent cell line). A kymograph analysis shows that the frequency of spiral rotation is low, but the wave velocity is the same as the parent. Expressing only cAR1 and cAR2 produced concentric waves from random positions. But, due to this randomness, they failed to aggregate, even though cell lines expressing only cAR1 could aggregate.

Measuring time intervals between successive waves showed that cells overexpressing cAR1 have a period of 11.6 min while the parent cell lines period is 3.5 min. cAR3 cells have a period of 9.9 min while cAR1 and cAR2 expressing cells have a period of 14.3 min. The wave velocity remains constant over

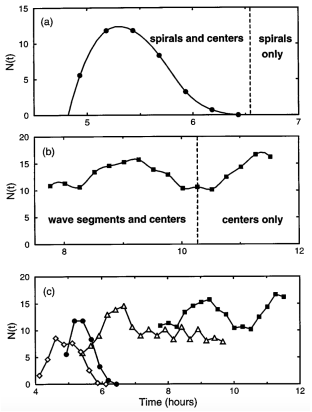

Figure 1.18: The change in the number of spirals formed for different cell densities as a function of time. (a) High cell density (b) low cell density (c) Combination of (a) and (b) Figure reprinted with permission from [30].

all the mutants [11]. This means the receptor affinity does not influence wave speeds. But the receptor affinity does affect the wave periods. The fact that even when the dominant cAR1 expression does not give the same period and wave pattern as the parent suggests that cAR1 could have a negative effect on cAMP relay. Since only spirals and no targets were observed when only cAR3 is expressed, it suggests that the cells are only excitable [11] because spirals can persist in excitable media, but targets need pacemaker cells in the center [12]. Previously, it was mentioned that the wave velocity decreases with time. However, in cAR mutants, no decrease in speed was seen; the wave speed was constant at around 250μm/min, which is approximately the lowest speed to which waves in the normal cases reduces to. In normal circumstances, initially there are few cAR receptors; the number of receptors increases with time. In the case of mutants, there are a very large number of receptors expressed from the beginning. This suggests that increasing the number of receptors decreases the speed of the waves [11].

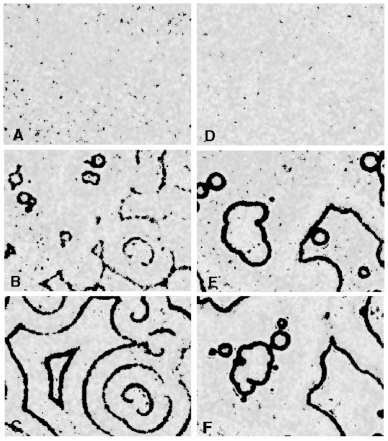

Figure 1.19: When cAMP is sprayed at 408 min (D) when patterns are well developed, only targets re-appear. Figure reprinted with permission from [31].

In a study that focused on the patterns formed by the starving *D.d* cells, it was found that at low cell densities mostly targets were observed whereas at high cell densities spirals were seen [30]. At high cell densities, spirals and spontaneous firing events compete, with the spirals eventually suppressing all the firing events. When the cell density was low, there were many firing centers and spirals failed to develop from the broken wave segments caused by inhomogeneities. At all the cell densities, a peak in the number of firing centers was observed at intermediate times. (Fig. 12) In high-density experiments, the decrease in the number is due to the suppression of the firing centers by the spirals. This is called entrainment of slow centers by the faster spirals.

An experiment to understand the evolution of the excitability of the cells was performed in [31]. cAMP was used to reset the waves by spraying a mist of it on the layer of cells. This extinguishes the spirals already present. If the resetting is done before 6h of starvation, spirals and targets re-emerge. (fig. 1.19) After 6 h, only targets are formed. It is interesting to note that the targets are re-formed in the same places that they had formed before spirals entrained

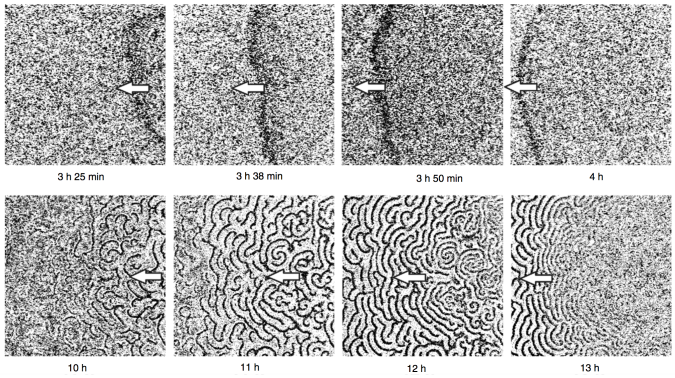

Figure 1.20: The top row shows the global wave propagating through the cell populations. The bottom row shows that the formation of patterns follows the global wave. Figure reprinted with permission from [48].

them [31]. Extracellular cAMP is regulated by secretion by cells, degradation by phosphodiesterase and inhibition of the phosphodiesterase by an inhibitor. This inhibitor is secreted only during the early hours of starvation. According to a model [41], local random pulses of the phosphodiesterase inhibitor cause wave initiation by locally increasing cAMP levels. Before 6 h of starvation, the cells can produce spirals because the inhibitor can still be secreted. But after 6 h, the inhibitor is no longer produced and so only targets are formed [31]. This shows that oscillations are a persistent feature of *D.d* signaling because they re-appear soon after the mist of cAMP has extinguished the spirals. These results suggest that spatial inhomogeneities may not be the cause for spiral formation.

Another experiment reveals the importance of cAMP on the pattern formation. cAMP was added to the agar substrate and the patterns were observed [48]. A large wave is seen to form spontaneously from random locations when cAMP is included in the substrate. This wave is the global wave and is accompanied by cell movement in the direction of propagation [48]. The time at which the global wave forms increases with increase in initial cAMP concentra-

tion linearly. The velocity of propagation, found using a kymograph, decreases non-linearly with increase in initial cAMP concentration. The speed of propagation is much faster, ranging from 0.1mm/min to 1.8mm/min. Above an initial concentration of 4.5mM and below an initial concentration of 6.25μM, no global wave was observed. Aggregation follows the global wave in the same direction. (Fig. 1.20) The time delay after which cAMP waves follow the global waves increases with increase in concentration of initial cAMP. These cAMP waves had similar velocities and periods as compared to the control experiments without cAMP in the substrate. The cAMP waves were only seen for agar concentrations lower than 1mM. The number of eventual aggregation territories is larger and increases with initial cAMP concentration. The streaming of cells showed a preferential direction opposite to the direction of the global wave. For initial cAMP concentrations larger than 1mM, aggregates were formed without streaming. It is proposed that the addition of cAMP desensitizes the cAMP receptors. A local cAMP gradient is set up due to heterogeneities. The global starts when the cAMP concentration drops to a low value that makes the cells move chemotactically into regions with higher cAMP concentrations. This hypothesis was tested by creating known cAMP gradients in the experiment. The global wave always propagated from region of lower cAMP concentration to regions of higher cAMP concentration [48].

Spiral waves in excitable media can be explained by using reaction-diffusion equations [26]. It is expected that systems obeying these equations should have a linear relation between normal velocity (N) of the wave and its curvature (K).

$$N = c - D.K \tag{1.44}$$

Here c is the velocity of plane wave and D is the diffusion coefficient. This is called the eikonal equation. In addition to relating the speed to curvature of the

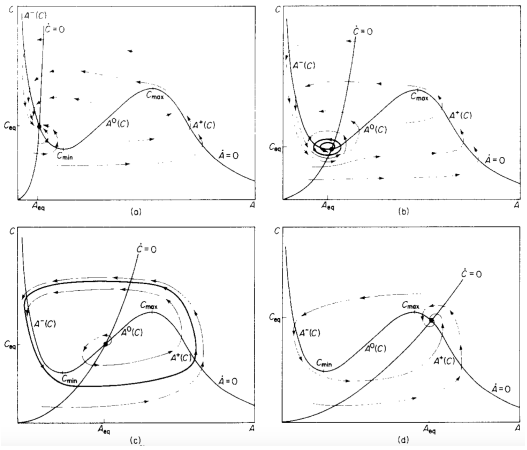

Figure 1.21: As the concentration of the stored reserves changes, different patterns are formed because the stability of the fixed point changes. Figure reprinted with permission from [24].

waves, this relation also sets the minimum radius of the core of the spiral which allows the speed of propagation to the be greater than zero. This is the critical radius. In [17], this relation was verified for the spiral waves of *D.d*. To measure negative curvature, isointensity points were taken along cusp like structures formed when waves collide. A hyperbola was fit to these points and curvature was measured. Velocity was calculated using a timer. To find positive curvatures, isointensity points along the edge of circular waves were used. A third order polynomial was fit to find the curvature. Fitting straight lines to the N vs. K data for negative curvatures gave diffusion coefficient to be 0.66 x 10^{-5} cm^2/s and a critical radius of 130μm. For positive curvature, the diffusion coefficient was 0.93 x $10^{-5} cm^2/s$. Extrapolation of the straight line yields a critical radius of 200μm. It was also seen that the pitch of the spirals was almost a constant. This suggests that the spirals are involutes of a circle rather then Archimedean [17].

1.3.2 Theoretical models

Early theoretical works make use of diffusion to characterize cAMP wave propagation [6]. Considering only diffusion of cAMP (in the absence of phosphodiesterase and phosphodiesterase inhibitors), they calculate the minimum density of cells required to cause the nearest neighbor to emit cAMP. Below this threshold density no aggregation is possible. They found that the time at which threshold cAMP concentration is reached decreased with increasing density of cells. This sets limits on the diffusion coefficient (which had not been measured at that time) and the refractory period of the cells. The observed delay time for the signal between two pulses of cAMP is about 0.25 min, which is 1000 times shorter than the upper limit for diffusion [6]. The authors therefore suggested that rather than diffusion, the refractory period sets the oscillation period. When diffusion was considered on a square lattice including contributions from all neighbors along the propagation axis, the results were similar to the previous case only for densities below a critical value. Above this density, several adjacent rows begin to signal spontaneously. Concentration of phosphodiesterase was assumed to be constant in time. Considering all neighbor interaction doubles the time needed to reach maximum concentration and the threshold concentration increases by a factor of four. The effect of this is to increase the critical density of cells required to aggregate [6].

An early model for the formation of spirals and targets was proposed by Hagan and Cohen [24]. They proposed a reaction-diffusion based on the assumption that the dynamics of the waves are governed by the extracellular cAMP, α, intracellular cAMP concentration $\tilde{A}$, inhibitor concentration C and stored reserves, S, which is related to the time after starvation. The authors explain the

formation of the wave patterns using nullclines of A and C for different values of S. (Fig. 1.21). When the C nullcline crosses the A nullcline before its minimum, the system is stable because the equilibrium is far away from the minimum. No pulses can propagate in this case. But as S decreases, the equilibrium moves towards the minimum value and pulses of cAMP propagate for strong perturbations. When S further decreases, the C nullcline crosses the A nullcline near the minimum and spiral waves can exist. As S decreases more, the C nullcline intersects the A nullcline between the minimum and the maximum value. Targets exist in this regime. With lower values of S, tip formation occurs [24].

One of the most widely used models for the formation of spiral waves in *D.d* is the one proposed by Martiel and Goldbeter [36]. Their model is based on the following reaction scheme. The receptor for cAMP has two conformational states, the active R state and the desensitized D state. The extracellular cAMP, P, binds to them with different affinities. When it binds to the active state R, the R-P complex activates the enzyme adenylate cyclase, C to form an active complex E. Both the active complex E and the inactive form C can catalyze the production of intracellular cAMP Pi, by combining with ATP, S. Part of this Pi is hydrolyzed inside the cell and the rest is transported out. Once outside, it can either diffuse away, be hydrolyzed by external phosphodiesterase or attach to the cAMP receptors of its own cell. The ATP, S, is also used for other processes. Considering all the binding steps to be faster than the transition between states, conservation equations for the receptor and the enzyme and that the level of ATP does not change much, the equations for a well-stirred system can be written as a set of three coupled differential equations.

$$\frac{d\rho}{dt} = -f_1(\gamma)\rho + f_2(\gamma)(1-\rho)$$

$$\frac{d\beta}{dt} = q\sigma\phi(\rho,\gamma) - (k_i + k_t)\beta$$

$$\frac{d\gamma}{dt} = (k_t\beta/h) - k_e\gamma$$

$$f_1(\gamma) = \frac{k_1 + k_2\gamma}{1+\gamma}$$

$$f_2(\gamma) = \frac{k_1L_1 + k_2L_2c\gamma}{1+c\gamma}$$

$$\phi(\rho,\gamma) = \frac{\alpha(\lambda\theta + \epsilon Y^2)}{1 + \alpha\theta + \epsilon Y^2(1+\alpha)}$$

$$Y = \frac{\rho\gamma}{1+\gamma}$$

The values of the constants can be found in [36]. Here, ρ_t is the fraction of active receptors, β denotes the concentration of intracellular cAMP and γ denotes the concentration of extracellular cAMP. Tyson et. al [54] extended this system of equations by adding a diffusive term to the extracellular cAMP equation, to account for the observation of traveling waves of cAMP seen in monolayers of cells. They also showed that for suitable values of parameters, the set of equations can be reduced to two. Numerical simulation showed that as period decreases, wave velocity decreases. (Fig. 20) Reasonable estimates for the period and the wave velocity are obtained for the parameter sets considered [54].

The set of equations have been modified in many ways to account for the formation of spirals and targets. The first one was by Pálsson and Cox [41]. They showed that regulating the concentration of phosphodiesterase inhibitor and by introducing stochastic variations in space and time, the formation of spirals could be explained. Their model is described by:

$$\frac{d\rho}{dt} = -f_1(\gamma)\rho + f_2(\gamma)(1-\rho)$$

$$\frac{d\beta}{dt} = s\phi(\rho,\gamma) - (k_i + k_t)\beta$$

$$\frac{d\gamma}{dt} = (k_t\beta/h) - k_e(t)\gamma + D\nabla^2\gamma$$

The activity of external phosphodiesterase (PDE), which is reflected in the value of k_e, was made to vary in space and time, inversely depending on the concentration of PDI. Since PDI secretion starts after starvation, there is a heterogeneity in the PDI, level because not all the cells are in the same stage of their life cycle at the onset of starvation. After the beginning of the propagation of cAMP waves, the production of PDI was stopped [41]. To simulate this, the initial PDI levels were set to random values around a mean, which caused random pulses of cAMP that initially gave rise to targets. Interaction with new pulses caused the targets to break. The broken wave segments evolved into spirals with one or more arms when new pulses were produced in regions where some cells were still refractory. In a second method, instead of having randomly distributed PDI levels, the authors increased PDI levels with time, because it is expected in early stages of aggregation. This also gave rise to spirals in a similar manner. But in this case, fewer spirals were formed, and the spirals tightened, decreasing their wavelength and increasing their rotational speeds with time. These changes were not observed in the spirals produced by the first method, but are in agreement with experimental results [23, 50]. The authors concluded that spatiotemporal heterogeneity can explain the formation of spirals.

To test this model, cells without the gene to form PDI were studied experimentally. These cells failed to form spirals and had much smaller aggregation territories [42]. Mostly targets and broken waves were seen. (Fig. 1.22) The oscillation frequency did not change, and the transition from excitable to oscillatory regimes occurred at the same times as the wild type cells. This proved that PDI is necessary for formation of spirals, which supported the model proposed earlier. The authors explained the experimental observations on the resetting of the cAMP by spraying cAMP over the cells [31], by assuming that the exter-

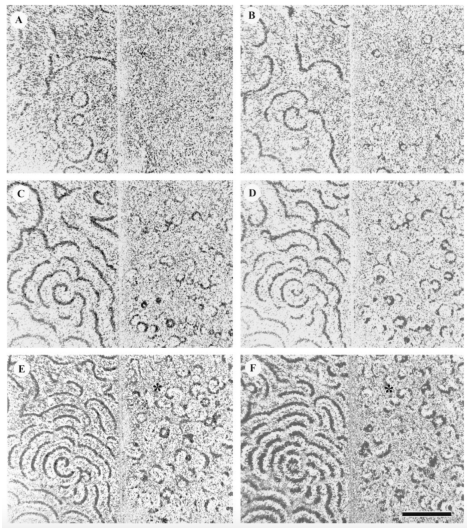

Figure 1.22: The patterns formed in wild type cells compared to the patterns formed by mutants with did not have the phosphodiesterase inhibitor. Figure reprinted from [42].

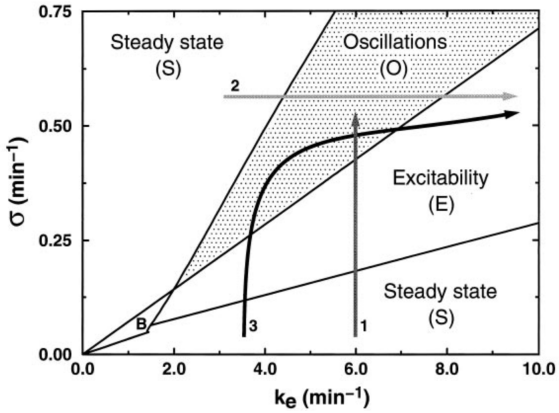

Figure 1.23: The phase-space of the model proposed by [36]. The three developmental paths considered in [29] are also shown here. Figure reprinted from [29].

nal cAMP halts the production PDI. The authors accounted for the observation that spirals fail to form at low cell densities [30] by saying that the frequency of the pulses in the low-density cells is insufficient to break the symmetry to form spirals.

Another method to extend the model [54] to account for formation of spirals was given in [29]. A stability analysis of the coupled partial differential equations of [54] shows the existence of steady state, oscillatory state, excitable state and bistable state. The phase diagram is as shown in fig. 1.23. σ is the rate of the enzyme adenylate cyclase, which is responsible for the production of intracellular cAMP and k_e is the rate of degradation by phosphodiesterase, which hydrolyzes cAMP. The cells are assumed to follow one of the three possible developmental paths shown in fig. 1.23. To start with, heterogeneity is introduced by randomly assigning cells different positions on the developmental path through en exponential probability distribution given by

$$P(t_s) = 1/e^{-t_s/\Delta} \tag{1.45}$$

This is equivalent to assigning different starting times for each cell. Δ in eq. 1.45 represents the extent of desynchronization. With time, the cells develop along one of the three developmental pathways. It was found that time taken to form spiral along path 1 does not match with experimental results. Path 2 fails to form spirals and only leads to bulk oscillations. Path 3 gives reasonable times for the formation of spirals with a desynchronization time of about 25 min [29].

A detailed analysis of this model was performed in [19]. They tracked the target waves and found that initially targets grow in time, but later the centers drift apart. The number of targets depended on the desynchronization parameter. A pulsing target wave fractured into several small centers that eventually formed spirals. The spirals either annihilated or formed a steady state. (Fig. 1.24) The times at which these transitions happened corresponded to the change in dynamical properties predicted by the model [29]. They also found that the location of spirals was not influenced by the cell properties. Instead, the authors

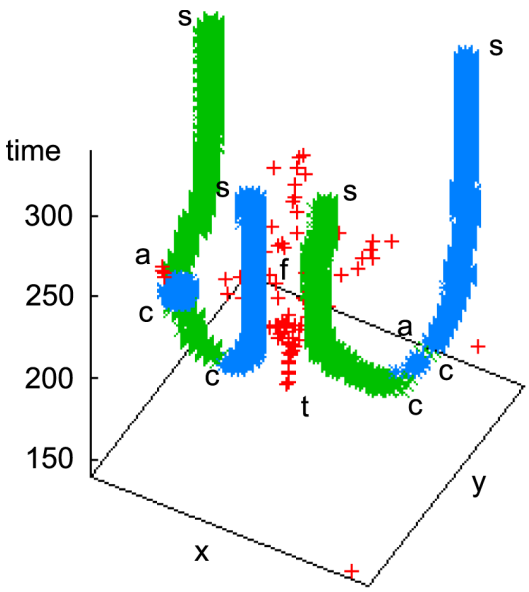

Figure 1.24: The formation of spirals and targets were tracked for the simulations of the model proposed in [29]. t - repeated targets, f - fractured targets, c - counter-rotating spirals, a - annihilated spirals, s - stable spirals. Figure reprinted from [19].

[19] reported that the spirals are formed parallel to and at a fixed distance from the Voronoi diagram of the pacemakers. The probability of spiral formation is higher near the vertices of the Voronoi diagram. [19]

Apart from inhomogeneities in the levels of PDI and developmental path, the other approach to obtain spirals from the modified Martiel- Goldbeter [36] model [54] was to include genetic feedback to account for changes in receptor and protein expression with time [16]. A new variable G – the ratio of the total amount of cAMP receptor to the initial amount – was introduced. The amount of ATP, α, was allowed to vary in time.

$$\frac{d\rho}{dt} = -f_1(\gamma)\rho + f_2(\gamma)(G-\rho)$$

$$\frac{d\beta}{dt} = q\Phi(G,\alpha,\rho,\gamma) - (k_I G^3 + k_t)\beta$$

$$\frac{d\gamma}{dt} = (k_t\beta/h) - k_E G^2\gamma + D\nabla^2\gamma$$

$$\frac{d\alpha}{dt} = \nu - k'\alpha - \Phi(G, \rho, \gamma, \alpha)$$
$$\frac{dG}{dt} = (1/80)\Big[\frac{Y^4}{0.25^4 + Y^4} - \frac{Y^4}{2^4 + Y^4}\Big]$$
$$\Phi(G, \rho, \gamma, \alpha) = \frac{\sigma\alpha G^2(\lambda\theta + \epsilon G^2 Y^2)}{1 + \alpha\theta + \epsilon G^2 Y^2(1 + \alpha)}$$

The forms of the dependences on G were inspired by experimental results. It is known that the concentration of adenyl cyclase increases with receptor density, which accounts for the form of Φ. To ensure that intracellular and extracellular cAMP does not exceed reasonable values, their degradation rates were scaled with G: $k_e = k_E G^2$ and $k_i = k_I G^3$. Pulsed cells show increased expression of genes, even without intracellular cAMP. This means extracellular cAMP plays an important role. So, the value of G does not depend on intracellular cAMP, but only on Y. The dynamics were fixed so that G was zero at high values and at basal values of Y, and was high around the concentration corresponding to the typical cAMP pulse peaks. Experimentally, an increase by a factor of 10-30 is observed in the cAMP receptors over the course of signaling. This set the scale for G. This model is excitable for $1.0 < G < 1.11$, oscillatory for $1.11 < G < 1.65$ and excitable for $1.65 < G < 2.24$. The initial condition for this simulation is a normal distribution of G. This inhomogeneity leads to formation of spirals through targets and broken wave segments [16]. Suppression of targets by spirals, increase in topological defects and G with time are observed. The results of [31], the waveform resetting by application of cAMP, are obtained in these simulations.

A different approach was adopted by Kessler and Levine [27]. Instead of dealing with the biochemical networks and signaling mechanisms as in the Martiel-Goldbeter model [36], they replaced each cell with a bion that can measure concentration and concentration gradients, change an internal state, sense

the presence of other nearby bions and move. These bions are on a 2D square lattice of size a, with a density ρ. The concentration of cAMP obeys the equation

$$\frac{\partial c}{\partial t} = a_2 \nabla^2 c - \gamma c + (sources)$$

where a^2 is the normalized diffusion constant and the degradation Γ is due to the action of the phosphodiesterase whose concentration is assumed to be uniform. The bion is in state 0 until it the concentration of cAMP exceeds a threshold concentration c_T. If $c > c_T$, the bion goes to state 1 and emits some amount of cAMP, δc over a time τ. After emission, the bion enters a quiescent state (state 2). In this is state the bion cannot respond to excitation. After a time t_R it goes back to state 0. Simulation of this model leads to the production of spiral waves. This model requires a minimum density ρ to sustain the waves [27]. This model belongs to a general class of models called cellular automata where rules are implemented for each point on the simulation grid. See Box 1.4 for more on cellular automata.

This model was further improved by Levine and co-workers [34]. The level of gene expression changes with starvation time. There is feedback loop that stimulates gene expression by detecting cAMP pulses. Also, the value of the threshold concentration of cAMP required to cause emission of cAMP is not constant. It changes from a maximum value C_{max} to a minimum value C_{min} depending on the time after the previous excitation. The threshold also depends on the how excitable the cells are. Including the excitability, the equation for c_T is

$$c_T = \frac{c_{max} - Ax}{(x + T_{ARP})} \times (1 - E) \tag{1.46}$$

Here, x is the time spent in the relative refractory period T_{RRP}, and T_{ARP} is the duration of the absolute refractory period where cells are incapable of emitting

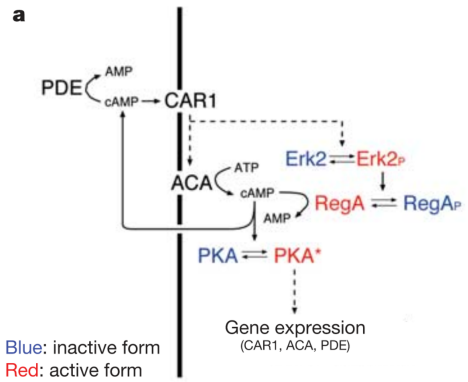

Figure 1.25: The auto-regulatory circuit proposed by Sawai et al [46], showing the PKA pathway. Figure reprinted with permission from [46].

cAMP. A is a constant chosen so that the threshold concentration is maximum at the beginning to the refractory period and minimum at the end of it. To incorporate the feedback for gene expression, the excitability varies with time.

$$\frac{dE}{dt} = -\eta E + \beta c \tag{1.47}$$

Here β controls the feedback. When this model was simulated, it produced spirals only when time dependent excitability was included. Though spirals are obtained even in the absence of feedback, they fail to form large coherent domains. The correlations are short ranged. But when genetic feedback was included, large spirals form which wind up with time as seen in experiments [34]. This is thought to be a symmetry breaking instability where one spiral center captures its neighbors territory. This model suggests that if genetic feedback is broken, spirals will not form. This can be verified using suitable mutants, where targets should be seen. The excitability, which is dependent on the genetic feedback is controlled by coupling between cAMP receptors and adenylate cyclase (ACA). External pulses of cAMP and protein Kinase A (PKA) control this coupling [46] (Fig. 1.25). Cells mutated in erkB, PKA (pkaR) and regA were used

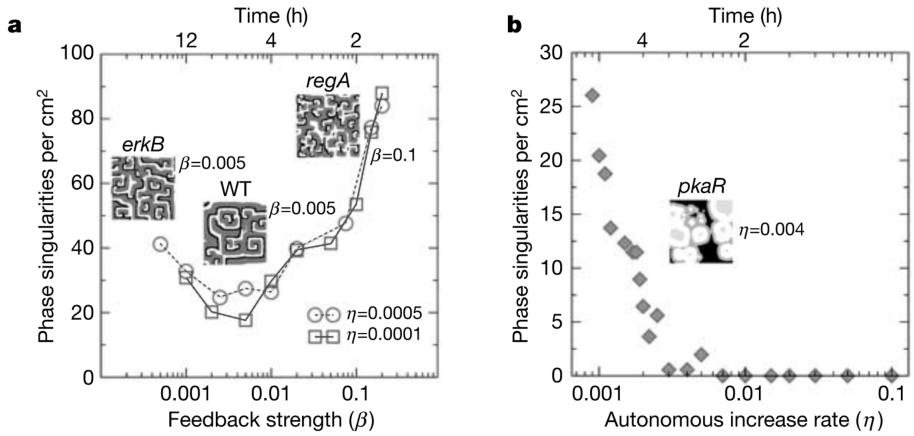

Figure 1.26: The effect of varying feedback strength and autonomous increase in excitability on number of spirals formed by the model proposed by Sawai et al [46]. Figure reprinted with permission from [46].

by Sawai et al. [46]. These mutant strains showed a twofold and fourfold increase in the number of spiral centers. The signals could not propagate over large distance because the waves from the many cores collided and annihilated frequently. However, they did show oscillations in the optical density. Thus, PKA was not necessary for oscillations, but was necessary for establishing wave territories. These mutants were used to verify the model proposed in [34]. If η was close to zero (i.e. autonomous increase in excitability is suppressed), β controlled the phase singularities non-monotonically. If β was either too high or too low, the number of phase singularities increased. If β was close to zero, as in the pkaR mutant, number of phase singularities decreased with increasing η. (Fig. 1.26) Experiments also showed that cells starved between 4 - 8h formed spirals whereas cells starved for 8 h failed because the excitability is too high after 8h. These results were verified by simulating the model using appropriate values for η and β. It has been found that for this model [34, 46], there is a strong anti-correlation in the position of the pacemaker cells and the position of the

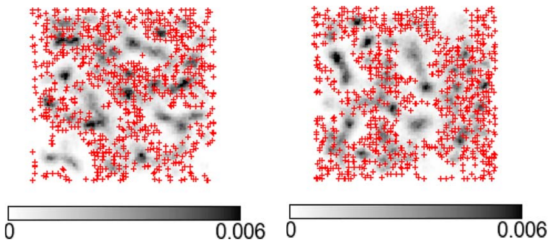

Figure 1.27: The red spots show the positions of the pacemakers. Dark value denotes high average tip occupancy. The two panels correspond to runs of the same simulations. The anti-correlation is apparent. Figure reprinted with permission from [18].

spiral tips [18] (Fig. 1.27). There is also no connection between cAMP patterns and pacemaker region. The authors of [18] suggest a different mechanism for the formation of spirals from pacemakers. If the pacemakers are aligned so as to have a region of no excitability in between, then the spirals form around this region. Depending on which pacemaker entrains the other, and the geometrical position of the centers, there can be for possible types of forming spirals for a simple three-pacemaker system. This also causes a chiral asymmetry as is seen in fig 1.28. The probability of entrainment depends on how the pacemakers are arranged geometrically [18]. In a novel approach, Gregor and co-workers performed a series of experiments on single cell level and population level in *D.d.* to create a model for pattern formation that explains the behavior at both these scales [22, 49, 40]. Using a model based on the Fitz-Hugh Nagumo model, the Gergor lab can explain the response of single cells to differing amounts of external cAMP stimulus, as well as pattern formation in systems with a constant flow. The model equations are given by

$$\frac{dA_i}{dt} = f(A_i) - R_i + I([cAMP]_{ext}) + \eta_i(t)$$

$$\frac{dR_i}{dt} = \epsilon(A_i - \gamma R_i) + \epsilon c_0$$

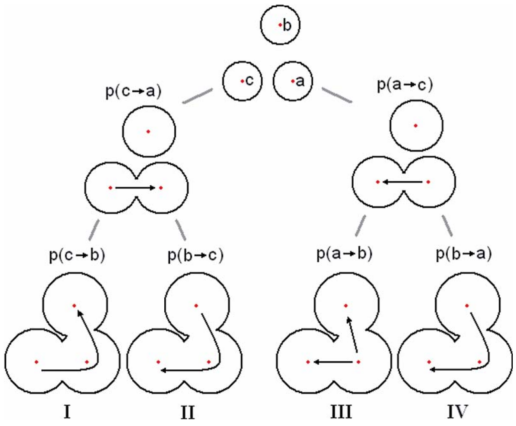

Figure 1.28: First a and c connect and then a and b connect. Case I is the probability of getting a right handed spiral. This is given by the product of the probability of c entraining a and then entraining b. Cases II and IV give left handed spirals. Case II is when c entrains a, and is in turn entrained by b. Case IV is when a entrains c, and is then entrained by b. Figure reprinted with permission from [18].

$$\frac{d[cAMP]_{ex}}{dt} = \alpha_f + \rho\alpha_0 + \rho S \frac{1}{N}\sum_{i=1}^{N} \Theta(A_i) - D[cAMP]_{ext}$$

The function f has the form $f(A) = A - (1/3)A^3$. A is an activator, R is a repressor, I is a function of the extra-cellular cAMP, $[\text{cAMP}]_{\text{ex}}$, η describes white noise, α_f is the amount of cAMP flown into the system, ρ is the cell density, Θ is a step function that is one if $A_i > 0$ and zero otherwise, D is the degradation rate, which combines the degradation due to the flow, and the phosphodiesterase, S is the rate at which each cell releases cAMP, and α_0 is the baseline rate of external cAMP.

This model was first successfully compared to response of single cells to stimuli of different strengths and shapes. Then, it was compared to experiments where a population of *D.d* were under a constant flow of cAMP. The model produced quantitatively similar results for different flow rates and time period of the response oscillations [22, 49]. By adding a diffusion term to the

equation for extracellular cAMP, the model reproduced spirals [40]. Further, the authors were able to provide insights into the function I, which represents a pre-processing module for signal processing. They found that this function is logarithmic.

Therefore, as detailed here, many models have been proposed to explain the behavior of starving populations of *D.d*.

Box 1.4: Cellular automata

The history of cellular automata is fascinating. Their origin dates back to 1940s, when von Neumann was interested in them, trying to answer the question if a machine or an "automaton" could reproduce itself. His idea was to create an automaton built of numerous small units and to think of a way in which this automaton could make copies of itself, if sufficient numbers of the small units were available. He deduced that such a replication should be possible, given that an automaton has a blueprint of itself. In such a a case, the automaton can make an exact copy of the blueprint and use it as an instruction to make a copy. Stanislaw Ulam reformulated the problem in terms of an abstract space of cells, with integers representing their state. By early 1950s, von Neumann was able to create systems capable of reproducing in a cellular automaton with 29 states.[45]

The next major event in the history of cellular automata was the publication of an article in *Scientific American* about John Conway's "Game of Life". In this article, Martin Gardner described Conway's game whose original objective was to find rules by which simple patterns could grow for ever. The publication of this article inspired scientists at MIT to come up with the configurations of a "glider gun", which enabled patterns to persist forever.

With the advent of computing powers, more self-sustaining patterns were discovered.

The idea of creating "artificial life" through cellular automata persisted. In 1980s, Langton proposed to use automata to study how bio-molecules behave [28]. His rules led to a plethora of dynamical behavior in cellular automata – from steady states to strange attractors. Further, Langton showed how these behaviors could model the various functions of biological molecules. Perhaps the most spectacular of all, he modeled an insect colony for "vants" – virtual ants! Depending on the rules, the vants displayed emergent behavior, including the construction of a highway [28]!

By the 1990s cellular automata were being used to model various biological systems, like excitable media, coat patterns, population dynamics, immunology, reaction diffusion systems, fibroblast aggregation, growth of microbes, and various other aspects [15].

BIBLIOGRAPHY

[1] FERNANDA ALCANTARA and MARILYN MONK. "Signal Propagation during Aggregation in the Slime Mould Dictyostelium discoideum". In: *Microbiology* 85.2 (1974), pp. 321–334.

[2] Eberhard Bodenschatz, Werner Pesch, and Guenter Ahlers. "Recent Developments in Rayleigh-Bénard Convection". In: *Annual Review of Fluid Mechanics* 32.1 (2000), pp. 709–778. DOI: 10.1146/annurev.fluid.32.1.709. eprint: http://dx.doi.org/10.1146/annurev.fluid.32.1.709. URL: http://dx.doi.org/10.1146/annurev.fluid.32.1.709.

[3] Michael Brenner and Stephen D. Thoms. "Caffeine blocks activation of cyclic AMP synthesis in Dictyostelium discoideum". In: *Developmental Biology* 101.1 (1984), pp. 136–146. ISSN: 0012-1606. DOI: https://doi.org/10.1016/0012-1606(84)90124-6. URL: http://www.sciencedirect.com/science/article/pii/0012160684901246.

[4] Gil Bub, Alvin Shrier, and Leon Glass. "Spiral Wave Generation in Heterogeneous Excitable Media". In: *Phys. Rev. Lett.* 88 (5 2002), p. 058101. DOI: 10.1103/PhysRevLett.88.058101. URL: http://link.aps.org/doi/10.1103/PhysRevLett.88.058101.

[5] Elena O. Budrene and Howard C. Berg. "Complex patterns formed by motile cells of Escherichia coli". In: *Nature* 349.6310 (Feb. 1991), pp. 630–633. URL: http://dx.doi.org/10.1038/349630a0.

[6] Morrel H. Cohen and Anthony Robertson. “Wave propagation in the early stages of aggregation of cellular slime molds”. In: *Journal of Theoretical Biology* 31.1 (1971), pp. 101–118. ISSN: 0022-5193. DOI: https://doi.org/10.1016/0022-5193(71)90124-X. URL: http://www.sciencedirect.com/science/article/pii/002251937190124X.

[7] M. C. Cross and P. C. Hohenberg. “Pattern formation outside of equilibrium”. In: *Rev. Mod. Phys.* 65 (3 1993), pp. 851–1112. DOI: 10.1103/RevModPhys.65.851. URL: http://link.aps.org/doi/10.1103/RevModPhys.65.851.

[8] Michael Cross and Henry Greenside. *Pattern Formation and Dynamics in Nonequilibrium Systems:* Cambridge University Press, 2009. ISBN: 9780511627200. DOI: 10.1017/CBO9780511627200.

[9] M Dinauer, TL Steck, and P Devreotes. “Cyclic 3′, 5′-AMP relay dictyostelium discoideum. V. Adaptation of the cAMP signaling response during cAMP stimulation”. In: *The Journal of Cell Biology* 86.2 (1980), pp. 554–561. ISSN: 0021-9525. DOI: 10.1083/jcb.86.2.554. eprint: http://jcb.rupress.org/content/86/2/554.full.pdf. URL: http://jcb.rupress.org/content/86/2/554.

[10] J.D. Dockery, J.P. Keener, and J.J. Tyson. “Dispersion of traveling waves in the belousov-zhabotinskii reaction”. In: *Physica D: Nonlinear Phenomena* 30.1 (1988), pp. 177–191. ISSN: 0167-2789. DOI: https://doi.org/10.1016/0167-2789(88)90105-4. URL: http://www.sciencedirect.com/science/article/pii/0167278988901054.

[11] Dirk Dormann et al. “cAMP receptor affinity controls wave dynamics, geometry and morphogenesis in Dictyostelium”. In: *Journal of Cell Science* 114.13 (2001), pp. 2513–2523. ISSN: 0021-9533. eprint: http://jcs.biologists.org/content/114/13/2513.full.pdf. URL: http://jcs.biologists.org/content/114/13/2513.

[12] A.J. Durston. “Dictyostelium discoideum aggregation fields as excitable media”. In: *Journal of Theoretical Biology* 42.3 (1973), pp. 483–504. ISSN: 0022-5193. DOI: http://dx.doi.org/10.1016/0022-5193(73)90242-7. URL: http://www.sciencedirect.com/science/article/pii/0022519373902427.

[13] A.J. Durston. “Pacemaker activity during aggregation in Dictyostelium discoideum”. In: *Developmental Biology* 37.2 (1974), pp. 225–235. ISSN: 0012-1606. DOI: http://dx.doi.org/10.1016/0012-1606(74)90144-4. URL: http://www.sciencedirect.com/science/article/pii/0012160674901444.

[14] L. Eichinger et al. “The genome of the social amoeba Dictyostelium discoideum”. In: *Nature* 435.7038 (May 2005), pp. 43–57. URL: http://dx.doi.org/10.1038/nature03481.

[15] G. B. Ermentrout and L. Edelstein-Keshet. “Cellular automata approaches to biological modeling”. In: *Journal of Theoretical Biology* 160 (1993), pp. 97–133.

[16] Martin Falcke and Herbert Levine. “Pattern Selection by Gene Expression in Dictyostelium Discoideum”. In: *Phys. Rev. Lett.* 80 (17 Apr. 1998), pp. 3875–3878. DOI: 10.1103/PhysRevLett.80.3875. URL: https://link.aps.org/doi/10.1103/PhysRevLett.80.3875.

[17] P. Foerster, S.C. Muller, and B. Hess. “Curvature and spiral geometry in aggregation patterns of Dictyostelium discoideum”. In: *Development* 109.1 (1990), pp. 11–16. ISSN: 0950-1991. eprint: http://dev.biologists.org/content/109/1/11.full.pdf. URL: http://dev.biologists.org/content/109/1/11.

[18] Daniel Geberth and Marc-Thorsten Hütt. “Predicting spiral wave patterns from cell properties in a model of biological self-organization”. In: *Phys. Rev. E* 78 (3 Sept. 2008), p. 031917. DOI: 10.1103/PhysRevE.78.031917. URL: https://link.aps.org/doi/10.1103/PhysRevE.78.031917.

[19] Daniel Geberth and Marc-Thorsten Hütt. “Predicting the Distribution of Spiral Waves from Cell Properties in a Developmental-Path Model of Dictyostelium Pattern Formation”. In: *PLOS Computational Biology* 5.7 (July 2009), pp. 1–10. DOI: 10.1371/journal.pcbi.1000422. URL: https://doi.org/10.1371/journal.pcbi.1000422.

[20] Irati Golvano-Escobal et al. “Spontaneous formation of spiral-like patterns with distinct periodic physical properties by confined electrodeposition of Co-In disks”. In: *Scientific Reports* 6 (July 2016), 30398 EP. URL: http://dx.doi.org/10.1038/srep30398.

[21] N. A. Gorelova and J. Bureš. “Spiral waves of spreading depression in the isolated chicken retina”. In: *Journal of Neurobiology* 14.5 (1983), pp. 353–363. ISSN: 1097-4695. DOI: 10.1002/neu.480140503. URL: http://dx.doi.org/10.1002/neu.480140503.

[22] Thomas Gregor et al. “The Onset of Collective Behavior in Social Amoebae”. In: *Science* 328.5981 (2010), pp. 1021–1025. ISSN: 0036-8075. DOI: 10.1126/science.1183415. eprint: http://science.sciencemag.

org/content/328/5981/1021.full.pdf. URL: http://science.sciencemag.org/content/328/5981/1021.

[23] J.D. Gross, M.J. Peacey, and D.J. Trevan. "Signal emission and signal propagation during early aggregation in Dictyostelium discoideum". In: *Journal of Cell Science* 22.3 (1976), pp. 645–656. ISSN: 0021-9533. eprint: http://jcs.biologists.org/content/22/3/645.full.pdf. URL: http://jcs.biologists.org/content/22/3/645.

[24] P.S. Hagan and M.S. Cohen. "Diffusion-induced morphogenesis in the development of Dictyostelium". In: *Journal of Theoretical Biology* 93.4 (1981), pp. 881–908. ISSN: 0022-5193. DOI: https://doi.org/10.1016/0022-5193(81)90346-5. URL: http://www.sciencedirect.com/science/article/pii/0022519381903465.

[25] S. Jakubith et al. "Spatiotemporal concentration patterns in a surface reaction: Propagating and standing waves, rotating spirals, and turbulence". In: *Phys. Rev. Lett.* 65 (24 1990), pp. 3013–3016. DOI: 10.1103/PhysRevLett.65.3013. URL: http://link.aps.org/doi/10.1103/PhysRevLett.65.3013.

[26] James P. Keener. "A Geometrical Theory for Spiral Waves in Excitable Media". In: *SIAM Journal on Applied Mathematics* 46.6 (1986), pp. 1039–1056. DOI: 10.1137/0146062. eprint: https://doi.org/10.1137/0146062. URL: https://doi.org/10.1137/0146062.

[27] David A. Kessler and Herbert Levine. "Pattern formation in Dictyostelium via the dynamics of cooperative biological entities". In: *Phys. Rev. E* 48 (6 Dec. 1993), pp. 4801–4804. DOI: 10.1103/PhysRevE.48.4801. URL: https://link.aps.org/doi/10.1103/PhysRevE.48.4801.

[28] Christopher G Langton. “Studying artificial life with cellular automata”. In: *Physica D* 22 (1986), pp. 120–149.

[29] Jacques Lauzeral, José Halloy, and Albert Goldbeter. “Desynchronization of cells on the developmental path triggers the formation of spiral waves of cAMP during Dictyostelium aggregation”. In: *Proceedings of the National Academy of Sciences of the United States of America* 94.17 (Aug. 1997), pp. 9153–9158. URL: http://www.ncbi.nlm.nih.gov/pmc/articles/PMC23083/.

[30] Kyoung J. Lee, Edward C. Cox, and Raymond E. Goldstein. “Competing Patterns of Signaling Activity in Dictyostelium Discoideum”. In: *Phys. Rev. Lett.* 76 (7 Feb. 1996), pp. 1174–1177. DOI: 10.1103/PhysRevLett.76.1174. URL: https://link.aps.org/doi/10.1103/PhysRevLett.76.1174.

[31] Kyoung J. Lee, Raymond E. Goldstein, and Edward C. Cox. “Resetting Wave Forms in Dictyostelium Territories”. In: *Phys. Rev. Lett.* 87 (6 July 2001), p. 068101. DOI: 10.1103/PhysRevLett.87.068101. URL: https://link.aps.org/doi/10.1103/PhysRevLett.87.068101.

[32] Herbert Levine and Wouter-Jan Rappel. “Directed Motility and Dictyostelium Aggregation”. In: *Cell Motility*. New York, NY: Springer New York, 2008, pp. 59–92. ISBN: 978-0-387-73050-9. DOI: 10.1007/978-0-387-73050-9_3. URL: http://dx.doi.org/10.1007/978-0-387-73050-9_3.

[33] Herbert Levine and Wouter-Jan Rappel. “Directed Motility and Dictyostelium Aggregation”. In: *Cell Motility*. New York, NY: Springer New York, 2008, pp. 59–92. ISBN: 978-0-387-73050-9. DOI: 10.1007/978-0-

387-73050-9_3. URL: https://doi.org/10.1007/978-0-387-73050-9_3.

[34] H Levine et al. "Positive genetic feedback governs cAMP spiral wave formation in Dictyostelium". In: *Proceedings of the National Academy of Sciences* 93.13 (1996), pp. 6382–6386. eprint: http://www.pnas.org/content/93/13/6382.full.pdf. URL: http://www.pnas.org/content/93/13/6382.abstract.

[35] Alfred J. Lotka. "Analytical Note on Certain Rhythmic Relations in Organic Systems". In: *Proceedings of the National Academy of Sciences* 6.7 (1920), pp. 410–415. DOI: 10.1073/pnas.6.7.410. eprint: http://www.pnas.org/content/6/7/410.full.pdf. URL: http://www.pnas.org/content/6/7/410.short.

[36] Jean-Louis Martiel and Albert Goldbeter. "A Model Based on Receptor Desensitization for Cyclic AMP Signaling in Dictyostelium Cells". In: *Biophysical Journal* 52.5 (1987), pp. 807–828. ISSN: 0006-3495. DOI: http://dx.doi.org/10.1016/S0006-3495(87)83275-7. URL: http://www.sciencedirect.com/science/article/pii/S0006349587832757.

[37] Stephen W. Morris et al. "Spiral defect chaos in large aspect ratio Rayleigh-Bénard convection". In: *Phys. Rev. Lett.* 71 (13 1993), pp. 2026–2029. DOI: 10.1103/PhysRevLett.71.2026. URL: http://link.aps.org/doi/10.1103/PhysRevLett.71.2026.

[38] James D. Murray. *Mathematical Biology*. Berlin, Heidelberg: Springer Berlin Heidelberg, 1993, pp. 232–253. ISBN: 978-3-662-08542-4. DOI: 10.1007/978-3-662-08542-4_9. URL: http://dx.doi.org/10.1007/978-3-662-08542-4_9.

[39] Peter C. Newell and Fiona M. Ross. “Inhibition by Adenosine of Aggregation Centre Initiation and Cyclic AMP Binding in Dictyostelium”. In: *Microbiology* 128.11 (1982), pp. 2715–2724. URL: http://mic.microbiologyresearch.org/content/journal/micro/10.1099/00221287-128-11-2715.

[40] Javad Noorbakhsh et al. “Modeling oscillations and spiral waves in Dictyostelium populations”. In: *Phys. Rev. E* 91 (6 June 2015), p. 062711. DOI: 10.1103/PhysRevE.91.062711. URL: https://link.aps.org/doi/10.1103/PhysRevE.91.062711.

[41] E Pálsson and E C Cox. “Origin and evolution of circular waves and spirals in Dictyostelium discoideum territories”. In: *Proceedings of the National Academy of Sciences* 93.3 (1996), pp. 1151–1155. eprint: http://www.pnas.org/content/93/3/1151.full.pdf.

[42] E Pálsson et al. “Selection for spiral waves in the social amoebae Dictyostelium”. In: *Proceedings of the National Academy of Sciences* 94.25 (1997), pp. 13719–13723. eprint: http://www.pnas.org/content/94/25/13719.full.pdf. URL: http://www.pnas.org/content/94/25/13719.abstract.

[43] Andrew M. Reynolds and Nicholas T. Ouellette. “Swarm dynamics may give rise to Lévy flights”. In: *Scientific Reports* 6 (July 2016), 30515 EP. URL: http://dx.doi.org/10.1038/srep30515.

[44] A. Robertson and D. J. Drage. “Stimulation of late interphase Dictyostelium discoideum amoebae with an external cyclic AMP signal”. In: *Biophysical Journal* 15.8 (), pp. 765–775. DOI: 10.1016/S0006-3495(75)85853-X. URL: http://dx.doi.org/10.1016/S0006-3495(75)85853-X.

[45] Rudy Rucker. *The Origins of Cellular Automata*. URL: http://psoup.math.wisc.edu/491/CAorigins.htm.

[46] Satoshi Sawai, Peter A. Thomason, and Edward C. Cox. "An autoregulatory circuit for long-range self-organization in Dictyostelium cell populations". In: *Nature* 433.7023 (Jan. 2005), pp. 323–326. URL: http://dx.doi.org/10.1038/nature03228.

[47] Jakob Schweizer et al. "Geometry sensing by self-organized protein patterns". In: *Proceedings of the National Academy of Sciences* 109.38 (2012), pp. 15283–15288. DOI: 10.1073/pnas.1206953109. eprint: http://www.pnas.org/content/109/38/15283.full.pdf. URL: http://www.pnas.org/content/109/38/15283.abstract.

[48] Hana Ševčíková et al. "A new traveling wave phenomenon of Dictyostelium in the presence of cAMP". In: *Physica D: Nonlinear Phenomena* 239.11 (2010). Emergent Phenomena in Spatially Distributed Systems, pp. 879–888. ISSN: 0167-2789. DOI: http://dx.doi.org/10.1016/j.physd.2009.06.019. URL: http://www.sciencedirect.com/science/article/pii/S0167278909001869.

[49] Allyson E Sgro et al. "From intracellular signaling to population oscillations: bridging size- and time-scales in collective behavior". In: *Molecular Systems Biology* 11.1 (2015). ISSN: 1744-4292. DOI: 10.15252/msb.20145352. eprint: http://msb.embopress.org/content/11/1/779.full.pdf. URL: http://msb.embopress.org/content/11/1/779.

[50] FLORIAN SIEGERT and CORNELIS WEIJER. "Digital image processing of optical density wave propagation in Dictyostelium discoideum and analysis of the effects of caffeine and ammonia". In: *Journal of Cell*

Science 93.2 (1989), pp. 325–335. ISSN: 0021-9533. URL: http://jcs.biologists.org/content/93/2/325.

[51] Steven H. Strogatz. *Nonlinear dynamics and chaos : with applications to physics, biology, chemistry, and engineering*. Second edition. Boulder, CO : Westview Press, a member of the Perseus Books Group, [2015]. URL: https://search.library.wisc.edu/catalog/9910223127702121.

[52] A Theibert and P N Devreotes. "Cyclic 3′, 5′-AMP relay in Dictyostelium discoideum: adaptation is independent of activation of adenylate cyclase." In: *The Journal of Cell Biology* 97.1 (1983), pp. 173–177. ISSN: 0021-9525. DOI: 10.1083/jcb.97.1.173. eprint: http://jcb.rupress.org/content/97/1/173.full.pdf. URL: http://jcb.rupress.org/content/97/1/173.

[53] A. M. Turing. "The Chemical Basis of Morphogenesis". In: *Philosophical Transactions of the Royal Society of London B: Biological Sciences* 237.641 (1952), pp. 37–72. ISSN: 0080-4622. DOI: 10.1098/rstb.1952.0012. eprint: http://rstb.royalsocietypublishing.org/content/237/641/37.full.pdf. URL: http://rstb.royalsocietypublishing.org/content/237/641/37.

[54] John J. Tyson et al. "Spiral waves of cyclic amp in a model of slime mold aggregation". In: *Physica D: Nonlinear Phenomena* 34.1 (1989), pp. 193–207. ISSN: 0167-2789. DOI: http://dx.doi.org/10.1016/0167-2789(89)90234-0. URL: http://www.sciencedirect.com/science/article/pii/0167278989902340.

[55] P J Van Haastert et al. "Competitive cAMP antagonists for cAMP-receptor proteins." In: *Journal of Biological Chemistry* 259.16 (1984), pp. 10020–10024.

eprint: http://www.jbc.org/content/259/16/10020.full.pdf+html. URL: http://www.jbc.org/content/259/16/10020.abstract.

[56] Tamás Vicsek et al. "Novel Type of Phase Transition in a System of Self-Driven Particles". In: *Phys. Rev. Lett.* 75 (6 1995), pp. 1226–1229. DOI: 10.1103/PhysRevLett.75.1226. URL: http://link.aps.org/doi/10.1103/PhysRevLett.75.1226.

[57] Vito Volterra. "Fluctuations in the abundance of a species considered mathematically". In: *Nature* 118 (1926), pp. 558–560. DOI: 10.1038/118558a0.

[58] Jeffrey G. Williams. "Dictyostelium Finds New Roles to Model". In: *Genetics* 185.3 (2010), pp. 717–726. ISSN: 0016-6731. DOI: 10.1534/genetics.110.119297. eprint: http://www.genetics.org/content/185/3/717.full.pdf. URL: http://www.genetics.org/content/185/3/717.

[59] Robin S.B. Williams et al. "Towards a molecular understanding of human diseases using Dictyostelium discoideum". In: *Trends in Molecular Medicine* 12.9 (2006), pp. 415–424. ISSN: 1471-4914. DOI: http://dx.doi.org/10.1016/j.molmed.2006.07.003. URL: http://www.sciencedirect.com/science/article/pii/S1471491406001444.

[60] A. T. Winfree. *The geometry of biological time*. Springer-Verlag, 1980. ISBN: 978-3-540-52528-8.

[61] Arthur T. Winfree. "Spiral Waves of Chemical Activity". In: *Science* 175.4022 (1972), pp. 634–636. ISSN: 0036-8075. DOI: 10.1126/science.

175 . 4022 . 634. eprint: http : / / science . sciencemag . org / content / 175 / 4022 / 634 . full . pdf. URL: http : / / science . sciencemag.org/content/175/4022/634.

[62] BERND WURSTER. "Temperature dependence of biochemical oscillations in cell suspensions of Dictyostelium discoideum". In: *Nature* 260.5553 (Apr. 1976), pp. 703–704. URL: http : / / dx . doi . org / 10 . 1038/260703a0.

CHAPTER 2

METHODS

2.1 Experiments

2.1.1 Strains

The wild type strain used in the experiments are AX2. They are grown axenically, i.e. without bacteria, in a growth medium. They are cryogenically stored as spores in liquid nitrogen.

For fluorescent measurements, HG1694 cells are used. These are AX2 cells with whose cytoplasm is tagged with Green Fluorescent Protein. These are also cryogenically stored as spores in liquid nitrogen.

acaA$^-$ cells are mutants cells in which the gene responsible for the production of the enzyme acaA has been knocked out. Because this enzyme is responsible for cAMP production, these mutants cannot produce cAMP. These cells are derived from AX3. We obtained them from the Kortholt group in the Netherlands.

2.1.2 Setup

The bulk of the data in this work was collected on a dark field set-up. Our dark field consists of a LED ring lamp that shines light onto the Petri-dish placed below. A CCD camera from QImaging is placed below the Petri-dish. For the later experiments, to obtain uniform illumination, a flat Fresnel lens was placed

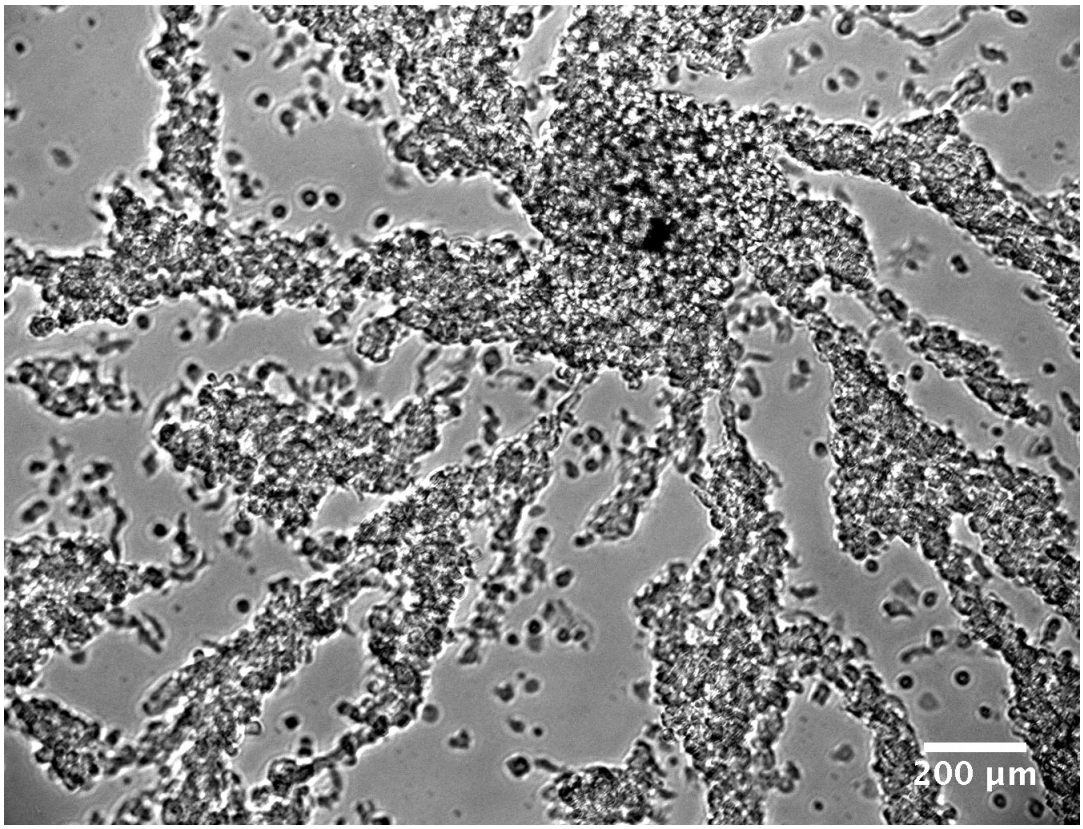

Figure 2.1: The bright-field image of a population of *D.d.* cells streaming.

between the LED ring lamp and the Petri-dish. The entire set up is placed in a room that is dark, and maintained at 22C. I take about a 1500 images separated by 20s each. Since the oscillation period is about 6 min, this sampling rate is higher than the minimum rate required by Nyquist-Shannon theorem.

For measurements needing higher magnification, a bright field microscope was used. An example image is shown in fig. 2.1. For fluorescent measurements, a confocal microscope was used.

2.1.3 Growth and harvesting

The AX2 spores are taken out from the liquid nitrogen and thawed to room temperature. Then, they are inoculated in a growth medium - the HL5 medium (35.5g of Formedium powder from Formedium Ltd., England, per liter of double distilled water, autoclaved and filtered) at 22^0C in a 8 cm diameter plastic Petri-dish. The spores regenerate in this favorable environment and begin to divide. After about 3 days, enough cells have divided to form a confluent layer in the Petri dish. The cells are harvested when confluent. First, the medium is removed using a pipette. The cells are left behind in the dish because they adhere to the bottom. These cells are then dislodged by vigorously washing the bottom of the plate with 10 ml phosphate buffer ($2g$ of KH_2PO_4, $0.36g$ of $Na_2HPO_4.2H_2O$) (This buffer is also called Sorenson's buffer). Thus, the cells are suspended in buffer. This cell solution is centrifuged three times to wash away traces of medium. Each Centrifugation runs at 1000rpm and lasts for 3min.

To get the desired density, the cells have to be counted. This is achieved by diluting a small amount of the cell solution (typically $10\mu l$) to a lower concentration. I used Trypan blue as the diluting agent and a dye. This dye stains everything that is dead blue, whereas the cells which are alive remain white. So only the cells that are alive appear white on a blue background. However, Trypan blue is toxic (to humans too), so the cell counting has to be performed within 10- 15 min, before the cells die. The cell solution can also be diluted by using phosphate buffer. The dilution factor depends on the number of expected cells - typically it is about 1:5. To count the cells, a hemocytometer is used. This a glass slide on which wells are etched. The depth of the wells are precisely known. We place a coverslip over the wells and add about $10\mu l$ of the diluted

cell solution in between the coverslip and the slide. The solution spread over the wells. Then, the number of cells in each well is counted and averaged. Since the depth of the well and the dilution factor is known, this average gives the average cell density of the cell solution. Depending on the cell density, appropriate dilutions of the cell solution is made using phosphate buffer.

The same procedure is used for other strains of cells.

2.2 Data Analysis

2.2.1 Image processing

The raw data obtained from the dark field set up are images of size 1392 x 1040 in either 8 bit or 16 bit format. To improve the signal to noise ratio, I first convert all the images to 32 bits, create an image that is the average of the first few slices. I divide all the images in the stack with this averaged image. This removes artifacts like marks on the dish, condensation, non-uniform illumination, etc. It is necessary to first convert the images to 32 bits because it provides a finer tuning capacity. To use the images for further analysis, I band-pass filter the images allowing only spatial structures larger than 0.3 mm and smaller than 3 mm to pass through. These numbers correspond to the smallest and the largest spatial structures seen during pattern formation. This process smoothes the images and increases the contrast.

If the images are just for visualization, before performing the bandpass filter, I subtract every image from the image taken a minute prior to it. Subtraction

highlights the changes between the frames. After band-pass filtering the waves can be easily seen - even for the noisy experiments. However, subtracted images must not be used for further analysis because subtraction affects the frequencies. This is because, subtraction is similar to taking a time derivative. In the subtracted signal, low amplitude oscillations of high frequency will get amplified, resulting in incorrect power spectra. Therefore, this procedure must only be used for visualization of the waves.

I performed these procedures using the software ImageJ.

2.2.2 Fourier analysis

For performing a Fourier analysis, the un-subtracted, band-pass filtered images were used. From the image stack, I can obtain the time series of the intensity of each pixel. With this, I find the Fourier Transform of the time series at each time point with a window of about 120 frames or 40 min, which corresponds to about 6-7 oscillations. With the Fourier transform of each pixel in an image, I find the power spectrum at each pixel. Then, I spatially average these power spectra, giving one power spectrum for all the pixels on the image. Repeating the process for the images at all time points, I get an averaged power spectrum for each time point. For example, we started with the first image of the image stack and found the time series of the intensity for all the pixels by collecting their intensity values from images corresponding to the next 40 *min*. Then, we took the Fourier transform of each of these time series and found their power spectra. These power spectra were then averaged to get one average power spectrum corresponding to the first image. Then we moved to the sec-

ond image in the image stack. Again, we found the intensity time series of each pixel by collecting its intensity values from images corresponding to the next 40 *min*. As before, we took the Fourier transform of each of these pixels and found their power spectra. The spatially averaged power spectrum corresponds to the power spectrum of the second image. This procedure was repeated resulting in a power spectrum for each time point. The magnitude of these power spectra were plotted over time to give a spectrogram.

Windows: Here it is important to note that the length of the window has to be chosen carefully. The length of the window is related to the frequency resolution of the Fourier transform. If the window is very short, a small error in in the Fourier frequency gives large deviations in the period. If it is too long, then the oscillation frequencies may change in the interval. Further, the introduction of the window leads to artificial effects like spectral leakage. This occurs when the window doesn't contain integer number of periods. The FFT algorithms assume that the first and the last points of the data set are connected. When the interval in the window doesn't have an integer number of periods, there is a discontinuity in the end points. This discontinuity are represented as high frequencies in the power spectrum. The amplitude of the actual frequency decreases, "leaking" the amplitude to higher frequencies. This is spectral leakage. In our algorithm, this effect is minimized by the technique of windowing. In this technique, the data set is multiplied by a time window whose amplitude decreases to zero smoothly towards the beginning and the end of the data set, ensuring that the endpoints of the data set have no discontinuity. Although this does not completely remove the high frequency components, it does decrease their amplitudes. In the algorithms used here, either Blackmann or Hanning windows were used.

Another artifact in the spectrogram is a strong peak in the power spectrum at a frequency corresponding to the length of the window. This is especially pronounced when the signal is weak.

2.2.3 Phase singularities

Phase singularities denote the spiral cores. To find the phase singularities, I begin with the result of the Fourier analysis, where I found the dominant frequency at each time point. The phase at each pixel is defined to be the phase of the oscillation at the dominant frequency (obtained from the real and imaginary parts of the Fourier transform). A map of this phase, ranging from from $-\pi$ to π for all the pixels is the phase map of that image. A phase singularity is a point where phase is not defined. One way to detect phase singularities is by integrating the gradient of the phase along a closed curve. Such an integral is non-zero only if the loop encloses a singularity.

$$\pm n.2\pi = \oint \vec{\nabla}\phi \cdot \vec{dl} = \oint \vec{k} \cdot \vec{dl} \tag{2.1}$$

Here $\vec{k}$ is the wave vector, and is equal to the gradient of the phase. It is assumed to lie in the xy plane. n is an integer. The wave vector at any point (i, j) is given by

$$k_x(i, j) = \phi(i + 1, j) - \phi(i, j) \tag{2.2}$$

$$k_y(i, j) = \phi(i, j + 1) - \phi(i, j) \tag{2.3}$$

Any difference in phase larger than π is replaced by its 2π complement. Further, Stokes' theorem gives

$$(\nabla \times \vec{k}) \cdot \hat{z} = \oint \vec{k} \cdot \vec{dl} \tag{2.4}$$

$$n.2\pi = \int (\vec{\nabla} \times \vec{k}) \cdot d\vec{A}. \tag{2.5}$$

The cross product in equation (4.8) was evaluated using the kernel method described in [1] to obtain the singularities in our patterns. The curl can be approximated as the convolution operator given by

$$\nabla_x = \begin{bmatrix} -0.5 & 0 & +0.5 \\ -1 & 0 & +1 \\ -0.5 & 0 & +0.5 \end{bmatrix} \tag{2.6}$$

$$\nabla_y = \begin{bmatrix} +0.5 & +1 & +0.5 \\ 0 & 0 & 0 \\ -0.5 & -1 & -0.5 \end{bmatrix} \tag{2.7}$$

For spirals, the winding number n, is either +1 or -1. Noise introduces spurious singularities. To eliminate such spurious singularities, we spatially filtered the phase map by first converting the phase to a complex number by raising it to an exponential of e and multiplying with i. In this complex plane, we filtered in 2D using a box-average filter. The filtered phase map was then obtained from the angles of the resulting complex numbers. [2]

However, this was not enough to remove the spurious singularities. So, we defined spirals to be the singularities that persisted for 40 *min*. To achieve this, we detected all the singularities in the first image, defined a tolerance length, and used the fact that the spiral cores are never very close to one another. In the next frame, we checked if the singularities of the first image persisted in a box around the original position, with side equal to the pre-defined tolerance length. If no singularity was detected in this box, the original singularity was discarded. Also, if two singularities were closer than a pre-defined distance, they were discarded. This process continued for all the frames involved in counting.

2.2.4 Onset of synchronization

The onset of synchronization is defined using the concept of spectral entropy (as described in [4]). Starting with the spatially averaged power spectrum at each time point of the data, as described in the previous section, I first normalized these power spectra and used the following definition of spectral entropy, S:

$$S = -\sum p_i log(p_i). \tag{2.8}$$

Here p_i is the amplitude of the i^{th} frequency of the normalized power spectrum. If a time series represents white noise, all frequencies are equally dominant (p_i is high for all the i frequencies) and this spectral entropy is high. This is the case in the initial images, where no patterns occur. If the signal comes from a single frequency source, the value of the spectral entropy is lower because p_i is close to zero for almost all frequencies except one. This occurs when all the pixels or cells oscillate at the same frequency. So, the spectral entropy has a high value for unsynchronized noisy states and a low value for synchronized states. A plot of spectral entropy as a function of time shows the emergence of the synchronized state, when the spectral entropy begins to decrease. We find the minimum of the second derivative of this spectral entropy, which gives the point of maximum curvature, and define it to be the onset of synchronization. The same procedure was performed for patterns in both experiments and simulations.

2.2.5 Oscillation period

From the spectrogram obtained in the previous section, I found the time at which the power spectrum has the highest amplitude. This time corresponds to the time when the patterns are well developed. I fit the peak of the power

spectrum at this point with a second degree polynomial to obtain the frequency corresponding to the maximum and converted this frequency to period of oscillations.

In some cases where the signal to noise ratio is poor, these methods do not work. In these cases, I use the technique of autocorrelation. When a periodic signal is correlated with itself, the lag at which the second peak (after the maximum at zero lag) occurs, corresponds to the period of the signal. For this process, I first take the spatially averaged intensity time series and de-trend it to get oscillations about zero. Then I find the autocorrelation for various lags, and find the lag corresponding to the second peak.

2.2.6 Spatial order

Spatial order is obtained as described in [3]. I first take an image of the spirals at the synchronization time (when they're most ordered). If all the pixel intensities are shuffled randomly, a random image with the same distribution of intensities is obtained. As a consequence of the central limit theorem, the distribution of the spatial Fourier coefficients of this random image is a Gaussian, whose variance is the variance of the intensities of original ordered image (Parseval's theorem). I find the variance of the intensities of the original image and use it to construct the Gaussian distribution, P_r, corresponding to the random image with the same intensity distribution. The information corresponding to this Gaussian distribution (Hks) is the information of the most random image with the same intensity distribution as the original image.

$$Hks = -\sum P_r log P_r \tag{2.9}$$

Next, I find the spatial Fourier coefficients of the ordered image, whose distribution P_o is typically non-Gaussian. I find the information corresponding to this distribution (Iks).

$$Iks = -\sum P_o log P_o \tag{2.10}$$

The spatial order is defined as the difference of the above two informations. It estimates how far away the ordered image is from a random image of the same intensity distribution.

$$Order = Hks - Iks \tag{2.11}$$

I use the spatially filtered phase maps for these calculations because they are less noisy.

BIBLIOGRAPHY

[1] Mark-Anthony Bray et al. "Experimental and Theoretical Analysis of Phase Singularity Dynamics in Cardiac Tissue". In: *Journal of Cardiovascular Electrophysiology* 12.6 (2001), pp. 716–722. ISSN: 1540-8167. DOI: 10.1046/j.1540-8167.2001.00716.x. URL: http://dx.doi.org/10.1046/j.1540-8167.2001.00716.x.

[2] Jan Christoph. "Intramural Visualization of Scroll Waves in the Heart". PhD thesis. Göttingen Graduate School for Neurosciences, Biophysics and Molecular Biosciences: Georg-August-University, Göttingen, Oct. 2014.

[3] W F. Heinz, J L. Werbin, E. Lattman, et al. "Computing Spatial Information from Fourier Coefficient Distributions". In: *J Membrane Biol* 241.2 (2011), pp. 59–68. DOI: http://dx.doi.org/10.1007/s00232-011-9362-x.

[4] G E Powell and I C Percival. "A spectral entropy method for distinguishing regular and irregular motion of Hamiltonian systems". In: *Journal of Physics A: Mathematical and General* 12.11 (1979), p. 2053. URL: http://stacks.iop.org/0305-4470/12/i=11/a=017.

CHAPTER 3

EFFECTS OF DEVELOPMENTAL VARIABILITY ON THE DYNAMICS AND SELF-ORGANIZATION OF CELL POPULATIONS.

Kaumudi H Prabhakara, Azam Gholami, Vladimir S Zykov, Eberhard Bodenschatz, New Journal of Physics, 2017

3.1 Abstract

We report experimental and theoretical results on spatiotemporal pattern formation in cell populations, where the parameters vary in space and time due to mechanisms intrinsic to the system, namely *Dictyostelium discoideum (D.d.)* in the starvation phase. We find that different patterns are formed when the populations are initialized at different developmental stages, or, when populations at different initial developmental stages are mixed. The experimentally observed patterns can be understood with a modified Kessler-Levine model that takes into account the initial spatial heterogeneity of the cell populations and a developmental path introduced by us, i.e., the time dependence of the various biochemical parameters. The dynamics of the parameters agree with known biochemical studies. Most importantly the modified model reproduces not only our results, but also the observations of an independent experiment published earlier. This shows that pattern formation can be used to understand and quantify the temporal evolution of the system parameters.

3.2 Introduction

Pattern formation has been broadly studied in living and non-living systems over a large range of scales [7, 35, 8], e.g., animal coats, shells, butterfly wings [36], in dynamics of cardiac tissues [9], in chemical reactions like the Belusov-Zhabotinsky reaction [51]. In some of these systems, for various cases, the dynamics change with time, leading to the formation of different patterns. In living systems the most common reason is the variation of gene expression levels. For example, during the embryogenesis of the fruit fly Drosophila, the activation of different genes at different stages causes the spatial patterning [34]. While these patterns can be visualized easily, correlating these patterns with the changing dynamics of the system is challenging.

One system that shows temporally varying patterns and self-organization is a starving population of *Dictyostelium discoideum* (*D.d.*). Ever since *D.d.*'s behavior was described [42, 2], it has been extensively studied to explore its chemotaxis [11, 18], pattern formation [19, 1], self-organization [37, 12], multicellularity [3], development [27] etc. Its natural environment is the soil, where it feeds on bacteria. The cells exhibit social behavior when they begin to starve [21]. They secrete a chemical called cyclic adenosine monophosphate (cAMP) as a response to starvation. The secreted cAMP diffuses through the surrounding medium. The neighboring cells detect the cAMP through their membrane bound receptors and, with the help of the enzyme adenyl cyclase, secrete more cAMP in response. Some of the cAMP molecules are degraded by an enzyme called phosphodiesterase, which is present in intracellular, extracellular, and membrane bound forms [17]. The response of the cells to cAMP's passage through the external medium can be visualized with dark field optics, either

as spirals or as targets [1, 10, 46, 45]. After starving for about 5 *h*, the cells respond to the external cAMP by migrating towards a higher concentration of cAMP - a process called chemotaxis. About 10^5 cells aggregate to form mounds. These mounds then form multi-cellular slugs that scout for food. On failing to find nutrients, the slug develops into a fruiting body; the cells that form its stalk die and the cells at its top become spores [49].

The developmental process from starvation to forming fruiting bodies takes about 24 *h*. Throughout this time, the cells continually undergo changes. For example, at different starvation times, different receptors of cAMP are expressed [23], the cells secrete different amounts of cAMP [25, 26], the expression of the amount of the degrading enzyme, phosphodiesterase, varies [43, 32], an inhibitor of phosphodiesterase is expressed at later stages of the development [52], etc. These changes are enabled by the expression of the respective genes [16, 28]. It is well known that expression of many genes are controlled by the number of cAMP pulses they received [24, 5]. Therefore, as the cells starve, they undergo a continuous process of development. An important question is whether these developmental changes influence the patterns formed by starving populations of *D.d.*

Various models have been proposed to explain the formation of patterns in starving populations of *D.d.* [33, 48, 15, 29, 39, 22, 31, 44]. The models describe mechanisms through which spirals could be generated in a system resembling populations of *D.d.* One of earliest models was proposed by Martiel and Goldbeter [33]. This model considers some of the biochemical reactions occurring in the system. The dynamics are reduced to three variables, corresponding to intracellular cAMP, extracellular cAMP and the fraction of occupied receptors.

This model was extended by Tyson et al. [48] to reproduce spatiotemporal patterns like spiral waves. It was further modified by Falcke and Levine [15] to include genetic variability of the membrane receptor of cAMP. The latter was achieved by introducing a new variable, which is the ratio of the total receptor concentration to the initial concentration. However, this modification assumes that the amounts of adenyl cyclase, intracellular phosphodiesterase and extracellular phosphodiesterase increase monotonically with this new variable. Further, to reflect the temporal changes that occur during the development of *D.d.*, Lauzeral et al. [29] modified the model to incorporate time variation in adenyl cyclase and rate of degradation. However the time dependence of the parameters does not match previous biochemical experiments [25, 26, 43, 32]. A further modification was proposed by Pálsson and Cox [39], in which the amount of phosphodiesterase in the system was regulated in two ways: by having a random initial distribution of the amount of phosphodiesterase, and by gradually decreasing the amount of phosphodiesterase with time to account for the increasing levels of the phosphodiesterase inhibitor. Next, they tested this experimentally, by observing patterns formed by mutants lacking the inhibitor [40]. They found that cells deficient in the gene of the inhibitor failed to form well developed spirals and formed smaller aggregates.

Another well-established model was proposed by Kessler and Levine [22]. This model mimics the behavior of *D.d.* by placing "bions" on a 2D grid. This is a cellular automata type of model, where each grid point, i.e., each bion, is governed by pre-determined rules. The bions are initially excitable. If the cAMP concentration surrounding them is higher than a threshold, the bions start to emit cAMP. Then they enter an absolute refractory phase where no secretion of cAMP is possible. After spending a specified amount of time in this phase, they

revert back to being excitable. This model was also successful in reproducing spiral waves with suitable initial conditions. To make the model more realistic, Levine et al. [31] modified it by introducing genetic feedback mediated by the pulses of cAMP. This was achieved by introducing a new variable called the excitability, which is coupled to the amount of cAMP, and in turn couples to the excitation threshold. This model was also able to simulate aggregation by including cell movement after the establishment of spirals. It was later slightly modified and used to account for patterns formed by populations deficient in certain genes of the signal transduction pathway [44]. Using a simpler form of cellular automata, another study numerically investigated the effects of variability [20] by simulating a system that models the spread of epidemics. They focused on the parameter corresponding to the excitability of the cells and the parameter regulating the impact of "infected" cells on the neighboring cells. To introduce variability, they assumed that these two parameters have a high value and a low background value. Each bion was assigned one of the two values for both parameters. The fraction of bions with the high value of the parameters was varied. This resulted in a variety of patterns. However, it is difficult to draw parallels with *D.d.* because the model used is far from the biochemical processes involved in *D.d.* Further, temporal variations of the parameters are not considered.

Although each of these models and their modifications explain various experiments, many results on pattern formation and selection in *D.d.* need further explanation. For instance, a study [13] showed that mutants expressing different kinds of cAMP receptors produce different kinds of patterns. In another experiment Lee et al. [30] perturbed pattern formation by spraying a mist of cAMP on populations showing spirals. Depending on how long after the starvation

the mist was sprayed, the populations either managed or failed to re-produce spirals. None of the models described above reproduced all the experimental results presented below.

In this work, we show that cell development and heterogeneity play an essential role in pattern formation of *D.d.* As stated before, while the populations starve, their gene expression levels vary. Therefore, in order to introduce genetic heterogeneity and variability, we starve populations for different initial durations (see Methods). In one set of experiments, we observe the patterns formed by single populations that have been starved for different initial durations. In the second set of experiments, we mix two populations containing equal number of cells that have been starved for different initial durations. We analyze the patterns formed in these experiments and simulate them with the modification of the Kessler-Levine model used by Sawai et al. [44]. We show that spatial heterogeneity of cell density and parameters combined with a specific temporal evolution of the system parameters (developmental path) semi-quantitatively reproduce the experimental results. Moreover, our modified model also reproduces the results of cAMP resetting experiments carried out by Lee et al. [30].

3.3 Results

3.3.1 Single populations

To systematically study the effect of development on pattern formation, we starved populations of AX2 wild type cells for different durations. After this initial starvation, the populations were plated on a Petri dish and observed un-

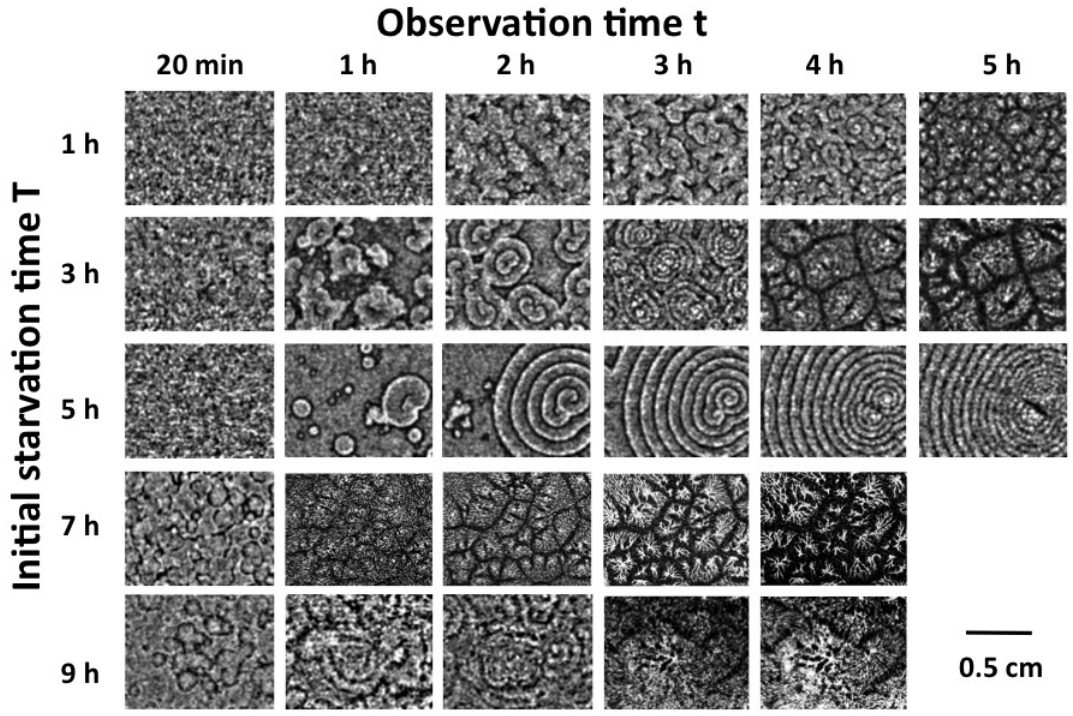

Figure 3.1: Sample patterns obtained in experiments for different initial starvation times T as a function of the observation time t.

der a dark field set-up. (See Methods.) This ensured that the populations started with different expression levels of the biochemical parameters. We observed different patterns depending on the initial starvation times as shown in figure 3.1. When populations were starved for short durations (less than 4 *h*), they formed numerous small spirals. These spirals started from broken wave segments. Populations starved for intermediate times (between 4 *h* and 6 *h*) formed fewer spirals. The patterns of these populations started differently - targets appeared at first, which were then replaced by spirals (compare supplementary movies S1 (https://youtu.be/oYRF7BaaaJY) and S2 (https://youtu.be/kT0R3wNbiro)). Populations starved for longer times (more than 7 *h*) only formed targets and began streaming soon after the formation of the initial patterns. Further important observations should be noted. Consider, for example, the patterns formed

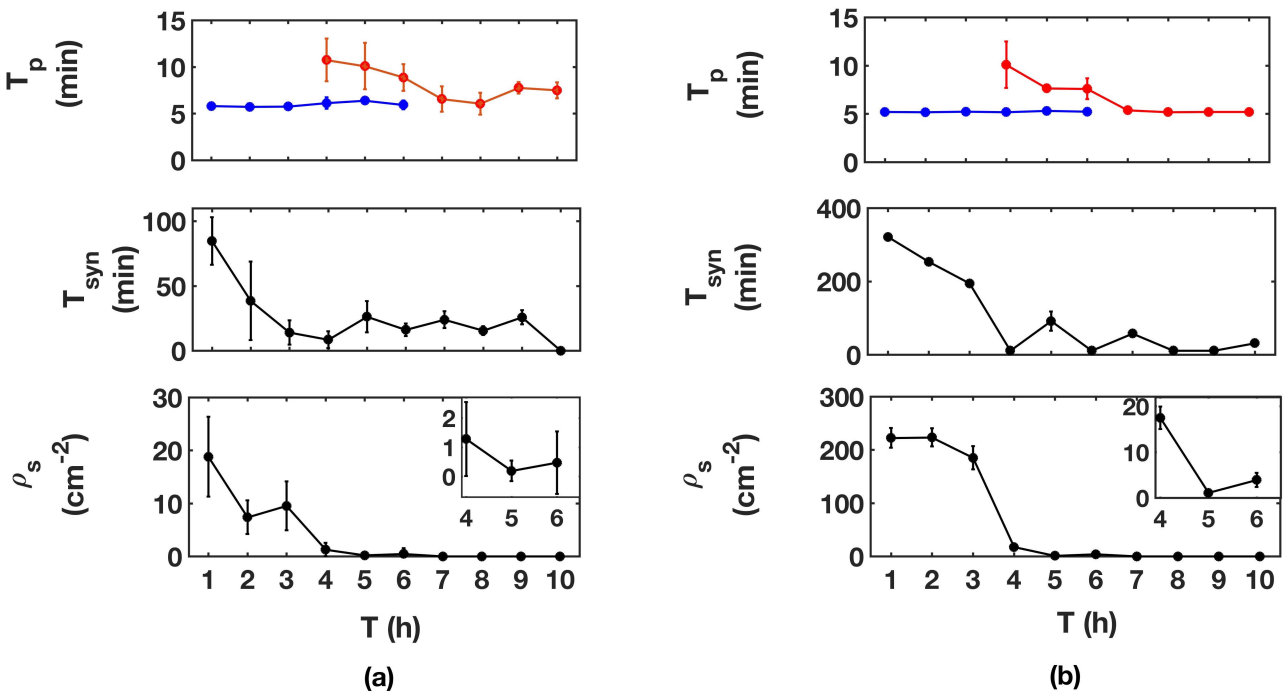

Figure 3.2: Parameters evaluated from the patterns (a) from experiments and (b) from simulations. The red lines (blue lines) in the top panels denote the oscillation period, T_p of target (spirals). The central panels show the time taken for onset of synchronization, T_{syn}, and the bottom panels show the spiral density, ρ_s. T denotes the initial starvation time of the populations. The insets in the bottom panel show the increase in spiral density after 5h. The error bars correspond to the standard deviation of the experiments and simulations. Different runs of the simulations (6 for each starvation time) were achieved by having different random initial conditions. See also Methods.

by a population starved initially for 3 *h*. Figure 3.1 shows the patterns observed after another 3 *h* of signaling. At this point, the population had starved for a total of 6 *h*. Now consider instead, a population initially starved for 5 *h*. Figure 3.1 shows the patterns observed after 1 *h* of signaling. At this point in time both populations had been starved for a total of 6 *h*. Please note that the patterns of the two populations strongly differ, clearly showing the importance of the developmental path and the associated gene expression on the pattern formation of *D.d.* To quantify the patterns, we use three order-parameters from

the experimental data: oscillation period T_p, onset of synchronization T_{syn}, and spiral density ρ_s. The Methods Section describes the exact procedure for the data analysis. Figure 3.2 shows the variation of these quantities as a function of initial starvation time T of the populations. Spirals have an oscillation period between 5 *min* and 6 *min*, irrespective of initial starvation time. The period of the spirals decreases with observation time and becomes approximately constant. Between 4 *h* and 6 *h* of initial starvation time, we observed a co-existence of spirals and targets. In this range, targets always had a longer oscillation period compared to spirals. This shorter period of the spirals enables them to take over the patterns. Spirals had a very small variation in oscillation period compared to targets as shown by the error bars. This indicates that spirals always have a fixed frequency of oscillation, whereas the frequency of target patterns varies. This is expected and well known from theoretical studies [47].

Next, let us consider the time it takes for the populations to exhibit a synchronization of cell dynamics. Such a time is quantified by the onset of synchronization plotted in the figure 3.2. With increasing initial starvation time, populations form patterns faster. The synchronization time decreases as initial starvation time increases.

Finally, we characterize the patterns by the number of spirals formed in a given area. It can already be seen in figure 3.1 that the number of spirals decreases with increasing initial starvation time. Figure 3.2 quantifies this: the spiral density reaches a minimum at 5 *h* of initial starvation time, and then increases slightly at 6 *h* (compare supplementary movies S3 (https://youtu.be/wEDe9NIeN0) and S4 (https://youtu.be/LGHIlz1oU24)). At 5 *h* of initial starvation time, due to the minimum in spiral density, very large spirals are

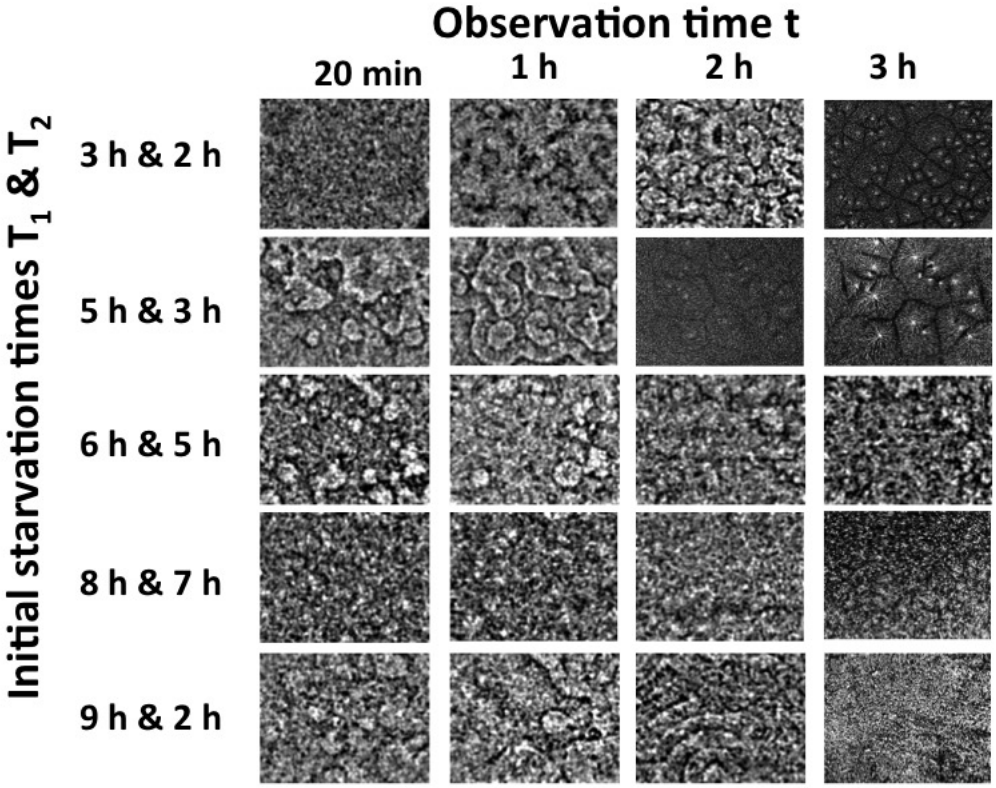

Figure 3.3: Sample patterns obtained in experiments for different mixtures as a function of the observation time t. T_1 and T_2 denote the initial starvation times of the two populations. The width of each panel is 1.8 *cm*.

formed, as is seen in figure 3.1. (Supplementary movie S3 (https://youtu.be/w-EDe9NIeN0).)

3.3.2 Binary population mixtures of different developmental stage

So far we have seen that developmental time plays an important role in pattern formation of *D.d.* Next, we study the effect of developmental heterogeneity on pattern formation. We starved populations containing equal number of cells

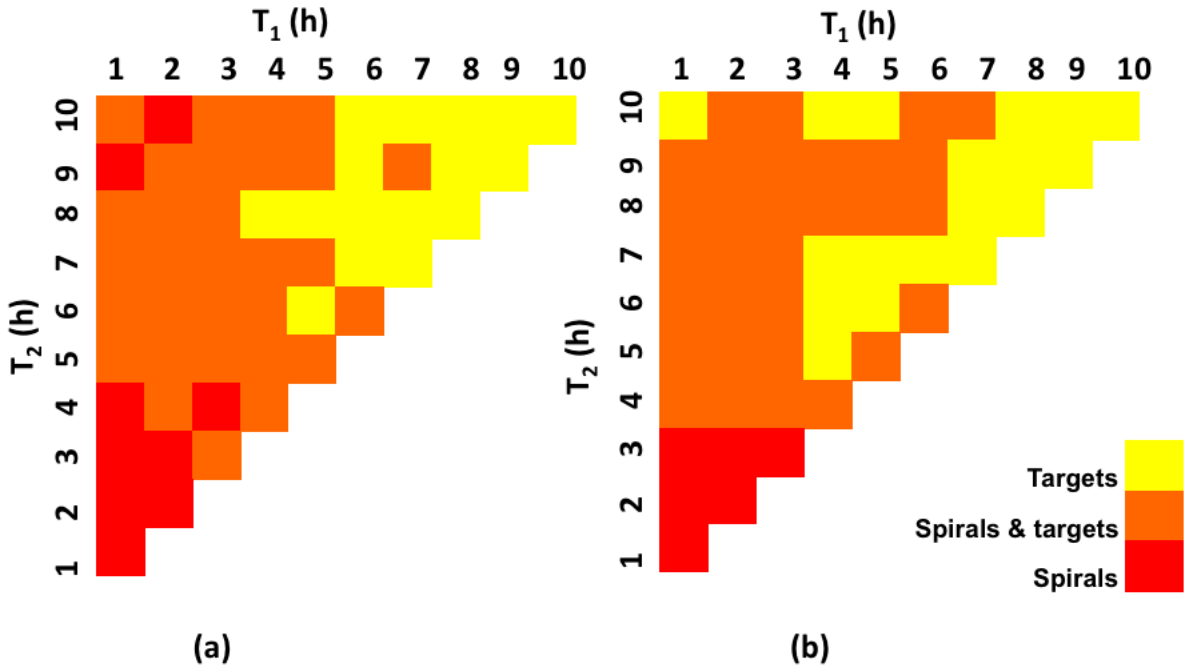

Figure 3.4: Phase diagram containing the classification of the patterns obtained in (a) experiments and (b) simulations. T_1 and T_2 denote the initial starvation times of the two populations.

for different initial starvation times (as we described under Methods) and then mixed them before observation. This way, cells with different gene expression levels interacted with each other. In the experiments we used all possible binary mixtures of populations initially starved between 1 *h* and 10 *h* (in 1 *h* intervals). For convenience, we call the populations initially starved for shorter (longer) durations, the younger (older) populations. The mixtures formed a variety of patterns as shown in figure 3.3.

A phase diagram (figure 3.4), summarizes the patterns observed. The two axes correspond to the initial starvation times of the two populations. The hypotenuse of the phase diagram corresponds to single populations. In the lowest part of the phase diagram, where the populations are initially starved for less than 4 *h* each, numerous small spirals were observed. These spirals formed from

broken wave segments. In the top left part of the phase diagram, where population 1 was initially starved for less than 5 h and population 2 was initially starved for more than 5 h, spirals co-existed with targets. In these mixtures, the populations formed targets first and then spirals. But the spirals, having a lower period took over the targets. Older populations (initially starved for longer than 8 h) that did not form spirals on their own, formed spirals when mixed with a younger populations. The patterns appeared faster in the mixtures than they would have in the younger populations only. These observations indicate that the older populations are important contributors to the pattern formation process. In the top right part of the phase diagram, both the populations were initially starved for longer than 5 h. These mixtures mostly failed to form spirals. After a few oscillations of the targets, they immediately began to stream. As in the case of single populations, the images of these mixtures had a low signal to noise ratio, which made measurement of spiral density less reliable.

3.3.3 Simulations

To understand our experimental results, we rely on the model originally proposed by Kessler and Levine [22] and modified by Sawai et al. [44]. Let us first summarize this model and its parameters before we show that our experimental results necessitate further modifications. The model simulates the collective dynamics of bions placed on a 2D grid. The location of a bion is denoted by the grid coordinates i and j. Each bion is characterized by the concentration of cAMP $C_{i,j}$, excitability $E_{i,j}$, and a threshold concentration of cAMP needed for excitation $C_{i,j}^{thresh}$. The dynamics of the bions obeys the following equations:

$$\dot{C}_{i,j} = D \cdot L(C_{i,j}) - \gamma \cdot C_{i,j} + \theta \cdot C_{rel} \tag{3.1}$$

$$\dot{E}_{i,j} = \eta + \beta \cdot C_{i,j}; \quad E_{i,j} \leq E_{max} \tag{3.2}$$

$$C_{i,j}^{thresh} = \left[C_{max} - A\frac{\tau}{\tau + T_{ARP}} \right](1 - E_{i,j}), 0 < \tau < T_{RRP} \tag{3.3}$$

In equation (5.6), L is the discrete Laplacian operator and θ is a step function - it is 1, if $C_{i,j} \geq C_{i,j}^{thresh}$ and 0 otherwise. (It is always zero in the absolute refractory phase, as described below.) Initially, the bions are excitable. If the concentration C of cAMP exceeds a threshold C^{thresh}, the bions emit cAMP at a rate $C_{rel} = 300/min$ for 1 min. Immediately after emission, they enter an absolute refractory state, where they are incapable of emitting cAMP for a fixed time, $T_{ARP} = 2\ min$. Next, the bions go into a relative refractory state, which has a high threshold for emission of cAMP. This state also lasts for a fixed time $T_{RRP} = 7\ min$. The threshold required for cAMP release decreases throughout this state (as τ, the time spent in the relative refractory phase, increases from 0 to T_{RRP}) and reaches a minimum at the end of this state (in accordance with equation (5.8)), after which the bions are excitable again and the cycle continues. The cAMP is degraded by an enzyme at a rate $\gamma = 8/min$. It is important to note that the degradation rate is the cumulative effect of phosphodiesterase and its inhibitor. The excitability of the cells E, increases autonomously, with $\eta = 0.0001/min$ and is proportional to C with a coupling $\beta = 0.005/min$. It saturates at a fixed value $E_{max} = 0.93$ (equation (5.7)). The time spent in the relative refractory phase (τ) and the excitability (E), determine the concentration of cAMP required to cause emission of cAMP by a bion. Highly excitable bions (high E) have a very low threshold for initiating cAMP emission and can be easily excited to release cAMP, whereas bions with low excitability have a higher threshold and are not

easily excitable. $C_{max} = 100$ is a constant describing the maximum value of the threshold required for emission of cAMP, D = 0.00138 mm^2/min is the diffusion coefficient and the constant $A = (T_{RRP} + T_{ARP})(C_{max} - C_{min})/T_{RRP}$ is chosen so that the threshold is maximum when the bions enter the relative refractory state and minimum when they leave it.

All bions fire randomly with a probability of 10^{-4}. The simulations were initialized with $E_0 = 0.5$ and $C = 0$ everywhere. A small fraction of bions were set to emit cAMP. Although the fraction used in Sawai at al. [44] is unknown, we found that 5 emitting bions randomly chosen out of 333 x 333 bions placed on a square grid reproduced their results. A bion that has already emitted cAMP atleast once, and has not emitted cAMP for about 15 *min* (the quiescence time) is forced to emit cAMP at the end of the quiescence time. The rules of the fixed durations of the refractory phases and the saturation of the excitability are implemented at each bion separately from these equations. The threshold required for cAMP release, C^{thresh} is calculated at each bion at each time step. The equations 5.6-5.8 are solved using the explicit Euler method with a grid size of $0.06mm$ and time step of $0.01min$.

In our simulations of the above model, we used populations at different initial starvation times [44], i.e., different initial starvation times correspond to different initial excitabilities of the bions. We studied both homogeneous populations and binary mixtures. In the latter case, each bion consisted of a 1:1 mixture of populations with different initial starvation times. The excitabilities, the cycle through the different phases, and the calculation of the threshold for cAMP release was conducted independently for each initially starved population. To our surprise, the model [44] did not reproduce the experimentally

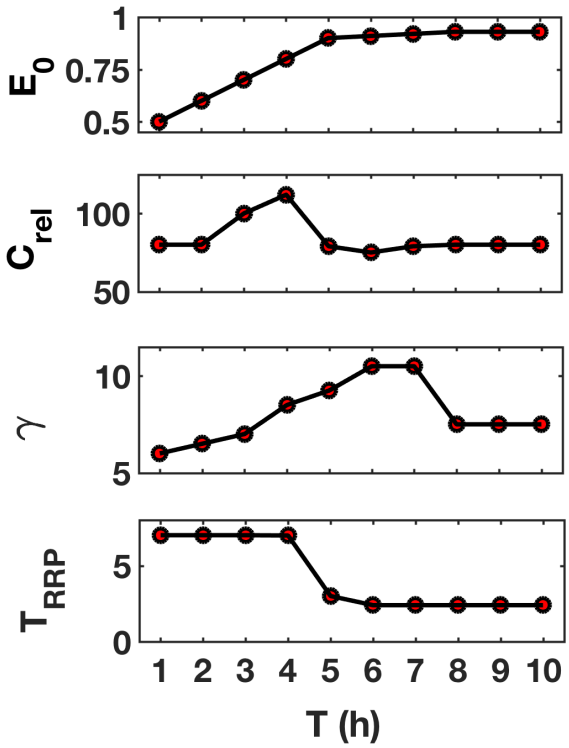

Figure 3.5: The temporal variation of the parameters used in the modified model. E_0 is the initial excitability for equation (5.7). C_{rel} denotes the amount of cAMP released by the cells. γ denotes the rate of degradation. It has units of min^{-1}. T_{RRP} denotes the duration of the relative refractory period. Its unit is *min*. For E_0, only the initial value is taken from the top panel. With time, the variable E evolves according to equation (5.7). However, the other three parameters start and evolve with time according the respective curves shown here. γ, C_{rel}, T_{RRP} and E_0 are all set manually after many trials. We used the biochemical experiments as a guide to have the right trend in γ and C_{rel}. The actual values are perturbations of the values used in the model proposed by Sawai et al [44]. For T_{RRP} we used an experimental result [14] that measured T_{RRP} at the beginning and the end of the signaling phase. The values we use in the model correspond exactly to this experimental result.

observed co-existence of spirals and targets for pure and mixed populations. Additionally, for large initial starvation times, the oscillation period of targets found in the simulations was about twice as long as those observed in experiments. Although the model was able to successfully capture the behavior of previous experiments by Sawai et al. [44], it is clearly insufficient to capture our experimental results. Thus, the model has to be modified. In our work, we conserve the structure of the model and introduce time dependence in some of its parameters.

Our first conjecture was that the oscillations period could depend on the time spent in the refractory period. Studies have shown that in *D.d.*, the refractory period for the relay of signals decreases from about 7 *min* to about 2 *min* during development [14]. We capture this by decreasing T_{RRP} with starvation time (figure 3.5). With this modification the oscillation period of targets agreed with the experimentally observed value of around 6 *min*. However, this modification alone did not reproduce the co-existence of spirals and targets and further modifications were necessary. Previous studies have shown that the activity of phosphodiesterase increases with starvation time in suspension of *D.d.* [43, 32]. To capture this, we modified the model to include a temporal variation of the rate of degradation of cAMP (γ in equation (5.6)) as shown in figure 3.5. Please note that this choice agrees with these biochemical studies [43, 32]. Furthermore, it is known that cells release different amounts of cAMP as they starve [25, 26]. Therefore, we varied the amount of cAMP emitted by the cells (C_{rel} in equation (5.6)) with starvation time in a manner compatible with these previous studies (figure 3.5). By varying these parameters, we are effectively varying the expression levels of the genes that regulate these parameters. In the simulations of the above model, the initial excitability was chosen according to

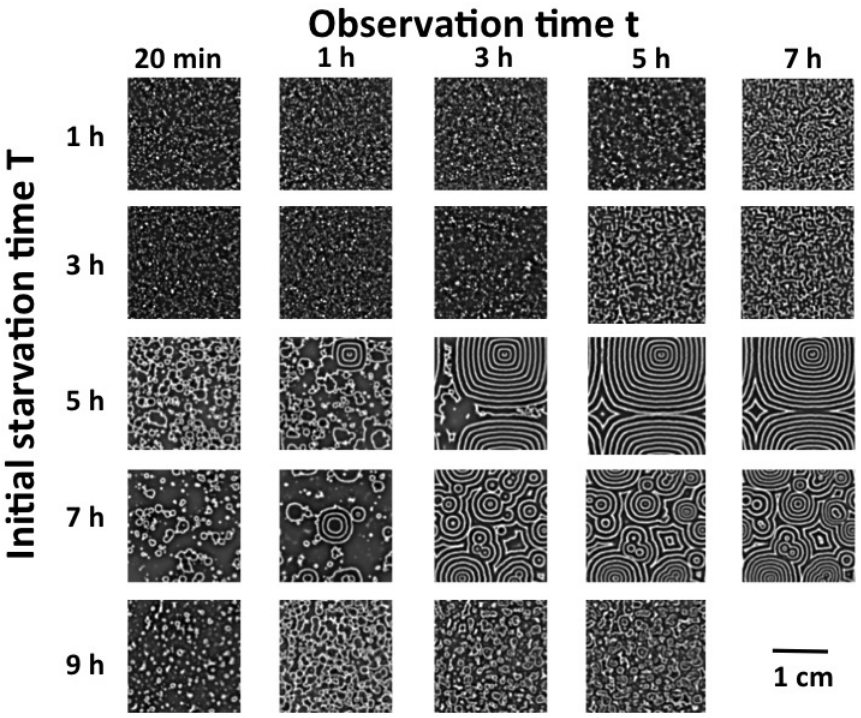

Figure 3.6: Sample patterns obtained in simulations for different initial starvation times, T as a function of the observation time t.

figure 3.5. Furthermore, to capture the initial conditions in the experiment as closely as possible, we included the spatial heterogeneity in the cell distribution in our model. See Methods for the details.

With these changes, i.e., the modification of the initial conditions and the time variation of the three parameters, the model semi-quantitatively reproduces our experimental results. Representative patterns obtained in the simulations are shown in figure 3.6 for single populations and in figure 3.7 for mixtures of populations. Please note that the square shape of the spirals is an artifact of the discretization of the model and the approximation of the Laplacian L, which takes into account only four nearest neighbors. Simulation results for all the mixtures and single populations are summarized in the phase diagram in figure 3.4b, which agrees very well with the phase diagram from the experiments

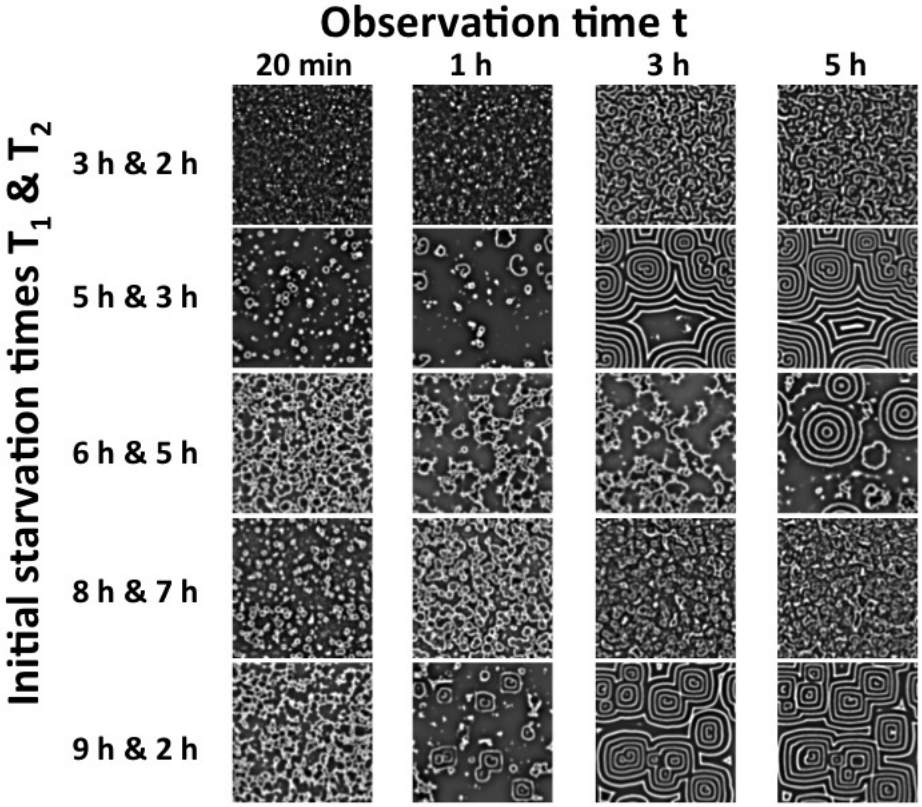

Figure 3.7: Sample patterns obtained in simulations of different mixtures as a function of the observation time t. T_1 and T_2 denote the initial starvation times of the two populations. The length of each panel is 2 *cm*.

(figure 3.4a). To further quantify our simulation results, we measured the three order-parameters using the same methods used in the experiments (see Methods). As shown in figure 3.2b, the measured order-parameters agree well with those in the experiments (figure 3.2a) for all cases investigated. Although the order parameters from the simulations qualitatively agree with the experimental order parameters, there is a discrepancy in the actual values of the spirals density and the onset of synchronization. However, the values of the oscillation period obtained from the experiments and the simulations agree well. We discuss the possible reasons in the next section.

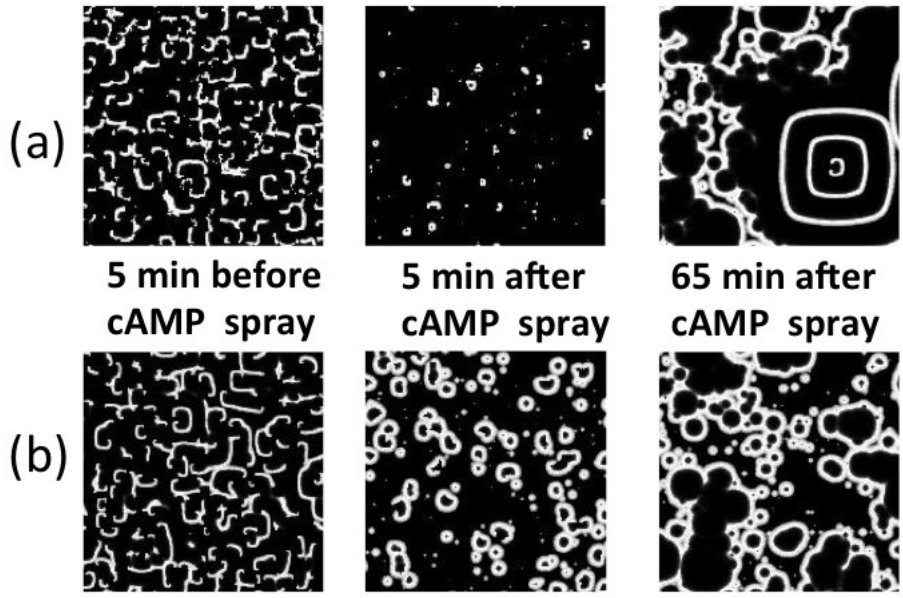

Figure 3.8: Patterns obtained by simulating experiments by Lee et al [30]. (a) Spirals re-emerge within an hour when the cAMP is sprayed at 4 h after start of simulations. (b) Only targets appear when cAMP is sprayed after 8.3 h of simulation. We performed the simulations on a 2 cm x 2 cm grid. For clarity, here we show a part of the simulation area. The length of each image is 1 cm.

At this point, one could argue that the model was modified to explain our experimental results and may not have any predictive value. Therefore it is imperative to test this model in an independent setting. In their seminal paper, Lee et al. [30] conducted experiments on the pattern formation of *D.d.* populations starving on agar. They observed targets and spirals if the system developed without any perturbation. However, when the cells were reset by spraying a mist of cAMP solution on the patterns, they showed different behavior depending on when the mist was sprayed. If cAMP was sprayed before 6 h of starvation, spirals and targets emerged; but if it was sprayed after 6 h, only targets emerged. These experimental findings have been simulated by Falcke and Levine [15] using a generalized version of the Martiel - Goldbeter model [33] which includes the coupling of the cAMP signaling to the expression levels of

aggregation genes, and qualitatively explained in other works [30, 40]. Here, we test if the modifications we made to the Sawai et al. [44] model to explain our experimental results can also reproduce the experimental results of Lee et al. [30]

To mimic the cAMP spray, for one time step we set the concentration of cAMP at all bions to a value of 20, which is about twice the maximum cAMP concentration of normal signaling. In all simulations, the populations had an initial starvation time of 3 h. If we "spray" cAMP 1.7 h after start of the simulation (4.7 h starvation) we observe patterns consisting of spirals and targets, just as in the experiment. As we increased the time at which we sprayed cAMP, the number of spirals that re-formed decreased. When cAMP was sprayed later than 4 h of simulation (7 h of starvation), no spirals were formed again. The results of the simulation for two cases are shown in the figure 3.8. It should be noted here that the experiments by Lee et al. [30] were conducted on 2% agar, whereas we modified the model to match experiments conducted on a plastic Petri dish. We know [38] that pattern formation and time taken for synchronization depend on the substrate. So, some differences between the patterns seen by Lee et al. [30] and patterns reproduced by our modified model are to be expected.

3.4 Discussion

Let us now discuss some possible implications of our results. We observe a change in the way spirals are formed at around 4 h of initial starvation. For initial starvation times lower than 4 h, the spirals form out of pre-existing sin-

gularities or broken wave segments. While for initial starvation times between 4 h and 6 h spirals co-exist with targets, for initial starvation times longer than 6 h, only targets are formed. A possible explanation of the transition in the way the spirals form can be found in our modified model. For equation (5.7), we assumed that the initial excitability increases linearly with time with a saturation after 6 h of initial starvation (figure 3.5). This implies that in the experiment where only targets are observed, the cells are highly excitable. These highly excitable cells have a short refractory period (figure 3.5) and a low threshold for cAMP emission (equation (5.8)). The low threshold, in turn, causes the cells to produce pulses of cAMP, if they detect even a small amount of cAMP in their surroundings. Furthermore, due to their short refractory periods, the cells can quickly become excitable again. Thus, the cells emit cAMP frequently, and there are few refractory cells to cause the wave break required to induce spirals, resulting in the formation of targets and a few large spirals. As the probability of encountering refractory cells decreases with increasing initial starvation times, only targets are formed.

It is important to note that when spirals formed by cells with lower excitabilities, they were sustained even when the cells reached high excitabilities. For example, a population with an initial starvation time of 1 h was able to maintain the spirals even after 5 h of starvation, when the cells become highly excitable, as seen in experiments and in simulations. The initial excitability of cells is therefore a very important factor in determining the kind of patterns formed.

However, it is not just the refractory period that determines the spiral density. For populations initially starved for shorter durations, the probability of random firing events plays an important role in setting the spiral density.

Choosing a lower probability would decrease the spiral density, but it would also qualitatively change the patterns formed in the simulations of the population mixtures. Further, decreasing the probability of random firing also increases the time taken by the populations to form patterns, i.e. T_{syn} increases. As a compromise, we used the value of the random firing probability that qualitatively reproduces the experimental patterns in the mixtures while keeping T_{syn} and spiral density within reasonable limits. For populations initially starved for intermediate and long durations, the combination of γ and C_{rel} is critical to obtain the right trend in spiral densities. For example, in experiments, we observed that the spiral density increased slightly after reaching a minimum at 5 h of initial starvation (see inset in bottom panel of figure 3.2). Such trends can be achieved in simulations only by using a particular set of γ and C_{rel} values (see supplementary movies S5 (https://youtu.be/Mt1AfTDreSk) and S6 (https://youtu.be/8CQzvBzOHOc)).

The combination of the γ and C_{rel} and the probability of random firing also control T_{syn}. Since we found these coefficients by trial and error by trying to match the patterns of the population mixtures as well as single populations, we had to use parameters that enabled the model to reasonably reproduce the patterns in both cases. The values we obtained may not be optimal. So if a mathematically rigorous method to estimate these parameters is found, then T_{syn} and ρ could match better with experimental values.

Therefore, the time variation of the three parameters, the refractory period, rate of degradation and amount cAMP released, is crucial in determining the kind of patterns observed. The degradation rate and the amount of cAMP released are controlled by the enzymes phosphodiesterase, phosphodiesterase in-

hibitor and adenyl cyclase. Therefore, it is the variation in the expression levels of the genes controlling these enzymes that is responsible for the pattern selection.

From figure 3.2 we see that the values of T_p match almost exactly between experiments and simulations. This is because it depends only on the parameters T_{RRP} and T_{ARP} (= 2 min). The oscillation period for all the patterns is approximately equal to the $T_{RRP} + T_{ARP}$; for populations initially starved for longer than 7 h, since the cells are oscillatory, the period is almost exactly equal to the $T_{RRP} + T_{ARP}$.

Further, from figure 3.2, we see that, both in experiments and simulations, the oscillation period of targets decreases with increasing initial starvation time and settles at about 5 min at high starvation times, whereas the oscillation period of spirals is almost always around 5 min. Why is that? Let us first consider the case of spirals. For populations starved for shorter durations i.e. 1 h - 3 h, spirals form after 5 h - 3 h respectively (from figure 3.2b). So, by the time the spirals form, T_{RRP} has evolved to about 3 min (from the temporal evolution of T_{RRP} in figure 3.5) for all the three cases. Adding T_{ARP} gives T_p to be 5 min. In populations where there is a co-existence of spirals and targets, spirals form later than the targets and are the stable structures until the end of signaling. Therefore, again, the oscillation period, $T_{RRP} + T_{ARP}$, is about 3 min + 2 min = 5 min.

Now let us consider the targets. For initial starvation times of 4 h - 6 h, the targets are formed almost immediately after the cells are plated (or after start of simulations.) At this point, T_{RRP} ranges from 7 min - 3.5 min (from the temporal evolution of T_{RRP} in figure 3.5 between 4 h - 6 h). So the period of oscillation of these targets ranges from approximately 9 min - 5.5 min ($T_{RRP} + T_{ARP}$). This

is within the error bars of the observed oscillation periods both in experiments and in simulations. At higher starvation times, T_{RRP} has evolved to about 3 min; so the oscillation period is 5 min. And since the populations are oscillatory here, the oscillation period is almost exactly equal to the sum of these two quantities.

To ascertain the importance of the quiescent time of 15 min, we performed further simulations. For populations initially starved for intermediate and long durations (>5 h), dropping this condition has no effect. This is because the cells are already highly excitable, and fire periodically without this condition. However, for populations initially starved for short durations (<4 h), dropping this condition significantly increased T_{syn}. But dropping this term after the onset of synchronization has no effect on the patterns. This is again because once patterns form, the cells are synchronized and will fire periodically even without this condition.

An interesting question about pattern formation in *D.d.* is whether the dynamics are excitable or oscillatory. The Kessler-Levine model always considers the dynamics of the cells to be excitable. This is true for the populations starved for short periods of time. However, as discussed above, after about 6 h of initial starvation, the excitability of the cells reaches a maximum value. So the right hand side of equation (5.7) is zero. Also, as mentioned earlier, the high excitability reduces the threshold of surrounding cAMP required to cause emission of cAMP (equation (5.8)). As a consequence cells immediately fire when they leave the refractory period ($T_{ARP} + T_{RRP}$), i.e., the cells are oscillatory.

Finally, heterogeneity is also an important factor for pattern formation. To reproduce patterns formed by older populations in simulations, it was essential to incorporate the initial spatial heterogeneity in the cell distribution — cells in

older population tend to form clusters, leaving empty spaces in between. Further, the importance of heterogeneity in parameters is best seen in mixtures. When older populations that formed targets on their own were mixed with younger populations, spirals were formed. The time taken to form these spirals is less than the time taken by the younger populations. Therefore, the synchronization of the population and the pattern selection depend on the heterogeneity of the parameters.

Before concluding, a note about our simulations is pertinent. We tried various combinations of parameters, with and without time variation. Since these changes were manual, it was impossible to test all possible parameter combinations. We chose the three parameters that are known to change with starvation time and changed them in a manner compatible with previous biochemical experimental results and in a manner that best reproduced our experimental patterns for both single populations and mixtures of two populations. We do not claim this to be the only way or the best way to modify this model, however our choice of parameter evolution seems to work remarkably well. A mathematically rigorous method of parameter estimation is highly desired, but currently unavailable.

Although the modified model semi-quantitatively reproduces all experimental results, it is far from perfect. The values of the onset of synchronization and spiral density don't match the experiments as shown in figure 3.2. Also, for the mixed populations, though the phase diagrams look similar, for short initial starvation times actual parameters like the spiral density are different from the experiments (quite similar to that of single populations). Another point to note is that in some cases, e.g. initial starvation time of 9 h, the simulations produce

small spirals after few hours of simulation time, while this is not the case for the experiments, where the cells have already streamed at that time. Thus, to classify the patterns in figure 3.4b, we considered only simulations over a time interval corresponding to the experimental one. One possible way to fix this issue would be the introduction of cell motility in our modified model [22]. Although cell density is a dynamic variable of the system, we do not incorporate its dynamics in our model. During signaling although there is some random cell movement, significant cell movement and density changes only occur during streaming. Since we are only considering the pattern formation stage, we have not incorporated the cell density dynamics.

3.5 Conclusions

We have studied the effects of development on pattern formation in *D.d.* experimentally, and explained the results with a modified model based on [22, 44]. To our knowledge, only the paper by Sawai et al. [44] reports patterns formed by populations starved for different durations. They report the patterns for two starvation times. Our systematic study of the effect of starvation on both single populations and mixtures are novel. From our analysis of the observed patterns, we conclude that the selection of patterns formed by *D.d.* depends on the temporal variability of the parameters, i.e., the initial excitability and the spatial heterogeneity of parameters and cell density.

Recapitulating, pattern formation in *D.d.* depends on how long the cells have been starved for. Older populations formed target patterns while younger ones formed spirals. The transition occurred around 4 h of initial starvation.

However, when old populations were mixed with younger populations, they formed spirals. We have quantified the patterns in terms of spiral density, synchronization time, and oscillation period. We have offered explanations for the variation of these quantities and the observed transition in the patterns. We found that our modified model describes the experimental results by Lee et al. [30]. We have shown that developmental variability is vital for pattern selection since the variation in parameters is brought about by the developmental path.

We can predict the time evolution of the properties of *D.d.* since our modifications lead to a semi-quantitative reproduction of the experimental observations. First, the excitability increases with starvation and saturates to a maximum value. At this maximum value the dynamics of the system can be thought of as oscillatory, whereas the system is excitable for short starvation times. Second, the refractory period of the cells decreases with starvation time. Third, the amount of cAMP released by the cells and the degradation rate of cAMP have a peak in their values during starvation. We can also propose certain rules for pattern selection: highly excitable cells cannot form spirals, but form targets; but highly excitable cells can sustain spirals, if their initial condition was a spiral. Not only do these results provide insights into the temporal behavior of *D.d.*, our results are a proof of concept that it is possible to deduce many properties of the system by analyzing the patterns only. Furthermore, since the mechanism of pattern formation in *D.d.* is similar to the mechanism of pattern formation in heart tissues and various chemical reactions, our results imply that an analysis of patterns in other excitable systems could also provide important information about the system parameters.

3.6 Methods

3.6.1 Experiments

AX2 cells were grown in HL5 medium (35.5g of Formedium powder from Formedium Ltd., England, per liter of double distilled water, autoclaved and filtered) at 22^0C and harvested when they became confluent. The cells were washed in phosphate buffer (2g of KH_2PO_4, 0.36g of $Na_2HPO_4.2H_2O$ per liter at pH 6, autoclaved) and centrifuged two times. The cells were then counted using a hemocytometer. Then they were poured into a conical flask and placed on a shaker for the desired initial starvation time. After the desired starvation time, they were centrifuged and diluted to a density of 4 x 10^6 cells/ml with fresh phosphate buffer. For mixtures, each population contributed 2 x 10^6 cells/ml, and were starved in separate conical flasks. They were then plated on a 8.6 *cm* diameter plastic Petri dish with 10 ml phosphate buffer. Dark-field optics was used to image the cell populations every 20 s [1, 10, 46, 45]. It consists of an LED ring lamp placed above the Petri dish and a CCD camera (QIClick-F-M-12 from QImaging) placed below the Petri dish. Parafilm was wrapped around the sides to prevent evaporation of the buffer. A table fan blew air above the dish to equilibrate the temperature. The entire room was dark during the experiment and maintained at 22^0C. The single populations experiments were repeated three times. The imaged area was split into four parts and each part was analyzed separately. Each mixture experiment was performed either once or twice. To find the spatial heterogeneity in the cell density, we experimentally analyzed the spatial distribution of cells for the different initial starvation times. We plated the starved cells at the same density on a Petri dish. After waiting for

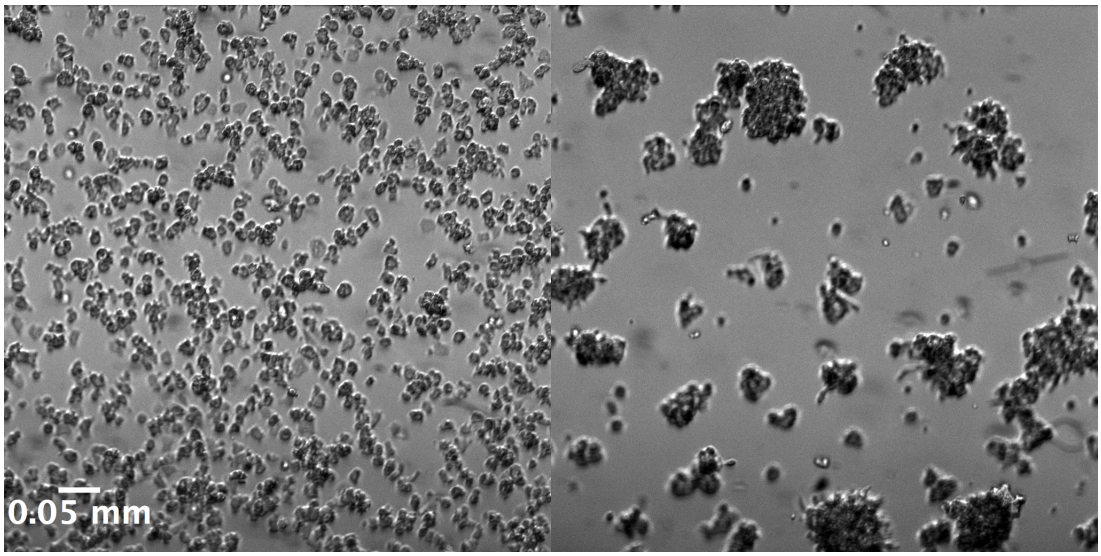

Figure 3.9: The initial distribution of the cells observed experimentally. The left panel shows the cell distribution for an initial starvation time of 2 *h*. The right panel shows the cell distribution for mixture of 10 *h* and 8 *h* initially starved populations.

about 10 *min* to allow the cells to attach to the surface, we imaged the dish at about 15 distinct regions using an inverted bright-field microscope, using a 10X objective. Figure 4.6 exemplarily shows the initial cell distributions for two different initial starvation times. To determine the ratio of the area occupied by the cells to the area of the grid, i.e., the occupation ratio, we divided the images of about 600 x 600 μm^2 into grids of size 60 x 60 μm^2 (corresponding to the size of the grids in the simulations). For these 600 x 600 μm^2 regions, we thus measured the spatial distribution of occupation ratios at 10 x 10 grid points (bions in the simulations). For each starvation time, we have about 15 such distributions. To cover the simulation region of 333 x 333 bions, we distribute these 10 x 10 distributions randomly on the simulation grid. We multiply the degradation rate γ and cAMP released C_{rel} for each bion with its respective occupation ratio, as the degradation rate and the amount of cAMP released depend on the number of cells in each bion. For mixtures, we assume that each population makes up half

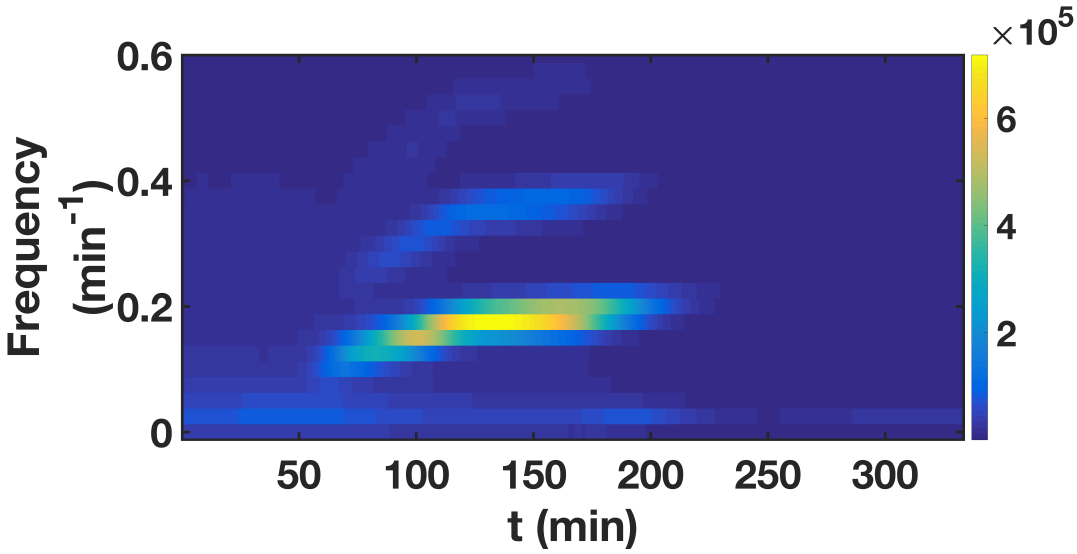

Figure 3.10: Sample spectrogram obtained from an experiment. The slight increase in frequency (the y-axis) with observation time t (the x-axis), mentioned in the results section, is visible. The colormap shows the amplitude of the power spectrum. In this case, it has a maximum at around 140 *min*. The power spectrum at this time is taken, its peak fit with a quadratic polynomial and the frequency at the maximum amplitude found.

the occupation ratio. This ensures that the effect of having clusters and sparsely occupied regions is incorporated into the simulation.

3.6.2 Data analysis

Oscillation period

First, the dark field images were filtered in space, only allowing structures between 3 *mm* and 0.2 *mm* to pass through. From these processed image stacks, we obtained the time series of the intensity for each pixel with a window of 40 *min* (corresponding to about 6 oscillations). Then, we took the Fourier transform of

these time series. The power spectra of the Fourier transforms thus obtained were spatially averaged giving one power spectrum for each time point. For example, we started with the first image of the image stack and found the time series of the intensity for all the pixels by collecting their intensity values from images corresponding to the next 40 *min*. Then, we took the Fourier transform of each of these time series and found their power spectra. These power spectra were then averaged to get one average power spectrum corresponding to the first image. Then we moved to the second image in the image stack. Again, we found the intensity time series of each pixel by collecting its intensity values from images corresponding to the next 40 *min*. As before, we took the Fourier transform of each of these pixels and found their power spectra. The spatially averaged power spectrum corresponds to the power spectrum of the second image. This procedure was repeated resulting in a power spectrum for each time point. The magnitude of these power spectra were plotted over time to give a spectrogram. An example spectrogram from an experiment is shown in figure 4.7. From the spectrogram, we found the time at which the power spectrum has the highest amplitude. This time corresponds to the time when the patterns are well developed. We fit the peak of the power spectrum at this point with a second degree polynomial to obtain the frequency corresponding to the maximum and converted this frequency to period of oscillations. In some cases, e.g. at large initial starvation times, only 2 or 3 oscillations of the targets were observed. In these cases, because it was not possible to use the Fourier transform technique, we obtained the period by finding the distance between peaks in the temporal intensity profile. The patterns formed in the simulations were analyzed with the same procedure as above. Here however, the limits of the band pass filter were 1.5 *mm* and 0.1 *mm* because the wavelengths are smaller.

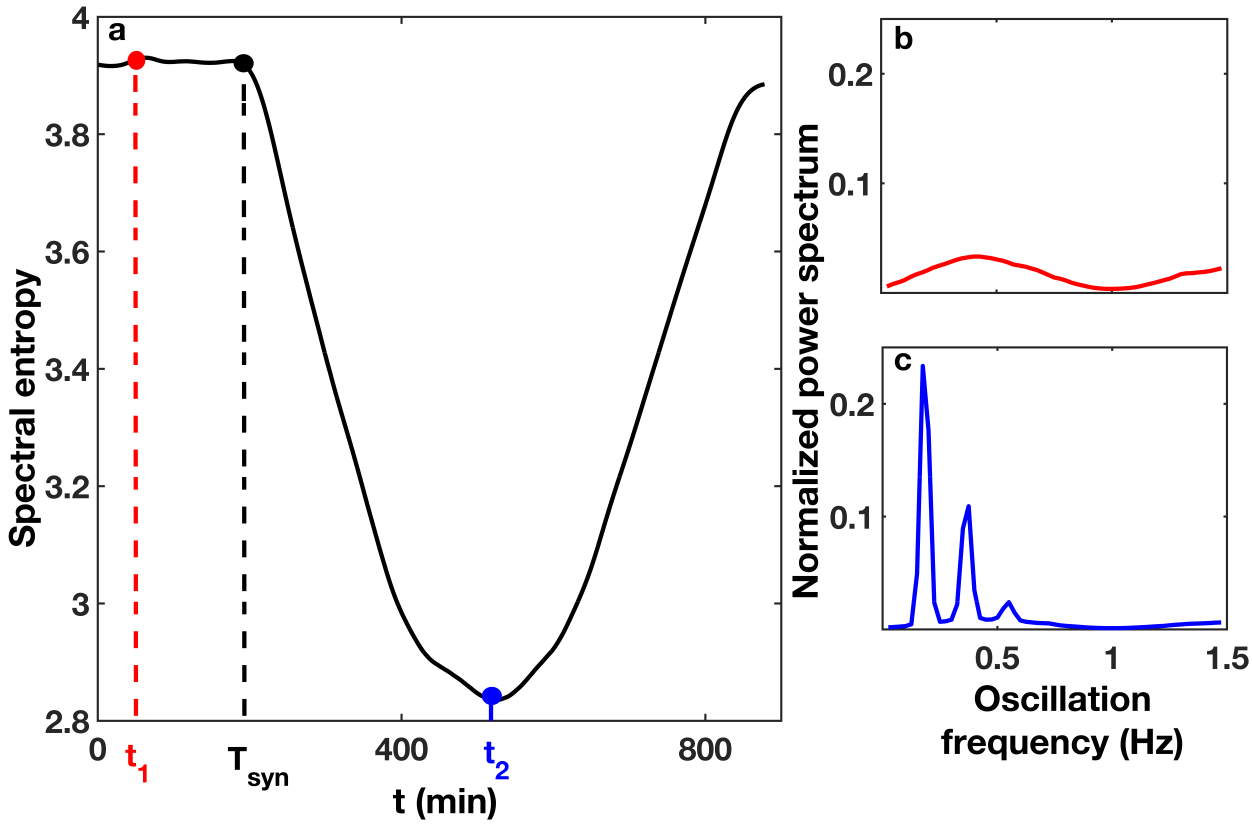

Figure 3.11: (a) The temporal variation of spectral entropy obtained from an experiment. The point of maximum curvature, defined to be the onset of synchronization, is denoted by T_{syn} (b) The normalized power spectrum corresponding to time t_1. It has a non-zero power for almost all frequencies. Using equation (4.6), the spectral entropy at this point is 3.92. (c) The normalized power spectrum corresponding to time t_2. The power is high only for a few frequencies and zero for all others. The spectral entropy is calculated to be 2.85.

Onset of synchronization

We define the onset of synchronization using the spectral entropy (as described in [41]). We found the spatially averaged power spectrum at each time point of the data, as described before. To find the onset of synchronization, we first normalized these power spectra and used the following definition of spectral

entropy, S:

$$S = -\sum p_i log(p_i). \tag{3.4}$$

Here p_i is the amplitude of the i^{th} frequency of the normalized power spectrum. If a time series represents white noise, all frequencies are equally dominant (p_i is high for all the i frequencies) and this spectral entropy is high (figure 4.8b). This is the case in the initial images, where no patterns occur. If the signal comes from a single frequency source, the value of the spectral entropy is lower because p_i is close to zero for almost all frequencies except one. (figure 4.8c) This occurs when all the pixels or cells oscillate at the same frequency. So, the spectral entropy has a high value for unsynchronized noisy states and a low value for synchronized states. A plot of spectral entropy as a function of time shows the emergence of the synchronized state, when the spectral entropy begins to decrease (figure 4.8a). We find the minimum of the second derivative of this spectral entropy, which gives the point of maximum curvature, and define it to be the onset of synchronization. The same procedure was performed for patterns in both experiments and simulations.

Spiral density

To find the spiral density, we began with the Fourier transform of the time series of the intensity of each pixel in the images, for a window of 40 *min*. After spatially averaging the power spectrum at each time point, we found the dominant frequency at each time point. We defined the phase at each pixel to be the phase of the oscillation at the dominant frequency (obtained from the real and imaginary parts of the Fourier transform). A map of this phase, ranging from from $-\pi$ to π for all the pixels is the phase map of that image. A spiral core is a

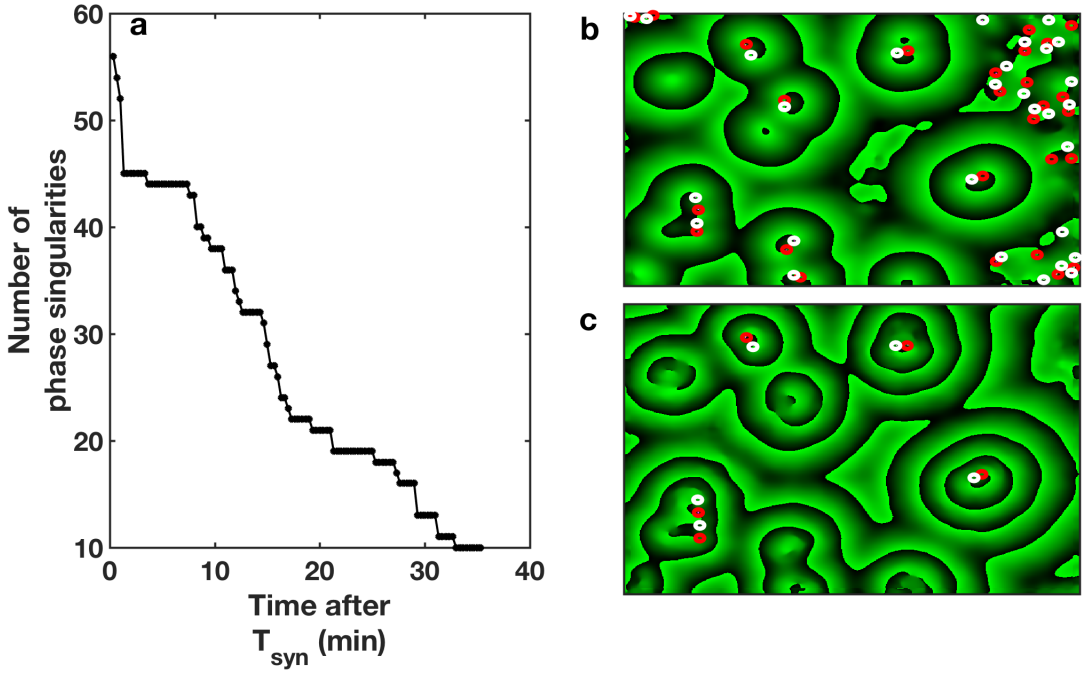

Figure 3.12: The result of our counting algorithm. The left panel shows the decrease in the number of phase singularities counted. Initially a lot of phase singularities are detected due to noise (top right panel). However, with time the number of singularities that persist decreases. At the end of the counting, the spurious singularities are discarded (bottom right panel)

phase singularity, a point where phase is not defined. (For more on phase singularities, see [50].) One way to detect phase singularities is by integrating the gradient of the phase along a closed curve. Such an integral is non-zero only if the loop encloses a singularity.

$$n.2\pi = \oint \vec{\nabla}\phi.\vec{dl} = \oint \vec{k}.\vec{dl} \tag{3.5}$$

Here $\vec{k}$ is the wave vector and n is an integer. Stokes theorem gives

$$n.2\pi = \int (\vec{\nabla} \times \vec{k}).\vec{dA}. \tag{3.6}$$

The cross product in equation (4.8) was evaluated using the kernel method described in [4] to obtain the singularities in our patterns. For spirals, the winding

number n, is either +1 or -1. Noise introduces spurious singularities. To eliminate such spurious singularities, we spatially filtered the phase map by first converting the phase to a complex number by raising it to an exponential of e and multiplying with i. In this complex plane, we filtered in 2D using a box-average filter. The filtered phase map was then obtained from the angles of the resulting complex numbers. [6]

However, this was not enough to remove the spurious singularities. So, we defined spirals to be the singularities that persisted for 40 *min*. To achieve this, we detected all the singularities in the first image, defined a tolerance length, and used the fact that the spiral cores are never very close to one another. In the next frame, we checked if the singularities of the first image persisted in a box around the original position, with side equal to the pre-defined tolerance length. If no singularity was detected in this box, the original singularity was discarded. Also, if two singularities were closer than a pre-defined distance, they were discarded. This process continued for all the frames involved in counting. The counting of the phase singularities started about 20 *min* after T_{syn}, when the patterns are well established. Figure 4.9 shows an example output of our algorithm. In figure 4.9b, we see the phase map of the first image considered for counting the singularities. The red and the white rings denote the +1 and -1 winding numbers respectively. Despite the filtering, it has many spurious singularities. Figure 4.9c shows the phase map of the last image considered for counting singularities. We see that all the spurious singularities have been eliminated by the tracking algorithm. Figure 4.9a shows the decrease in the number of singularities with time.

As described earlier, for the experiments and simulations with large initial

starvation times, the signal to noise ratio is very poor, resulting in numerous spurious singularities even when no spirals are visible. The method just described fails for these cases. Therefore, to disregard such cases, we found the actual amplitude of the signal by finding the absolute value of the Fourier transform at each time point for the data. We compared the maximum values of the signal for all experiments. As expected, there was a clear decrease in the signal amplitude at 7 h of initial starvation time. We set this value as a cut-off. Any experiment (single population and population mixtures) that had a lower signal amplitude than this cut off was classified as forming targets.

3.7 ACKNOWLEDGEMENTS

The authors thank Dr. Noriko Oikawa and Dr. Albert J Bae for their programs for the data analysis. Further, the authors thank Ms. Katharina Gunkel, Ms. Maren S Müller and Ms. Tina Althaus for their cheerful help with the preparation of the cells. The authors also thank Dr. Jan Christoph for suggesting the filtration method to detect phase singularities. This work has been supported by the Max Planck Society. A.G. acknowledges the MaxSynBio Consortium which is jointly funded by the Federal Ministry of Education and Research of Germany and the Max Planck Society.

BIBLIOGRAPHY

[1] FERNANDA ALCANTARA and MARILYN MONK. "Signal Propagation during Aggregation in the Slime Mould Dictyostelium discoideum". In: *Microbiology* 85.2 (1974), pp. 321–334. URL: http://microbiologyresearch.org/content/journal/micro/10.1099/00221287-85-2-321.

[2] John T. Bonner. "A Descriptive Study of the Development of the Slime Mold Dictyostelium discoideum". In: *American Journal of Botany* 31.3 (1944), pp. 175–182. ISSN: 00029122, 15372197. URL: http://www.jstor.org/stable/2437641.

[3] John Tyler Bonner et al. "The orientation to light and the extremely sensitive orientation to temperature gradients in the slime mold Dictyostelium discoideum". In: *Journal of Cellular and Comparative Physiology* 36.2 (1950), pp. 149–158. ISSN: 1553-0809. DOI: 10.1002/jcp.1030360203. URL: http://dx.doi.org/10.1002/jcp.1030360203.

[4] Mark-Anthony Bray et al. "Experimental and Theoretical Analysis of Phase Singularity Dynamics in Cardiac Tissue". In: *Journal of Cardiovascular Electrophysiology* 12.6 (2001), pp. 716–722. ISSN: 1540-8167. DOI: 10.1046/j.1540-8167.2001.00716.x. URL: http://dx.doi.org/10.1046/j.1540-8167.2001.00716.x.

[5] Mei-Yu Chen, Robert H. Insall, and Peter N. Devreotes. "Signaling through chemoattractant receptors in Dictyostelium". In: *Trends in Genetics* 12.2 (1996), pp. 52–57. ISSN: 0168-9525. DOI: http://dx.doi.org/10.1016/0168-9525(96)81400-4. URL: http:

/ / www . sciencedirect . com / science / article / pii / 0168952596814004.

[6] Jan Christoph. “Intramural Visualization of Scroll Waves in the Heart”. PhD thesis. Göttingen Graduate School for Neurosciences, Biophysics and Molecular Biosciences: Georg-August-University, Göttingen, Oct. 2014.

[7] M. C. Cross and P. C. Hohenberg. “Pattern formation outside of equilibrium”. In: *Rev. Mod. Phys.* 65 (3 July 1993), pp. 851–1112. DOI: 10.1103/RevModPhys.65.851. URL: https://link.aps.org/doi/10.1103/RevModPhys.65.851.

[8] Michael Cross and Henry Greenside. *Pattern Formation and Dynamics in Nonequilibrium Systems*. Cambridge University Press, 2009. ISBN: 978-0-521-77050-7.

[9] Jorge M. Davidenko, Arcady V. Pertsov, and et al et. “Stationary and Drifting Spiral Waves of Excitation in Isolated Cardiac Muscle”. English. In: *Nature* 355.6358 (Jan. 1992). Copyright - Copyright Macmillan Journals Ltd. Jan 23, 1992; Last updated - 2012-11-14; CODEN - NATUAS, pp. 349–51. URL: https://search.proquest.com/docview/204425923?accountid=104741.

[10] Peter N. Devreotes, Michael J. Potel, and Stephen A. MacKay. “Quantitative analysis of cyclic AMP waves mediating aggregation in Dictyostelium discoideum”. In: *Developmental Biology* 96.2 (1983), pp. 405–415. ISSN: 0012-1606. DOI: http://dx.doi.org/10.1016/0012-1606(83)90178-1. URL: http://www.sciencedirect.com/science/article/pii/0012160683901781.

[11] Peter N. Devreotes and Sally H. Zigmond. "Chemotaxis in Eukaryotic Cells: A Focus on Leukocytes and Dictyostelium". In: *Annual Review of Cell Biology* 4.1 (1988). PMID: 2848555, pp. 649–686. DOI: 10.1146/annurev.cb.04.110188.003245. URL: https://doi.org/10.1146/annurev.cb.04.110188.003245.

[12] Dirk Dormann and Cornelis J. Weijer. "Propagating chemoattractant waves coordinate periodic cell movement in Dictyostelium slugs". In: *Development* 128.22 (2001), pp. 4535–4543. ISSN: 0950-1991. eprint: http://dev.biologists.org/content/128/22/4535.full.pdf. URL: http://dev.biologists.org/content/128/22/4535.

[13] Dirk Dormann et al. "cAMP receptor affinity controls wave dynamics, geometry and morphogenesis in Dictyostelium". In: *Journal of Cell Science* 114.13 (2001), pp. 2513–2523. ISSN: 0021-9533. eprint: http://jcs.biologists.org/content/114/13/2513.full.pdf. URL: http://jcs.biologists.org/content/114/13/2513.

[14] A.J. Durston. "Pacemaker activity during aggregation in Dictyostelium discoideum". In: *Developmental Biology* 37.2 (1974), pp. 225–235. ISSN: 0012-1606. DOI: http://dx.doi.org/10.1016/0012-1606(74)90144-4. URL: http://www.sciencedirect.com/science/article/pii/0012160674901444.

[15] Martin Falcke and Herbert Levine. "Pattern Selection by Gene Expression in Dictyostelium Discoideum". In: *Phys. Rev. Lett.* 80 (17 Apr. 1998), pp. 3875–3878. DOI: 10.1103/PhysRevLett.80.3875. URL: https://link.aps.org/doi/10.1103/PhysRevLett.80.3875.

[16] Jakob Franke et al. "Cyclic nucleotide phosphodiesterase of Dictyostelium discoideum and its glycoprotein inhibitor: Structure and expression of

their genes". In: *Developmental Genetics* 12.1-2 (1991), pp. 104–112. ISSN: 1520-6408. DOI: 10.1002/dvg.1020120118. URL: http://dx.doi.org/10.1002/dvg.1020120118.

[17] Gene L Garcia et al. "The Group Migration of Dictyostelium Cells Is Regulated by Extracellular Chemoattractant Degradation". In: *Molecular Biology of the Cell* 20.14 (July 2009). Ed. by Jean E Schwarzbauer, pp. 3295–3304. DOI: 10.1091/mbc.E09-03-0223. URL: http://www.ncbi.nlm.nih.gov/pmc/articles/PMC2710833/.

[18] G Gerisch. "Chemotaxis in Dictyostelium". In: *Annual Review of Physiology* 44.1 (1982). PMID: 6280593, pp. 535–552. DOI: 10.1146/annurev.ph.44.030182.002535. URL: https://doi.org/10.1146/annurev.ph.44.030182.002535.

[19] Günther Gerisch. "Cell Aggregation and Differentiation in Dictyostelium". In: *Current Topics in Developmental Biology* 3 (1968), pp. 157–197. ISSN: 0070-2153. DOI: http://dx.doi.org/10.1016/S0070-2153(08)60354-3. URL: http://www.sciencedirect.com/science/article/pii/S0070215308603543.

[20] Christiane Hilgardt, Stefan C Müller, and Marc-Thorsten Hütt. "Reconstruction of cellular variability from spatiotemporal patterns of Dictyostelium discoideum". In: *Nonlinear Biomedical Physics* 1 (2007), pp. 10–10. DOI: 10.1186/1753-4631-1-10. URL: http://www.ncbi.nlm.nih.gov/pmc/articles/PMC2034575/.

[21] R. H. Kessin. *Dictyostelium*. Cambridge University Press, 2001. ISBN: 0521583640.

[22] David A. Kessler and Herbert Levine. “Pattern formation in Dictyostelium via the dynamics of cooperative biological entities”. In: *Phys. Rev. E* 48 (6 Dec. 1993), pp. 4801–4804. DOI: 10.1103/PhysRevE.48.4801. URL: https://link.aps.org/doi/10.1103/PhysRevE.48.4801.

[23] J.Y. Kim, J.A. Borleis, and P.N. Devreotes. “Switching of Chemoattractant Receptors Programs Development and Morphogenesis in Dictyostelium:Receptor Subtypes Activate Common Responses at Different Agonist Concentrations”. In: *Developmental Biology* 197.1 (1998), pp. 117–128. ISSN: 0012-1606. DOI: http://dx.doi.org/10.1006/dbio.1998.8882. URL: http://www.sciencedirect.com/science/article/pii/S0012160698988820.

[24] Alan R. Kimmel and Richard A. Firtel. “cAMP signal transduction pathways regulating development of Dictyostelium discoideum”. In: *Current Opinion in Genetics & Development* 1.3 (1991), pp. 383–390. ISSN: 0959-437X. DOI: https://doi.org/10.1016/S0959-437X(05)80304-1. URL: http://www.sciencedirect.com/science/article/pii/S0959437X05803041.

[25] Claudette Klein. “Adenylate cyclase activity in Dictyostelium discoideum amoebae and its changes during differentiation”. In: *FEBS Letters* 68.1 (1976), pp. 125–128. ISSN: 0014-5793. DOI: http://dx.doi.org/10.1016/0014-5793(76)80419-X. URL: http://www.sciencedirect.com/science/article/pii/001457937680419X.

[26] Claudette Klein. “Changes in adenylate cyclase during differentiation of Dictyostelium discoideum”. In: *FEMS Microbiology Letters* 1.1 (1977),

pp. 17–19. ISSN: 0378-1097. DOI: http://dx.doi.org/10.1016/0378-1097(77)90102-1. URL: http://www.sciencedirect.com/science/article/pii/0378109777901021.

[27] PS Klein et al. "A chemoattractant receptor controls development in Dictyostelium discoideum". In: *Science* 241.4872 (1988), pp. 1467–1472. ISSN: 0036-8075. DOI: 10.1126/science.3047871. eprint: http://science.sciencemag.org/content/241/4872/1467.full.pdf. URL: http://science.sciencemag.org/content/241/4872/1467.

[28] Paul Kriebel and Carole Parent. "Adenylyl Cyclase Expression and Regulation During the Differentiation of Dictyostelium Discoideum". In: *IUBMB Life* 56.9 (2004), pp. 541–546. ISSN: 1521-6551. DOI: 10.1080/15216540400013887. URL: http://dx.doi.org/10.1080/15216540400013887.

[29] Jacques Lauzeral, José Halloy, and Albert Goldbeter. "Desynchronization of cells on the developmental path triggers the formation of spiral waves of cAMP during Dictyostelium aggregation". In: *Proceedings of the National Academy of Sciences of the United States of America* 94.17 (Aug. 1997), pp. 9153–9158. URL: http://www.ncbi.nlm.nih.gov/pmc/articles/PMC23083/.

[30] Kyoung J. Lee, Raymond E. Goldstein, and Edward C. Cox. "Resetting Wave Forms in Dictyostelium Territories". In: *Phys. Rev. Lett.* 87 (6 July 2001), p. 068101. DOI: 10.1103/PhysRevLett.87.068101. URL: https://link.aps.org/doi/10.1103/PhysRevLett.87.068101.

[31] H Levine et al. “Positive genetic feedback governs cAMP spiral wave formation in Dictyostelium”. In: *Proceedings of the National Academy of Sciences* 93.13 (1996), pp. 6382–6386. eprint: http://www.pnas.org/content/93/13/6382.full.pdf. URL: http://www.pnas.org/content/93/13/6382.abstract.

[32] D Malchow et al. “Membrane-Bound Cyclic AMP Phosphodiesterase in Chemotactically Responding Cells of Dictyostelium discoideum”. In: *European Journal of Biochemistry* 28.1 (1972), pp. 136–142. ISSN: 1432-1033. DOI: 10.1111/j.1432-1033.1972.tb01894.x. URL: http://dx.doi.org/10.1111/j.1432-1033.1972.tb01894.x.

[33] Jean-Louis Martiel and Albert Goldbeter. “A Model Based on Receptor Desensitization for Cyclic AMP Signaling in Dictyostelium Cells”. In: *Biophysical Journal* 52.5 (1987), pp. 807–828. ISSN: 0006-3495. DOI: http://dx.doi.org/10.1016/S0006-3495(87)83275-7. URL: http://www.sciencedirect.com/science/article/pii/S0006349587832757.

[34] Hans Meinhardt. “Models of Biological Pattern Formation: From Elementary Steps to the Organization of Embryonic Axes”. In: *Current Topics in Developmental Biology* 81 (2008). Multiscale Modeling of Developmental Systems, pp. 1–63. ISSN: 0070-2153. DOI: http://dx.doi.org/10.1016/S0070-2153(07)81001-5. URL: http://www.sciencedirect.com/science/article/pii/S0070215307810015.

[35] Ehud Meron. “Pattern formation in excitable media”. In: *Physics Reports* 218.1 (1992), pp. 1–66. ISSN: 0370-1573. DOI: http://dx.doi.org/10.1016/0370-1573(92)90098-K. URL: http:

/ / www . sciencedirect . com / science / article / pii / 037015739290098K.

[36] James D. Murray. *Mathematical Biology*. Berlin, Heidelberg: Springer Berlin Heidelberg, 1993, pp. 232–253. ISBN: 978-3-662-08542-4. DOI: 10.1007/978-3-662-08542-4_9. URL: http://dx.doi.org/10.1007/978-3-662-08542-4_9.

[37] Peter C. Newell. "Aggregation and Cell Surface Receptors in Cellular Slime Molds". In: *Microbial Interactions*. Ed. by J. L. Reissig. Boston, MA: Springer US, 1977, pp. 1–57. ISBN: 978-1-4615-9698-1. DOI: 10.1007/978-1-4615-9698-1_1. URL: http://dx.doi.org/10.1007/978-1-4615-9698-1_1.

[38] N. Oikawa et al. "Effect of substrate on pattern formation and synchronization time in cell-cell signaling". Manuscript in preparation.

[39] E Pálsson and E C Cox. "Origin and evolution of circular waves and spirals in Dictyostelium discoideum territories". In: *Proceedings of the National Academy of Sciences* 93.3 (1996), pp. 1151–1155. eprint: http://www.pnas.org/content/93/3/1151.full.pdf.

[40] E Pálsson et al. "Selection for spiral waves in the social amoebae Dictyostelium". In: *Proceedings of the National Academy of Sciences* 94.25 (1997), pp. 13719–13723. eprint: http://www.pnas.org/content/94/25/13719.full.pdf. URL: http://www.pnas.org/content/94/25/13719.abstract.

[41] G E Powell and I C Percival. "A spectral entropy method for distinguishing regular and irregular motion of Hamiltonian systems". In: *Journal of*

Physics A: Mathematical and General 12.11 (1979), p. 2053. URL: http://stacks.iop.org/0305-4470/12/i=11/a=017.

[42] Kenneth B Raper. "Dictyostelium discoideum, a new species of slime mold from decaying forest leaves". In: *Journal of Agricultural Research* 50.2 (1935), pp. 135–148.

[43] V. Riedel and G. Gerisch. "Regulation of extracellular cyclic-AMP-phosphodiesterase activity during development of dictyostelium discoideum". In: *Biochemical and Biophysical Research Communications* 42.1 (1971), pp. 119–124. ISSN: 0006-291X. DOI: http://dx.doi.org/10.1016/0006-291X(71)90370-6. URL: http://www.sciencedirect.com/science/article/pii/0006291X71903706.

[44] Satoshi Sawai, Peter A. Thomason, and Edward C. Cox. "An autoregulatory circuit for long-range self-organization in Dictyostelium cell populations". In: *Nature* 433.7023 (Jan. 2005), pp. 323–326. URL: http://dx.doi.org/10.1038/nature03228.

[45] FLORIAN SIEGERT and CORNELIS WEIJER. "Digital image processing of optical density wave propagation in Dictyostelium discoideum and analysis of the effects of caffeine and ammonia". In: *Journal of Cell Science* 93.2 (1989), pp. 325–335. ISSN: 0021-9533. URL: http://jcs.biologists.org/content/93/2/325.

[46] KJ Tomchik and PN Devreotes. "Adenosine 3',5'-monophosphate waves in Dictyostelium discoideum: a demonstration by isotope dilution–fluorography". In: *Science* 212.4493 (1981), pp. 443–446. ISSN: 0036-8075. DOI: 10.1126/science.6259734. eprint: http://science.

sciencemag.org/content/212/4493/443.full.pdf. URL: http://science.sciencemag.org/content/212/4493/443.

[47] John J. Tyson and James P. Keener. "Singular perturbation theory of traveling waves in excitable media (a review)". In: *Physica D: Nonlinear Phenomena* 32.3 (1988), pp. 327–361. ISSN: 0167-2789. DOI: http://dx.doi.org/10.1016/0167-2789(88)90062-0. URL: http://www.sciencedirect.com/science/article/pii/0167278988900620.

[48] John J. Tyson et al. "Spiral waves of cyclic amp in a model of slime mold aggregation". In: *Physica D: Nonlinear Phenomena* 34.1 (1989), pp. 193–207. ISSN: 0167-2789. DOI: http://dx.doi.org/10.1016/0167-2789(89)90234-0. URL: http://www.sciencedirect.com/science/article/pii/0167278989902340.

[49] Cornelis J Weijer. "Dictyostelium morphogenesis". In: *Current Opinion in Genetics & Development* 14.4 (2004), pp. 392–398. ISSN: 0959-437X. DOI: https://doi.org/10.1016/j.gde.2004.06.006. URL: http://www.sciencedirect.com/science/article/pii/S0959437X04000851.

[50] A. T. Winfree. *The geometry of biological time*. Springer-Verlag, 1980. ISBN: 978-3-540-52528-8.

[51] Arthur T. Winfree. "Spiral Waves of Chemical Activity". In: *Science* 175.4022 (1972), pp. 634–636. ISSN: 0036-8075. DOI: 10.1126/science.175.4022.634. eprint: http://science.sciencemag.org/content/175/4022/634.full.pdf. URL: http://science.sciencemag.org/content/175/4022/634.

[52] R.P. Yeh, F.K. Chan, and M.B. Coukell. “Independent regulation of the extracellular cyclic AMP phosphodiesterase-inhibitor system and membrane differentiation by exogenous cyclic AMP in Dictyostelium discoideum”. In: *Developmental Biology* 66.2 (1978), pp. 361–374. ISSN: 0012-1606. DOI: http://dx.doi.org/10.1016/0012-1606(78)90245-2. URL: http://www.sciencedirect.com/science/article/pii/0012160678902452.

CHAPTER 4

CELLS "REMEMBER" HUNGER

Kaumudi H Prabhakara, Azam Gholami, Vladimir S Zykov, Eberhard Bodenschatz *To be submitted*

4.1 Abstract

We demonstrate the existence of long-term starvation memory in the amoebae *Dictyostelium discoideum (D.d.)* for the first time. We subject populations of *D.d.* to starvation, feeding and starvation again. By analyzing patterns formed by the starving populations of *D.d.* for different intermediate feeding durations, we find that the populations have a starvation memory of about an hour. We explain the origin of this memory through the de-regulation of the biochemical parameters involved in signaling. We simulate our experiment using a modified version of a well-known model, and reproduce its basic features.

4.2 Introduction

Memory is an intriguing concept. It is usually associated with the brain, the complexity of which is slowly being unraveled. Surprisingly, many primitive life forms that do not possess brains have recently been shown to exhibit memory. In populations of *Escherichia coli*, two kinds of memory have been discovered [17]. One, termed phenotypic memory, functions by the transmission of proteins through generations, and the other, the response memory, occurs due

to a hysteric behavior in the genetic network, which allows the cells to respond even after the stimulus is removed. Recently, Nakagaki and co-workers found that the amoebae *Physarum polycephalum* can not only "learn" patterns of shocks that it is subjected to, but also anticipate upcoming shocks by altering its behavior [26, 20]. The memory of the shock pattern persists for hours after the shocks have been stopped [21]. This behavior has been ascribed to intelligence and memory. In another study, it was found that the bacterium *Caulobacter crescentus* on its own cannot "remember" stress; but populations of these bacteria displayed memory-like response to periodic salt stresses [19]. Populations of yeast evolve special genetic pathways to anticipate changing stressful environments [8].

While the above examples provide evidence of the existence of memory in microbes, it is to be noted that the concepts of adaptation and memory have been used interchangeably. Therefore, before continuing, it is imperative to define what we mean by memory. Following [4], we define a system to have memory if its present state is determined not only by the present conditions, but also by the path by which the system reached the present state. With this definition in mind, we see that all the systems described above qualify as having memory. In this work, we probe the existence of memory in the amoebae *Dictyostelium discoideum (D.d)*.

D.d. is a unicellular organism that lives in the soil. When food is available in plenty, it feeds and divides. But when nutrients become scarce, it emits a chemical, cyclic adenosine monophosphate (cAMP), which diffuses into the surroundings [25, 2]. An enzyme, phosphodiesterase (PDE), also secreted by the cells, degrades cAMP, creating a reaction-diffusion system [12]. The response

of the cells to cAMP can be visualized as large scale (wavelength $\approx$ 2 mm) spiral and target waves using dark-field optics [1, 11, 30, 28]. After a few hours of signaling, the cells stream towards the center of the spirals or target waves through chemotaxis [7, 10] and form aggregates. These aggregates then form multicellular slugs and fruiting bodies with spores on the top. The spores can germinate into amoebae when the conditions are more favorable. Thus, this signaling mechanism enables *D.d.* to survive stressful starvation periods.

Consider a situation where these populations of *D.d.*, after a period of starvation, find nutrients for some time, and then starve again. Does their previous experience of starvation change their behavior? In other words, do these cells have a memory of starvation? So far, memory in *D.d* has only been studied on short time scales. When a cAMP wave passes over a cells, during the wave front, the chemotactic gradient is towards the center of the pattern, whereas during the wave-back, it is in the opposite direction. So the cell should move towards the center for half the wave period and reverse its direction for the second half of the period, rendering aggregation impossible. This has been termed the "chemotactic paradox". But it is well-known, that the cell only moves towards the center of the pattern. What prevents it from moving in the reverse direction during the wave-back? In a previous work, it was shown that cells have a short term adaptive memory that ensures that they do not travel backwards during the wave-back [29]. Previous theoretical works also postulated the presence of adaptations for the cells to overcome the paradox [13]. While these works deal with memory and adaptation on the order of a few minutes, long term memory in populations of *D.d.* has not been explored.

In our previous work, we showed that the patterns formed by the starving

populations of *D.d.* depend on their developmental stage [24]. To have populations at different developmental stages, we starved the populations in a flask under constant shaking for different durations before plating them on a dish. We observed that the spiral density decreases as the populations are initially starved for longer durations. In particular, the spiral density was a minimum for 5 h of initial starvation time [24]. As a consequence, the domains of the spirals was largest there. Further, the populations initially starved for longer durations synchronized faster. (See figures 1 and 2 in [24].) In this work, we use this knowledge to answer the question: can populations remember being starved? As described below, our experiments show the existence of "memory" in populations of *D.d*.

4.3 Results

We starved populations of *D.d* (about 3.5 million cells/ml) in a shaker for 5h. Then, we re-suspended the populations in a nutrient rich medium for different durations. Next, we starved the populations on a Petri-dish, observing the patterns formed with dark field optics. (See Supplementary material.) We varied the feeding duration from 20 min to 4 h and found that the patterns formed by the starving populations depended on the feeding duration. Fig. 4.1 shows some of the different patterns observed. With 20 min - 40 min of feeding, the pattern formation began within an hour with targets patterns. A few, large spirals were formed, which entrained the targets. For feeding times of around an hour, target patterns began to form around 1h or 1.5 h after start of starvation, and the spirals took over at later stages. The number of spirals formed increased with increasing feeding time. For feeding times longer then 2 h, pattern forma-

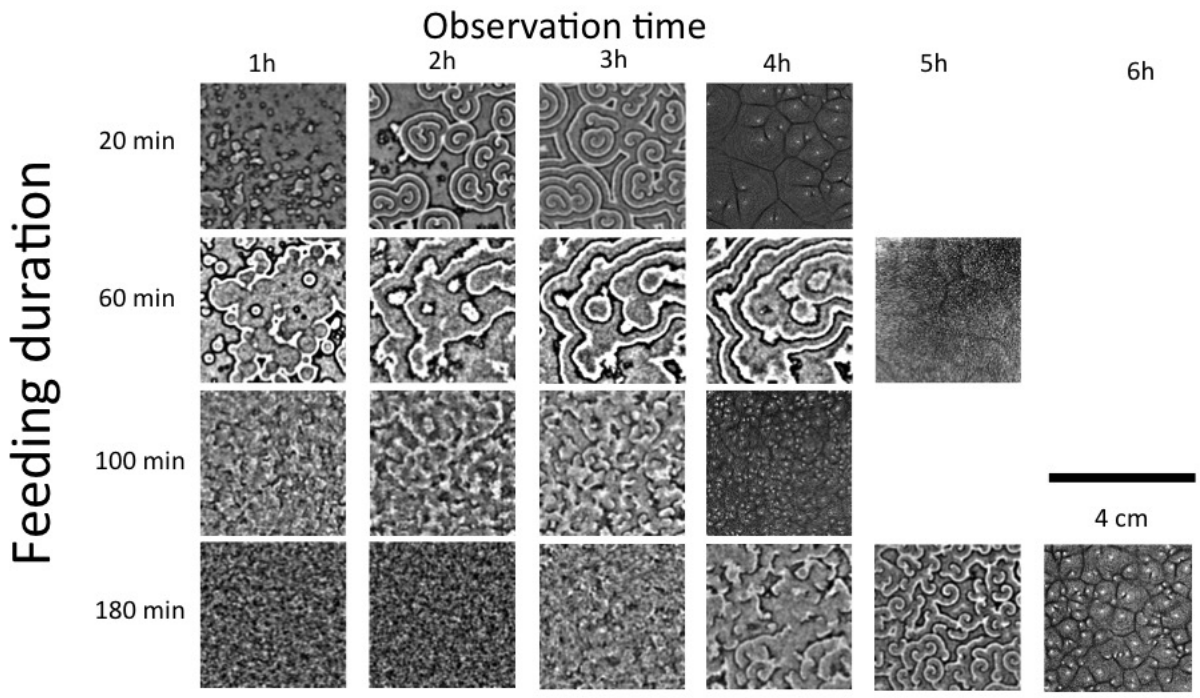

Figure 4.1: Patterns observed as a function of time for different feeding durations.

tion began after a longer time. In these cases, no targets were observed, but numerous small spirals were formed. The pattern formation was similar to the patterns formed by populations without a history of starvation. From fig. 4.1 it can be noted that for feeding durations of about one hour, the patterns were very different. Large scale waves that are almost planar are formed. This hinted that one hour of feeding was close to the transition point.

To quantify these patterns, we measured two order parameters. First, we measured the time taken by the populations to synchronize with each other to form the large scale patterns. This onset of synchronization, T_{syn}, is quantified by the time at which the spectral entropy, S, given by eq. 4.1, begins to decrease, indicating an increase in order.

$$S(t) = -\sum_i p_i log(p_i) \tag{4.1}$$

Here, p_i refers to the amplitude of the i^{th} frequency of the normalized power spectrum. (See supplementary material.)

The second order parameter is the spiral density, i.e., the number of spiral cores in unit area. Spiral cores are phase singularities. The winding number n, (± 1 for one armed spirals), is non-zero only if the integral over the phase ϕ in eq. 4.2 encloses a singularity.

$$n.2\pi = \oint \vec{\nabla}\phi.\vec{dl} \tag{4.2}$$

We quantify the spiral density ρ_s by counting the number of persistent phase singularities in the patterns. (See supplementary material.) The results are shown in fig. 4.2. We measured the oscillation period for the different patterns by taking the Fourier transform of the intensity time series. All the spirals have a lower oscillation period of around 5-6 min, whereas the targets have a higher oscillations period of about 10 min. This is a well-known phenomenon, which enables the spirals to entrain the targets, if they co-exist. As the feeding time increases from zero feeding, the populations need more time to synchronize. Between 40 min and 1h40 min, the populations need about the same time to synchronize. For feeding times longer than 1h40min, the populations need a longer time to synchronize. The blue dashed lines in fig. 4.2a correspond to the upper and lower limit of T_{syn} for populations that have had no history of starvation, i.e., populations which just started starving for the first time. Fig. 4.2b shows the variation in spiral density for different feeding durations. The spiral density initially does not change appreciably; for feeding durations around 40 min to 1 h, very few spirals are formed. The spiral density then increases with feeding duration. As before, the dashed lines in fig. 4.2b correspond to the upper and lower limit of ρ_s for populations that have had no history of starvation.

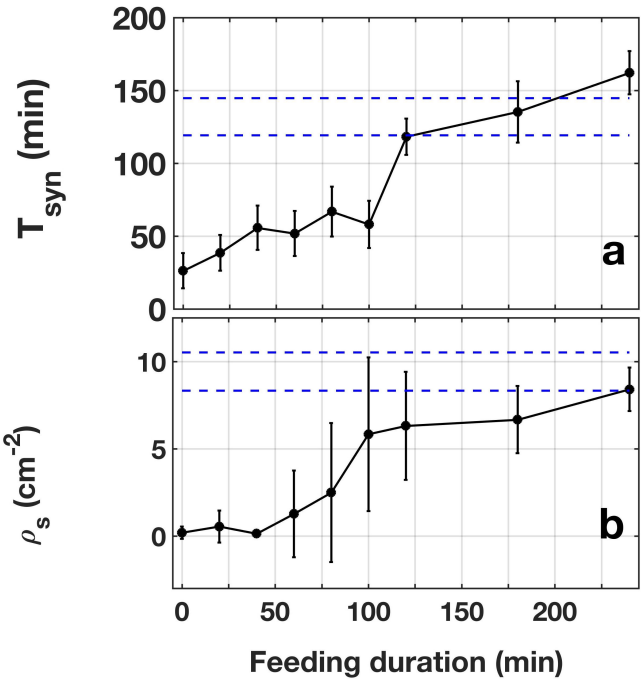

Figure 4.2: The order parameters (a) T_{syn}, representing the onset of synchronization, and (b) ρ_s, representing spiral density, as a function of feeding duration for the experimental data. The dashed blue lines represent the limits of the two parameters for a population without any starvation history.

4.4 Discussion

We have observed that the behavior of cell populations depends on their history. Our earlier definition of memory implies that *D.d* populations indeed possess memory. Populations that were fed for around 2 h and more behaved very similar to populations that had not been starved before. So, we hypothesize that feeding the populations for 2 h or longer erases the memory of starvation. Further, in fig. 4.2, we notice that the error bars in spiral density are much larger for populations that were fed for around an hour than for other feeding durations. The error bars represent standard deviations from different experiments. For populations fed for around 1 h, very few spirals were formed in some experi-

ments while large number of spirals were formed in others, giving rise to the large error bars. In statistical mechanics, it is well-known that large fluctuations occur close to phase transitions [22]. Therefore, we propose that the transition from having a starvation memory to having no memory occurs around 1h of feeding. However, it is important to note that the time at which the transition from memory to no memory could very well be dependent on the initial starvation duration, which was fixed to be 5 h for all the experiments here. In a population starved for just an hour, for example, the effect of intermediate feeding may be negligible. We chose 5 h of initial starvation time because (1) the patterns formed in these populations are drastically different from the patterns formed in populations with zero initial starvation time, as we have shown in our previous work [24] and (2) for populations starved longer than 5 h, the signal quality decreases [24].

But what does memory mean in the context of populations of *D.d*, which do not have developed nervous systems? In our previous work [24], we had proposed that as populations of *D.d* starve, their biochemical parameters, such as rate of degradation of cAMP, amount of cAMP produced, the refractory period, etc., vary in a certain manner (see fig. 5 in [24] or the grey dashed lines in fig. 4.3). This variation was necessary to simulate the experimental results. Biochemical experiments by various groups found similar trends in for the variation of these parameters with starvation time for populations of *D.d.* [18, 16, 32, 15, 9]. Here, we interpret memory in terms of de-regulation of these biochemical parameters.

The populations were initially starved for 5h, during which time, the biochemical parameters evolved to certain values. At 5h of starvation, these pop-

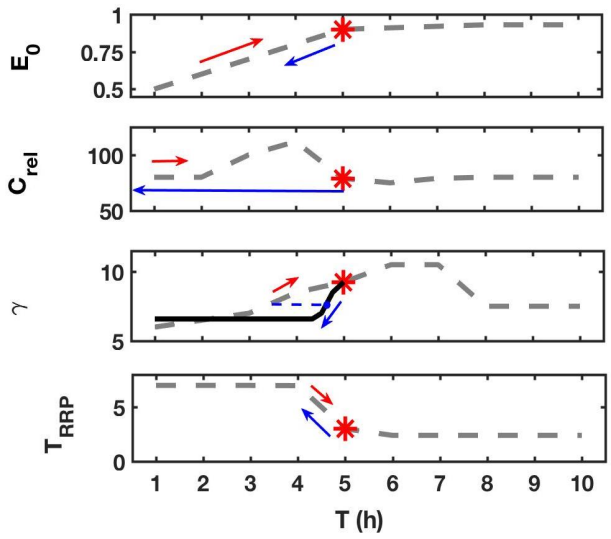

Figure 4.3: The grey dashed lines represent the temporal variation of the parameters E_0, the initial excitability, C_{rel}, the amount of cAMP released, γ, the degradation rate, and T_{RRP}, the duration of the relative refractive period, as a function of the initial starvation time T, as presented in our previous work [24]. The red star represents the parameters values after 5h of initial starvation. The blue arrows represent the path along which the parameters de-regulate during feeding. The red arrows indicate the evolution of the parameters when the populations starve again. E_0 and T_{RRP} are deregulated along the dashed curve. Since C_{rel} is close to the basal value, no matter how long the feeding time, it increases from its value at zero initial starvation. γ decreases rapidly and then stays constant, as represented by the thick black line. After a feeding duration, suppose γ has decreased to the point represented by the blue dot. If the population begins to starve at this point, the evolution of γ will continue along the grey dashed line from the value corresponding to the value of γ at that time.

ulations were fed. What happens to the parameters during feeding? Do they remain where they are, do they return to their basal values, or do they continue to evolve? Our experiments clearly indicate that the parameters do not remain where they are – if they did, no matter how long the feeding duration, the patterns formed during the subsequent starvation should have looked like the patterns formed in populations starved for 5h with no feeding, which is not what we observe. Further, our results also suggest that the parameters do not continue to evolve. Consider, for example, a population that was fed for 2 h. If the parameters had continued to evolve, then after 2 h, the parameters would have reached values corresponding to 7 h of starvation. From our previous work [24], we know what the patterns formed in populations starved for 7 h look like – only target patterns and no spirals are formed, and these patterns are formed within an hour. However, here we have seen that the populations fed for 2 h form spirals and no target patterns, after a couple of hours. Therefore, we can rule out the possibility of the parameters continuing to evolve when the cells are in a nutrient rich environment. This leaves us with the idea that the populations de-regulate their parameters during nutrient availability.

Before exploring the de-regulation of the parameters, it is important to understand what these parameters mean. A detailed discussion is available in [24]. Here, we present the main features of the model and its parameters. We use the model originally proposed Kessler-Levine [14], modified by Sawai et al. [27] and modified by us in a previous work [24]. The model simulates the collective dynamics of bions placed on a 2D grid, each point of which is represented by (i, j). $C_{i,j}$, $E_{i,j}$ and $C_{i,j}^{thresh}$ represent the concentration of cAMP, the excitability and the threshold concentration required for emission of cAMP at a grid point. The dynamics of the bions obeys the following equations:

$$\dot{C}_{i,j} = D \cdot L(C_{i,j}) - \gamma(t) \cdot C_{i,j} + \theta \cdot C_{rel}(t) \tag{4.3}$$

$$\dot{E}_{i,j} = \eta + \beta \cdot C_{i,j}; \quad E_{i,j} \leq E_{max} \tag{4.4}$$

$$C_{i,j}^{thresh} = \left[C_{max} - A(T_{RRP}(t)) \frac{\tau}{\tau + T_{ARP}} \right] (1 - E_{i,j}) \tag{4.5}$$

$$0 < \tau < T_{RRP}(t)$$

L is the discrete Laplacian operator, controlling diffusion, and θ is a step function – it is 1, if $C_{i,j} \geq C_{i,j}^{thresh}$ and 0 otherwise. (It is always zero in the absolute refractory phase, as described below.) Initially, the bions are excitable. If the concentration C of cAMP exceeds a threshold C^{thresh}, the bions emit cAMP at a rate C_{rel}/min for 1 min. Immediately after emission, they enter an absolute refractory state, where they are incapable of emitting cAMP for a fixed time, $T_{ARP} = 2\ min$. Next, the bions go into a relative refractory state, which has a high threshold for emission of cAMP. This state lasts for T_{RRP} min. The threshold required for cAMP release decreases throughout this state (as τ, the time spent in the relative refractory phase, increases from 0 to T_{RRP}) and reaches a minimum at the end of this state (in accordance with equation (5.8)), after which the bions are excitable again and the cycle continues. The cAMP is degraded at a rate γ/min. It is important to note that the degradation rate is the cumulative effect of the enzyme phosphodiesterase and its inhibitor. The excitability of the cells E, increases autonomously, with $\eta = 0.0001/min$ and is proportional to C with a coupling $\beta = 0.005/min$. It saturates at a fixed value $E_{max} = 0.93$ (equation (5.7)). The time spent in the relative refractory phase (τ) and the excitability (E), determine the concentration of cAMP required to cause emission of cAMP by a bion. Highly excitable bions (high E) have a very low threshold for initiating cAMP emission and can be easily excited to release cAMP, whereas bions with

low excitability have a higher threshold and are not easily excitable. C_{max} = 100 is a constant describing the maximum value of the threshold required for emission of cAMP, D = 0.00138 mm^2/min is the diffusion coefficient and the constant $A = (T_{RRP} + T_{ARP})(C_{max} - C_{min})/T_{RRP}$ is chosen so that the threshold is maximum when the bions enter the relative refractory state and minimum when they leave it. All bions fire randomly with a probability of 10^{-4} per grid point per time step. The rules of the fixed duration of the absolute refractory phase and the saturation of the excitability are implemented at each bion separately from these equations. The threshold required for cAMP release, C^{thresh} is calculated at each bion, at each time step. The equations (5.6 - 5.8) are solved using the explicit Euler method with a grid size of 0.06 mm and time step of 0.01 min. We chose the initial excitabilities based on initial starvation time - longer the initial starvation time, higher the initial excitability (fig. 4.3). To capture the spatial heterogeneity, we measured the cell distribution (see Supplementary material), and incorporated it into the model. Most importantly, we introduced a temporal variation for three parameters of the model, the degradation rate, the amount of cAMP released, and the duration of the relative refractory phase. These three parameters change with starvation time, as shown in fig. 4.3.

To understand our experimental results here, first consider the parameter C_{rel}. From fig. 4.3, we see that at 5 h after starvation, C_{rel} is already at the basal level (indicated by a star in fig. 4.3). Since cAMP is not required when nutrients are available, we assume that rather than following the path backwards, which calls for increasing C_{rel}, it remains at that value throughout the feeding stage. On subsequent starvation, C_{rel} increases as if it were starting from that basal value and continues along the developmental path (shown by the red arrow in fig. 4.3). The degradation rate is at a value higher than its basal value after 5h of

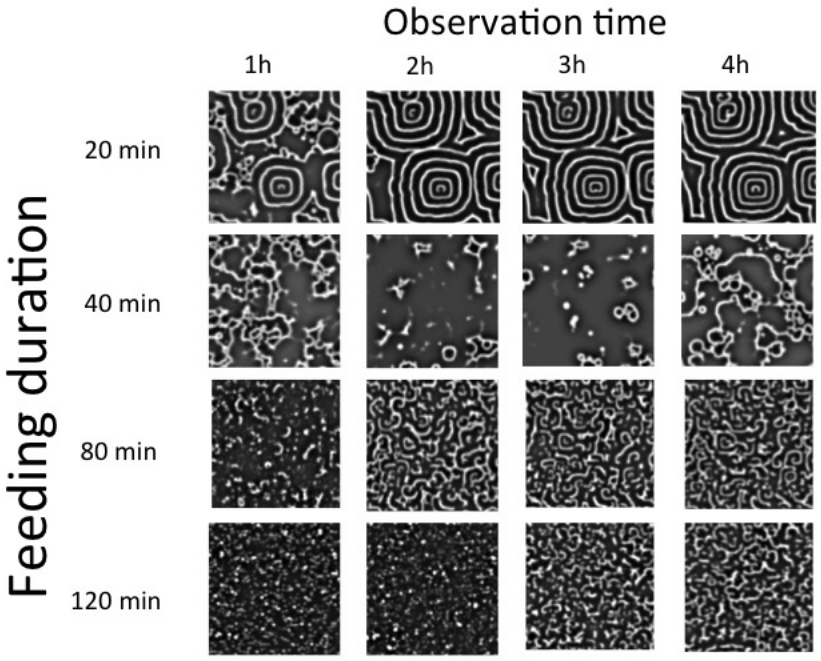

Figure 4.4: Patterns observed as a function of time for different feeding durations in simulations. The side corresponds to 1 cm. The feeding durations shown here are different from the feeding durations shown in fig. 4.1. These feeding durations were chosen to represent the different kinds of patterns produced by the model.

starvation (indicated by a star in fig. 4.3). For this parameter, we tried various paths of de-regulation. The path that best reproduced our experimental results was decreasing it about 4.25 times faster than a linear decrease in time and saturation at a value higher than the basal value. For instance, when the population was fed for 20 min, γ decreased 4.25 times faster than a linear decrease, and at the end of feeding its value corresponded to the value at 5 h - (4.25 x 20/60) h = 3.6 h, rather than 5 h - (20/60) h = 4.7 h. However, for populations fed for longer than 40 min, γ was around 6 /min. The black line in fig. 4.3 shows this de-regulation. On subsequent starvation, the value of γ increases along the dashed line starting from the point corresponding to its current value. This is

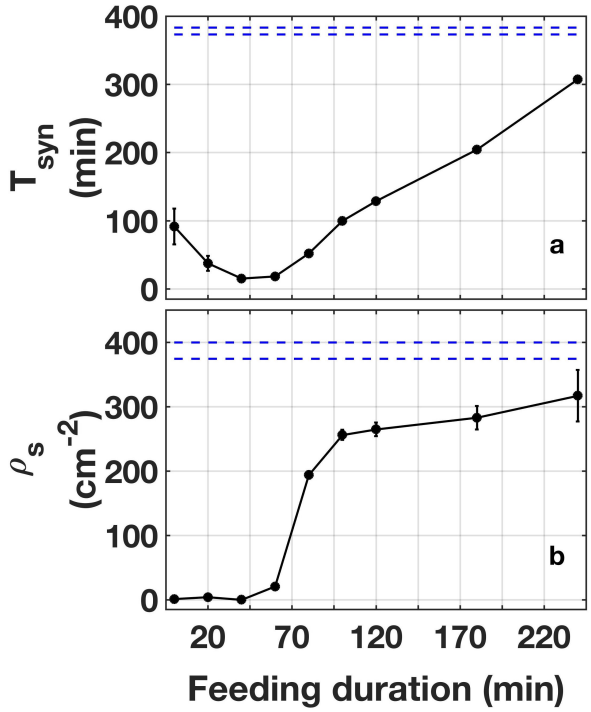

Figure 4.5: The order parameters (a) T_{syn}, representing the onset of synchronization, and (b) ρ_s, representing spiral density, as a function of feeding duration for the patterns obtained in simulations. The dashed blue lines represent the limits of the two parameters for a population without any starvation history.

shown by the blue dashed line in fig. 4.3.

The initial excitability and the duration of the refractory period were decreased linearly with time i.e., these two parameters returned to their basal values along the curves shown in fig. 4.3.

With these assumptions, we were able to semi-quantitatively reproduce our experimental results. Representative patterns produced in the simulations are shown in fig. 4.4. Fig. 4.5 shows the order parameters of these simulation patterns, measured similar to experimental patterns. Comparing these two figures to fig. 4.1 and fig. 4.2, we see that there is a qualitative agreement – the spi-

ral density decreases to zero around 40 min of feeding and then increases. The synchronization time increases with increasing feeding time after a plateau.

However, in the simulation results, the plateau in T_{syn} around 1 h of feeding occurs at a value lower than T_{syn} for 0 h of feeding, whereas in experiments, the plateau occurs at a value higher than T_{syn} for 0 h of feeding. We attribute the lack of quantitative agreement to our assumptions. The aim of the simulations presented here, is only to put forth the idea that memory can be explained by the manner in which the parameters are de-regulated. Given the large dimensional parameter space of the model, a mathematically rigorous method is necessary to find the "correct" de-regulation.

To conclude, we have shown the existence of long term starvation memory that lasts for about an hour, for the first time in populations of *D.d*. Despite the assumptions made, we can hypothesize that memory is manifested through the de-regulation of the biochemical parameters. Further, we have shown through an analysis of patterns, that different parameters are de-regulated differently. With the recent surge in interest in understanding memory and adaptations in microbes, our results provide insights into memory in social amoebae.

4.5 ACKNOWLEDGEMENTS

We thank S. Leibler for suggesting to look for memory in *D.d*. This work would not have been possible without the support of our laboratory assistants M. S. Müller and K. Gunkel, whose help in the preparation of cells for the experiments was invaluable. This work has been supported by the Max Planck Society. A.G. acknowledges the MaxSynBio Consortium which is jointly funded

by the Federal Ministry of Education and Research of Germany and the Max Planck Society.

4.6 Supplementary Materials

4.6.1 Cell preparation

AX2 cells were grown in HL5 medium (35.5g of Formedium powder from Formedium Ltd., England, per liter of double distilled water, autoclaved and filtered) at 22^0C and harvested when they became confluent. The cells were washed in phosphate buffer (2g of KH_2PO_4, 0.36g of $Na_2HPO_4.2H_2O$ per liter at pH 6, autoclaved) and centrifuged two times. The cells were then poured into a conical flask and placed on a shaker for 5 h. After 5 h, they were centrifuged, and the supernatant was removed, and the cells were suspended in 20 ml of HL5 medium. This cell solution was then poured into two 8.6 cm diameter Petri-dishes and incubated for the desired feeding time. After the desired feeding duration, all the cells in the dish were collected in the medium and centrifuged. The supernatant was discarded, and replaced with buffer. The cells we re-suspended in this buffer and centrifuged again. This process was repeated two more times with fresh buffer. (Note that this is not the usual procedure to harvest the cells. Normally, the medium is removed and only the cells adhered to the bottom of the dish are used. In these experiments, we followed a slightly different procedure because, some of our feeding times were as short as 20 min, and it was possible that not all the cells had adhered to the bottom of the dish. This modified procedure ensured minimal cell loss.) The cells were then

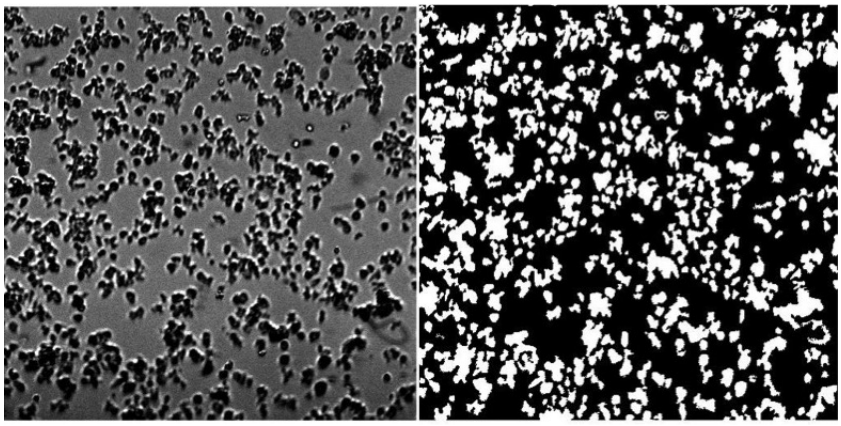

Figure 4.6: The initial distribution of the cells observed experimentally. The left panel shows the cell distribution for an initial starvation time of 1 h. The right panel shows the corresponding binarized cell distribution. The length of the figure is about 1.4 mm.

counted using a hemocytometer and diluted to a density of 3.5 x 10^6 cells/ml with fresh phosphate buffer. They were then plated on a 8.6 cm diameter plastic Petri dish with 10 ml phosphate buffer. Dark-field optics was used to image the cell populations every 20 s [1, 6, 30, 28]. It consists of an LED ring lamp placed above the Petri dish and a CCD camera (QIClick-F-M-12 from QImaging) placed below the Petri dish. Parafilm was wrapped around the sides to prevent evaporation of the buffer. A modified dryer blew air above the dish to equilibrate the temperature. The entire room was dark during the experiment and maintained at 22^0C.

4.6.2 Cell distribution

The cells are not homogeneously distributed. As explained in the our previous work [24], at different developmental stages, the cell distribution is different. For the simulating the experiments with non-zero feeding times, we assumed

that the cell distribution closely resembles the distribution of a cell population initially starved for an hour. For the experiments with zero feeding time, we measured the cell distribution of a population initially starved for 5 h. We plated the starved cells at the same density on a Petri dish. After waiting for about 10 min to allow the cells to attach to the surface, we imaged the dish at about 15 distinct regions using an inverted bright-field microscope, using a 10X objective. Figure 4.6 exemplarily shows the initial cell distribution for a population initially starved for an hour. To determine the ratio of the area occupied by the cells to the area of the grid, i.e., the occupation ratio, we divided the images of about 600 x 600 μm^2 into grids of size 60 x 60 μm^2 (corresponding to the size of the grids in the simulations). For these 600 x 600 μm^2 regions, we thus measured the spatial distribution of occupation ratios at 10 x 10 grid points (bions in the simulations). For both starvation times (1 h and 5 h), we have about 15 such distributions. To cover the simulation region of 333 x 333 bions, we distribute these 10 x 10 distributions randomly on the simulation grid. We multiply the degradation rate γ and cAMP released C_{rel} for each bion with its respective occupation ratio, as the degradation rate and the amount of cAMP released depend on the number of cells in each bion.

4.6.3 Data analysis

First, the dark field images were filtered in space, only allowing structures between 3 mm and 0.2 mm to pass through. From these processed image stacks, we obtained the time series of the intensity for each pixel with a window of 40 *min* (corresponding to about 6 oscillations). Then, we took the Fourier transform of these time series. The power spectra of the Fourier transforms thus obtained

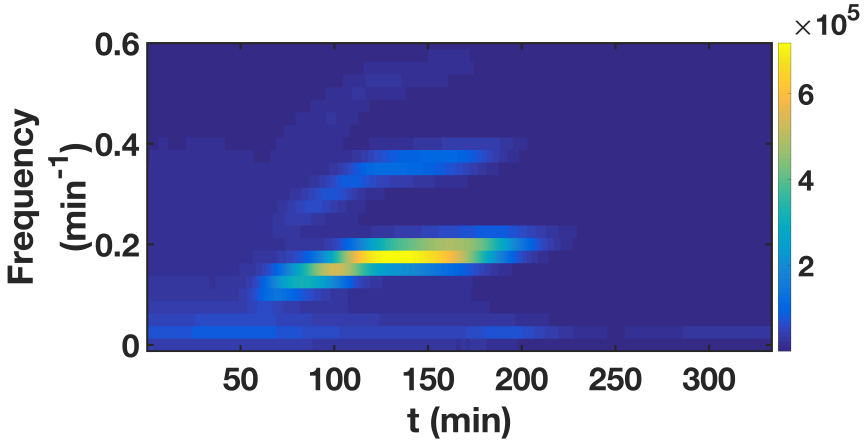

Figure 4.7: Sample spectrogram obtained from an experiment. The slight increase in frequency (the y-axis) with observation time t (the x-axis), mentioned in the results section, is visible. The colormap shows the amplitude of the power spectrum. In this case, it has a maximum at around 140 *min*. The power spectrum at this time is taken, its peak fit with a quadratic polynomial and the frequency at the maximum amplitude found.

were spatially averaged giving one power spectrum for each time point. For example, we started with the first image of the image stack and found the time series of the intensity for all the pixels by collecting their intensity values from images corresponding to the next 40 min. Then, we took the Fourier transform of each of these time series and found their power spectra. These power spectra were then averaged to get one average power spectrum corresponding to the first image. Then we moved to the second image in the image stack. Again, we found the intensity time series of each pixel by collecting its intensity values from images corresponding to the next 40 min. As before, we took the Fourier transform of each of these pixels and found their power spectra. The spatially averaged power spectrum corresponds to the power spectrum of the second image. This procedure was repeated resulting in a power spectrum for each time point. The magnitude of these power spectra were plotted over time to give a spectrogram. An example spectrogram from an experiment is shown in figure

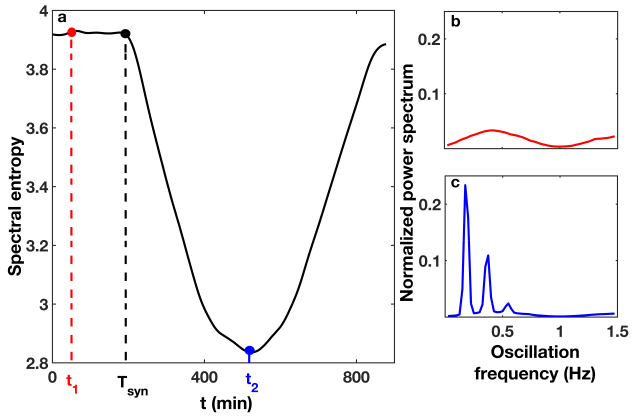

Figure 4.8: (a) The temporal variation of spectral entropy obtained from an experiment. The point of maximum curvature, defined to be the onset of synchronization, is denoted by T_{syn} (b) The normalized power spectrum corresponding to time t_1. It has a non-zero power for almost all frequencies. Using equation (4.6), the spectral entropy at this point is 3.92. (c) The normalized power spectrum corresponding to time t_2. The power is high only for a few frequencies and zero for all others. The spectral entropy is calculated to be 2.85.

4.7. From the spectrogram, we found the time at which the power spectrum has the highest amplitude. This time corresponds to the time when the patterns are well developed. We fit the peak of the power spectrum at this point with a second degree polynomial to obtain the frequency corresponding to the maximum and converted this frequency to period of oscillations. In some noisy cases, when it was not possible to use the Fourier transform technique, we obtained the period by autocorrelating the de-trended, and spatially averaged temporal intensity profile. The patterns formed in the simulations were analyzed with the same procedure as above. Here however, the limits of the band pass filter were 1.5 mm and 0.1 mm because the wavelengths are smaller.

Onset of synchronization

We define the onset of synchronization using the spectral entropy (as described in [23]). We found the spatially averaged power spectrum at each time point of the data, as described before. To find the onset of synchronization, we first normalized these power spectra and used the following definition of spectral entropy, S:

$$S = -\sum p_i log(p_i). \tag{4.6}$$

Here p_i is the amplitude of the i^{th} frequency of the normalized power spectrum. If a time series represents white noise, all frequencies are equally dominant (p_i is high for all the i frequencies) and this spectral entropy is high (figure 4.8b). This is the case in the initial images, where no patterns occur. If the signal comes from a single frequency source, the value of the spectral entropy is lower because p_i is close to zero for almost all frequencies except one. (figure 4.8c) This occurs when all the pixels or cells oscillate at the same frequency. So, the spectral entropy has a high value for unsynchronized noisy states and a low value for synchronized states. A plot of spectral entropy as a function of time shows the emergence of the synchronized state, when the spectral entropy begins to decrease (figure 4.8a). We find the minimum of the second derivative of this spectral entropy, which gives the point of maximum curvature, and define it to be the onset of synchronization. The same procedure was performed for patterns in both experiments and simulations.

Spiral density

To find the spiral density, we began with the Fourier transform of the time series of the intensity of each pixel in the images, for a window of 40 min. After spatially averaging the power spectrum at each time point, we found the dominant frequency at each time point. We defined the phase at each pixel to be the phase of the oscillation at the dominant frequency (obtained from the real and imaginary parts of the Fourier transform). A map of this phase, ranging from from $-\pi$ to π for all the pixels is the phase map of that image. A spiral core is a phase singularity, a point where phase is not defined. (For more on phase singularities, see [31].) One way to detect phase singularities is by integrating the gradient of the phase along a closed curve. Such an integral is non-zero only if the loop encloses a singularity.

$$n.2\pi = \oint \vec{\nabla}\phi.\vec{dl} = \oint \vec{k}.\vec{dl} \tag{4.7}$$

Here $\vec{k}$ is the wave vector and n is an integer. Stokes theorem gives

$$n.2\pi = \int (\vec{\nabla} \times \vec{k}).\vec{dA}. \tag{4.8}$$

The cross product in equation (4.8) was evaluated using the kernel method described in [3] to obtain the singularities in our patterns. For spirals, the winding number n, is either +1 or -1. Noise introduces spurious singularities. To eliminate such spurious singularities, we spatially filtered the phase map by first converting the phase to a complex number by raising it to an exponential of e and multiplying with i. In this complex plane, we filtered in 2D using a box-average filter. The filtered phase map was then obtained from the angles of the resulting complex numbers. [5]

However, this was not enough to remove the spurious singularities. So, we

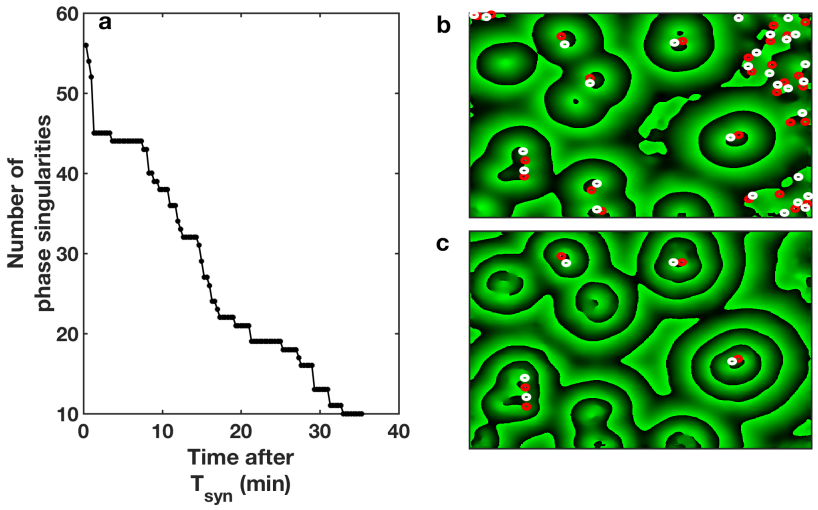

Figure 4.9: The result of our counting algorithm. The left panel shows the decrease in the number of phase singularities counted. Initially a lot of phase singularities are detected due to noise (top right panel). However, with time the number of singularities that persist decreases. At the end of the counting, the spurious singularities are discarded (bottom right panel)

defined spirals to be the singularities that persisted for 40 *min*. To achieve this, we detected all the singularities in the first image, defined a tolerance length, and used the fact that the spiral cores are never very close to one another. In the next frame, we checked if the singularities of the first image persisted in a box around the original position, with side equal to the pre-defined tolerance length. If no singularity was detected in this box, the original singularity was discarded. Also, if two singularities were closer than a pre-defined distance, they were discarded. This process continued for all the frames involved in counting. The counting of the phase singularities started about 20 *min* after T_{syn}, when the patterns are well established. Figure 4.9 shows an example output of our algorithm. In figure 4.9b, we see the phase map of the first image considered for counting the singularities. The red and the white rings denote the +1 and -1 winding numbers respectively. Despite the filtering, it has many spurious singularities.

Figure 4.9c shows the phase map of the last image considered for counting singularities. We see that all the spurious singularities have been eliminated by the tracking algorithm. Figure 4.9a shows the decrease in the number of singularities with time.

BIBLIOGRAPHY

[1] FERNANDA ALCANTARA and MARILYN MONK. "Signal Propagation during Aggregation in the Slime Mould Dictyostelium discoideum". In: *Microbiology* 85.2 (1974), pp. 321–334. URL: http://microbiologyresearch.org/content/journal/micro/10.1099/00221287-85-2-321.

[2] John T. Bonner. "A Descriptive Study of the Development of the Slime Mold Dictyostelium discoideum". In: *American Journal of Botany* 31.3 (1944), pp. 175–182. ISSN: 00029122, 15372197. URL: http://www.jstor.org/stable/2437641.

[3] Mark-Anthony Bray et al. "Experimental and Theoretical Analysis of Phase Singularity Dynamics in Cardiac Tissue". In: *Journal of Cardiovascular Electrophysiology* 12.6 (2001), pp. 716–722. ISSN: 1540-8167. DOI: 10.1046/j.1540-8167.2001.00716.x. URL: http://dx.doi.org/10.1046/j.1540-8167.2001.00716.x.

[4] Josep Casadesús and Richard D'Ari. "Memory in bacteria and phage". In: *BioEssays* 24.6 (2002), pp. 512–518. ISSN: 1521-1878. DOI: 10.1002/bies.10102. URL: http://dx.doi.org/10.1002/bies.10102.

[5] Jan Christoph. "Intramural Visualization of Scroll Waves in the Heart". PhD thesis. Göttingen Graduate School for Neurosciences, Biophysics and Molecular Biosciences: Georg-August-University, Göttingen, Oct. 2014.

[6] Peter N. Devreotes, Michael J. Potel, and Stephen A. MacKay. "Quantitative analysis of cyclic AMP waves mediating aggregation in Dictyostelium discoideum". In: *Developmental Biology* 96.2 (1983), pp. 405–415. ISSN: 0012-1606. DOI: http://dx.doi.org/10.1016/0012-

1606(83)90178-1. URL: http://www.sciencedirect.com/science/article/pii/0012160683901781.

[7] Peter N. Devreotes and Sally H. Zigmond. "Chemotaxis in Eukaryotic Cells: A Focus on Leukocytes and Dictyostelium". In: *Annual Review of Cell Biology* 4.1 (1988). PMID: 2848555, pp. 649–686. DOI: 10.1146/annurev.cb.04.110188.003245. URL: https://doi.org/10.1146/annurev.cb.04.110188.003245.

[8] R Dhar et al. "Yeast Adapts to a Changing Stressful Environment by Evolving Cross-Protection and Anticipatory Gene Regulation". In: *Molecular Biology and Evolution* 30.3 (2013), pp. 573–588. DOI: 10.1093/molbev/mss253. URL: +%20http://dx.doi.org/10.1093/molbev/mss253.

[9] A.J. Durston. "Pacemaker activity during aggregation in Dictyostelium discoideum". In: *Developmental Biology* 37.2 (1974), pp. 225–235. ISSN: 0012-1606. DOI: http://dx.doi.org/10.1016/0012-1606(74)90144-4. URL: http://www.sciencedirect.com/science/article/pii/0012160674901444.

[10] G Gerisch. "Chemotaxis in Dictyostelium". In: *Annual Review of Physiology* 44.1 (1982). PMID: 6280593, pp. 535–552. DOI: 10.1146/annurev.ph.44.030182.002535. URL: https://doi.org/10.1146/annurev.ph.44.030182.002535.

[11] Günther Gerisch. "Cell Aggregation and Differentiation in Dictyostelium". In: *Current Topics in Developmental Biology* 3 (1968), pp. 157–197. ISSN: 0070-2153. DOI: http://dx.doi.org/10.1016/S0070-2153(08)60354-3. URL: http://www.sciencedirect.com/science/article/pii/S0070215308603543.

[12] G. Gerisch et al. “Cyclic AMP Phosphodiesterase and its Inhibitor in Slime Mould Development”. In: *Nature* 235 (1972), pp. 90–92.

[13] T. Höfer et al. “A resolution of the chemotactic wave paradox”. In: *Applied Mathematics Letters* 7.2 (1994), pp. 1–5. ISSN: 0893-9659. DOI: https://doi.org/10.1016/0893-9659(94)90020-5. URL: http://www.sciencedirect.com/science/article/pii/0893965994900205.

[14] David A. Kessler and Herbert Levine. “Pattern formation in Dictyostelium via the dynamics of cooperative biological entities”. In: *Phys. Rev. E* 48 (6 Dec. 1993), pp. 4801–4804. DOI: 10.1103/PhysRevE.48.4801. URL: https://link.aps.org/doi/10.1103/PhysRevE.48.4801.

[15] Claudette Klein. “Adenylate cyclase activity in Dictyostelium discoideum amoebae and its changes during differentiation”. In: *FEBS Letters* 68.1 (1976), pp. 125–128. ISSN: 0014-5793. DOI: http://dx.doi.org/10.1016/0014-5793(76)80419-X. URL: http://www.sciencedirect.com/science/article/pii/001457937680419X.

[16] Claudette Klein. “Changes in adenylate cyclase during differentiation of Dictyostelium discoideum”. In: *FEMS Microbiology Letters* 1.1 (1977), pp. 17–19. ISSN: 0378-1097. DOI: http://dx.doi.org/10.1016/0378-1097(77)90102-1. URL: http://www.sciencedirect.com/science/article/pii/0378109777901021.

[17] G. Lambert and E. Kussell. “Memory and Fitness Optimization of Bacteria under Fluctuating Environments”. In: *PLOS Genetics* 10.9 (2014),

e1004556. URL: https://doi.org/10.1371/journal.pgen.1004556.

[18] D Malchow et al. "Membrane-Bound Cyclic AMP Phosphodiesterase in Chemotactically Responding Cells of Dictyostelium discoideum". In: *European Journal of Biochemistry* 28.1 (1972), pp. 136–142. ISSN: 1432-1033. DOI: 10.1111/j.1432-1033.1972.tb01894.x. URL: http://dx.doi.org/10.1111/j.1432-1033.1972.tb01894.x.

[19] Roland Mathis and Martin Ackermann. "Response of single bacterial cells to stress gives rise to complex history dependence at the population level". In: *Proceedings of the National Academy of Sciences* 113.15 (2016), pp. 4224–4229. DOI: 10.1073/pnas.1511509113. URL: http://www.pnas.org/content/113/15/4224.abstract.

[20] Toshiyuki Nakagaki, Hiroyasu Yamada, and Agota Toth. "Intelligence: Maze-solving by an amoeboid organism". In: *Nature* 407.6803 (Sept. 2000), pp. 470–470. URL: http://dx.doi.org/10.1038/35035159.

[21] T. Nakagaki et al. "Obtaining multiple separate food sources: behavioural intelligence in the Physarum plasmodium". In: *Proceedings of the Royal Society of London B: Biological Sciences* 271.1554 (2004), pp. 2305–2310. ISSN: 0962-8452. DOI: 10.1098/rspb.2004.2856. URL: http://rspb.royalsocietypublishing.org/content/271/1554/2305.

[22] R. K. Pathria. *Statistical Mechanics*. Second. Academic Press, 2009.

[23] G E Powell and I C Percival. "A spectral entropy method for distinguishing regular and irregular motion of Hamiltonian systems". In: *Journal of Physics A: Mathematical and General* 12.11 (1979), p. 2053. URL: http://stacks.iop.org/0305-4470/12/i=11/a=017.

[24] Kaumudi Hassan Prabhakara et al. “Effects of developmental variability on the dynamics and self-organization of cell populations.” In: *New Journal of Physics* (2017). *Accepted*. URL: http://iopscience.iop.org/10.1088/1367-2630/aa9391.

[25] Kenneth B Raper. “Dictyostelium discoideum, a new species of slime mold from decaying forest leaves”. In: *Journal of Agricultural Research* 50.2 (1935), pp. 135–148.

[26] Tetsu Saigusa et al. “Amoebae Anticipate Periodic Events”. In: *Phys. Rev. Lett.* 100 (1 Jan. 2008), p. 018101. DOI: 10.1103/PhysRevLett.100.018101. URL: https://link.aps.org/doi/10.1103/PhysRevLett.100.018101.

[27] Satoshi Sawai, Peter A. Thomason, and Edward C. Cox. “An autoregulatory circuit for long-range self-organization in Dictyostelium cell populations”. In: *Nature* 433.7023 (Jan. 2005), pp. 323–326. URL: http://dx.doi.org/10.1038/nature03228.

[28] FLORIAN SIEGERT and CORNELIS WEIJER. “Digital image processing of optical density wave propagation in Dictyostelium discoideum and analysis of the effects of caffeine and ammonia”. In: *Journal of Cell Science* 93.2 (1989), pp. 325–335. ISSN: 0021-9533. URL: http://jcs.biologists.org/content/93/2/325.

[29] Monica Skoge et al. “Cellular memory in eukaryotic chemotaxis”. In: *Proceedings of the National Academy of Sciences* 111.40 (2014), pp. 14448–14453. DOI: 10.1073/pnas.1412197111. URL: http://www.pnas.org/content/111/40/14448.abstract.

[30] KJ Tomchik and PN Devreotes. "Adenosine 3′,5′-monophosphate waves in Dictyostelium discoideum: a demonstration by isotope dilution–fluorography". In: *Science* 212.4493 (1981), pp. 443–446. ISSN: 0036-8075. DOI: 10.1126/science.6259734. eprint: http://science.sciencemag.org/content/212/4493/443.full.pdf. URL: http://science.sciencemag.org/content/212/4493/443.

[31] A. T. Winfree. *The geometry of biological time*. Springer-Verlag, 1980. ISBN: 978-3-540-52528-8.

[32] R.P. Yeh, F.K. Chan, and M.B. Coukell. "Independent regulation of the extracellular cyclic AMP phosphodiesterase-inhibitor system and membrane differentiation by exogenous cyclic AMP in Dictyostelium discoideum". In: *Developmental Biology* 66.2 (1978), pp. 361–374. ISSN: 0012-1606. DOI: http://dx.doi.org/10.1016/0012-1606(78)90245-2. URL: http://www.sciencedirect.com/science/article/pii/0012160678902452.

CHAPTER 5

EFFECTS OF CELL-CELL VARIABILITY ON PATTERN FORMATION

Kaumudi H Prabhakara, Albert J Bae, Eberhard Bodenschatz *To be submitted*

5.1 Abstract

Pattern formation and aggregation in starving populations of the social amoebae *Dictyostelium discoideum (D.d)*, have been widely studied due to their importance as survival strategies for *D.d*. The chemical cyclic Adenosine Monophosphate (cAMP) that the cells secrete on starvation is known to form patterns and lead to aggregation. However, neither do all cells release the same amount of cAMP nor is there always a sufficient density of cells to sustain pattern formation and aggregation. In this work, we address these two issues by mixing wild type *D.d.* cells with mutants that are unable to produce cAMP, and by varying the cell density. Surprisingly, we find that replacing a large fraction of wild type cells with the non cAMP producing mutants does not affect pattern formation drastically. Further, we observe that the populations require the same amount of time to form patterns and aggregate irrespective of the fraction of the mutants present in the population. Further experiments enabled us to deduce that the effect of the mutants is not mechanical, but chemical. However, we do not know what this chemical is, yet. Simulations of a model reproduced some of our results, like the variation of oscillation period, but it could not reproduce the result that replacing wild type cells with mutants has no effect on the time needed for synchronization. This indicates that the models need to take into account the effect of this chemical. Our work paves the way for future investigations on

the robustness of the signaling mechanism.

5.2 Introduction

Pattern formation is ubiquitous in nature, be it patterns on animal coats, in chemical reactions or on heart tissues. One biological system well known for pattern formation is a starving population of the amoeba *Dictyostelium discoideum (D.d.)*, which creates large scale spiral waves and targets. *D.d.* is a solitary organism that generally lives in the soil. When deprived of nutrients, these cells become social by emitting a chemical - cyclic adenosine monophosphate (cAMP) that diffuses into the medium. The diffusing cAMP is detected by the surrounding cells through the cAMP receptors on their membranes. Extracellular cAMP binds to the receptors, starting a signaling cascade inside the cells resulting in the production of cAMP. Most of this cAMP is transported out of the cell where some of it is degraded by an enzyme, phosphodiesterase, which is present in the extracellular medium and on the cell membranes. The remaining cAMP diffuses and similarly stimulates neighboring cells, constituting a reaction-diffusion system. After 2-3 hours of random cAMP emission, the cells in the population synchronize with each other, i.e. they emit cAMP at the same frequency. This is the signaling phase. When observed under a dark-field set-up, the response of the cells to the external cAMP appears as spiral waves and targets during the signaling phase. After a couple of hours, the cells aggregate via chemotaxis up the cAMP gradient to reach the centre of the spirals and form mounds. The mounds then form multicellular slugs composed of about a million cells, that crawl around looking for food. If nutrients are still unavailable, they form stalks with spores on the top, which can be dispersed and form

cells in presence of food. [14, 17, 7] This is a survival mechanism for the cells, so that their species can survive in unfavorable conditions.

Though the spiral and circular wave patterns in D.d have been studied for decades [6, 4, 3, 13], and many theoretical models have been proposed to explain the formation of such patterns, [9, 11, 12, 5, 16, 15] the exact mechanism for the selection of patterns remains unclear. The current understanding of the aggregation of *D.d.* is that cAMP signaling is responsible for synchronizing the cells. In all stages of the cells' life cycle, cAMP is thought to be the organizing chemical. However, due to genetic heterogeneity, not all cells are similar; some cells synthesize more cAMP than others. In this work, we subject starving cells through adverse conditions like extreme densities, and mix them with the mutant cells acaA$^-$, which lack the enzyme responsible for producing cAMP, and analyze the resulting patterns to study the effect of cell-cell variability on synchronization.

5.3 Methods

We used AX2 wild type cells, grown in HL5 medium. The wild type D.d cells were removed from the medium, washed and centrifuged thrice in phosphate buffer, counted and diluted to the required values and finally plated on a plastic Petri dish (8.7 cm diameter) with 10 ml phosphate buffer. The dish is sealed form the sides with Parafilm to reduce evaporation. The mutant cells, acaA$^-$ (a gift from the Kortholt lab), that lack the ability to produce cAMP, were similarly harvested. For the experiments with beads, polystyrene beads 10 and 20 microns in diameter (from Dynoseeds TS) were used. This diameter is comparable

to the typical diameter of D.d cells. Beads larger than or comparable to the typical cell size were used to ensure they weren't eaten by the cells. The beads were similarly washed and centrifuged in the phosphate buffer. All the experiments were repeated thrice, and four videos were obtained from each experiment. For fluorescence measurements, HG1694 cells - AX2 wild type cells with cytosolic green fluorescent protein - were used.

The cells were imaged every 20 s for about 7 h. The spatially averaged power spectrum of the time series of the intensities was found at each instant of time with a window of 40 min - corresponding to 6-7 typical oscillations. When most of the cells oscillate at the same frequency, the power spectrum has the highest amplitude. The time at which this occurs is defined as the synchronization time. The oscillation period, the spatial order and the spiral density were measured at the synchronization time. To find the spiral density, we first found the Fourier transform of each pixel in the images, for a window of 40 min. Using this, we find the phase of the oscillation of the dominant frequency. This gives a phase map for each image. A spiral core is a phase singularity. A closed integral of the phase gradient is non-zero only if the loop encloses a singularity.

$$n.2\pi = \oint \vec{\nabla}\phi.\vec{dl} = \oint \vec{k}.\vec{dl} \tag{5.1}$$

Here $\vec{k}$ is the wave vector and n is an integer. Stoke's theorem gives

$$n.2\pi = \int (\vec{\nabla} \times \vec{k}).\vec{dA}. \tag{5.2}$$

The cross product was evaluated using the kernel method described in [2]. To eliminate spurious singularities, we spatially filtered the phase map and define spirals to be the singularities that persist for 20 min before and 20 min after the synchronisation time.

Spatial order is obtained as described in [10]. We first take an image of the spirals at the synchronization time (when they're most ordered). If all the pixel intensities are shuffled randomly, we get a random image with the same distribution of intensities. As a consequence of the central limit theorem, the distribution of the spatial Fourier coefficients of this random image is a Gaussian, whose variance is the variance of the intensities of original ordered image (Parseval's theorem). So, we find the variance of the intensities of the original image and use it to construct the Gaussian distribution, P_r, corresponding to the random image with the same intensity distribution. The information corresponding to this Gaussian distribution (Hks) is the information of the most random image with the same intensity distribution as the original image.

$$Hks = -\sum P_r log P_r \tag{5.3}$$

Next, we find the spatial Fourier coefficients of the ordered image, whose distribution P_o is typically non-Gaussian. We find the information corresponding to this distribution (Iks).

$$Iks = -\sum P_o log P_o \tag{5.4}$$

The spatial order is defined as the difference of the above two informations. It estimates how far away the ordered image is from a random image of the same intensity distribution.

$$Order = Hks - Iks \tag{5.5}$$

We use the spatially filtered phase map for these calculations because they are less noisy.

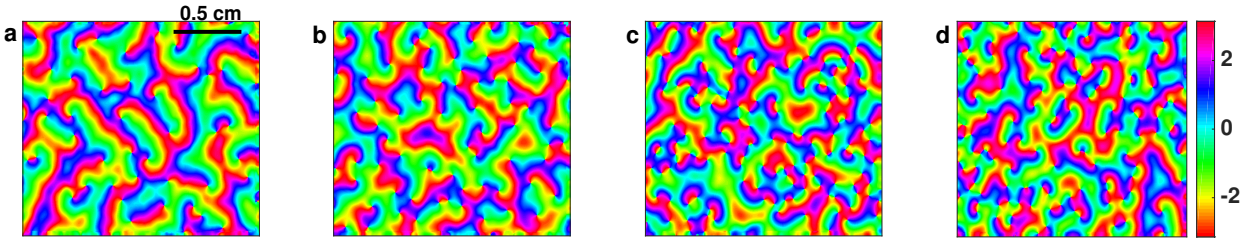

Figure 5.1: Spirals are observed for all the densities studied. Phase maps of four densities at their synchronization time are shown: a. 0.5 million/ml b. 3 million/ml c. 6 million/ml d. 9.36 million/ml

5.4 Results and discussion

5.4.1 Experiments

We increase the number of cells in the Petri dish systematically - corresponding to increasing the spatial density. We observe spirals for all the densities studied (Fig. 5.1). This result is different from [13], where target patterns were observed on agar substrate for low cell densities. Although we always observe spirals, their properties are different (Fig. 5.2). The oscillation period is independent of population density (Fig. 5.2a). As the density increases, the populations synchronize faster until the synchronization time saturates. (Fig. 5.2b) This could be due to the increasing amounts of cAMP released into the system and a higher degradation, which could reach a limiting value for high densities. The denser populations also tend to form more spirals and hence have a lower spatial order - higher the spiral density, smaller the spirals, and smaller regions in space are ordered. (Fig. 5.2 c and d) A conditioned medium factor (CMF) [8] is said to be involved in sensing the density of starving cells by regulating the number of cells in an aggregate. This could also cause the increase in spiral density (and the consequent decrease in spatial order) with population density. Note that

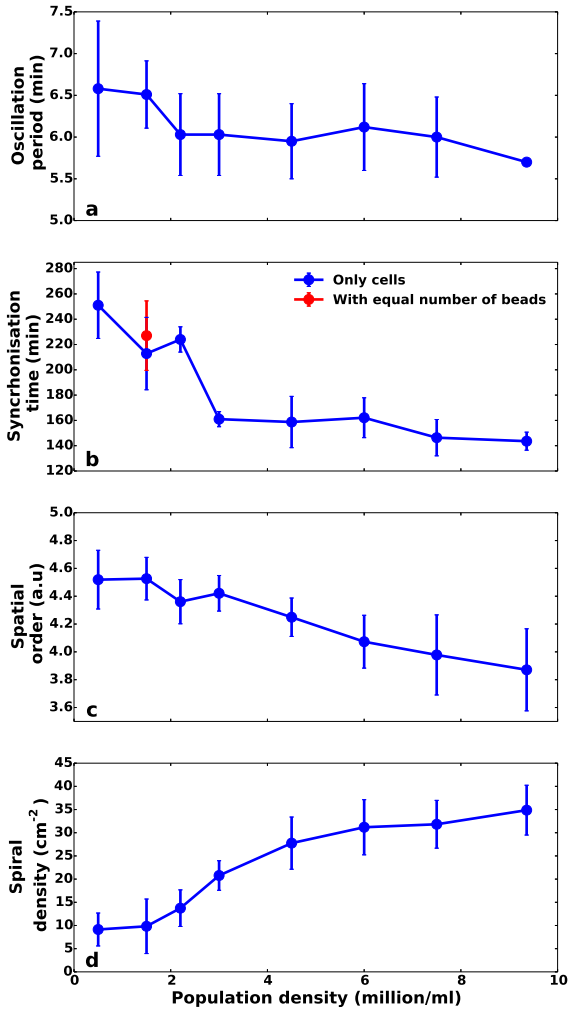

Figure 5.2: Parameters measured from the patterns of populations of different cell densities : a. Oscillation period b. Synchronization time c. Spatial order d. Spiral density

spatial order is a reliable measure of order and can be used in noisy cases as well.

We fixed the total cell density and varied the ratio of mutants to wild type cells from 15% to 100%, and repeated this for three different cell densities. (We have no points in between 85% and 100% mutants (that cannot produce cAMP) because the cell counting technique is not precise enough.) We always observed spirals, even for a high ratio of mutants; i.e. as low as 15% signaling cells are suf-

ficient to synchronize the entire population. Bright field movies of the mixtures verified that all the cells aggregate, confirming that the mutants can chemotax in a cAMP gradient. A control population of 100% mutants did not show any waves. Fig. 5.3 shows the results of varying the percentage of mutants in populations of 3 different fixed cell densities - 1.5, 3 and 4.5 million cells/ml of buffer. The surprising result is that increasing the percentage of mutants does not alter the synchronization time (Fig. 5.3b). This is unexpected because, if cAMP signaling was the major component in the synchronizing mechanism, as the percentage of mutants increased, the synchronization time should have increased, following the trend of decreasing cell density (Fig. 5.2b). This implies that the mutants are involved in synchronization, and since they don't produce cAMP, the synchronizing mechanism is not critically dependent on cAMP. The oscillation period increases with increasing percentage of mutants (Fig. 5.3a), in contrast to the case where the oscillation period remained constant on changing cell density (Fig. 5.2a). A difference is expected in this case because though the mutants don't produce cAMP, they can still degrade cAMP: as the ratio of mutants increases, the amount of cAMP released into the system decreases while the amount of degradation remains the same. From this, we infer that the combination of degradation rate and the amount of cAMP released affects the periodicity. Because of the inherent noise, we don't calculate the spiral densities for this case and restrict ourself to the spatial order. Spatial order decreases as the ratio of mutants increases (Fig. 5.3c). This is intuitive because increasing the ratio of mutants decreases the signal to noise ratio.

We mixed wild type cells labelled with cytosolic fluorescent protein with mutants. This helped us visualize the distribution of the two kinds of cells. Experiments with a 50 - 50 mixture and 85 -15 mixture, showed that the system

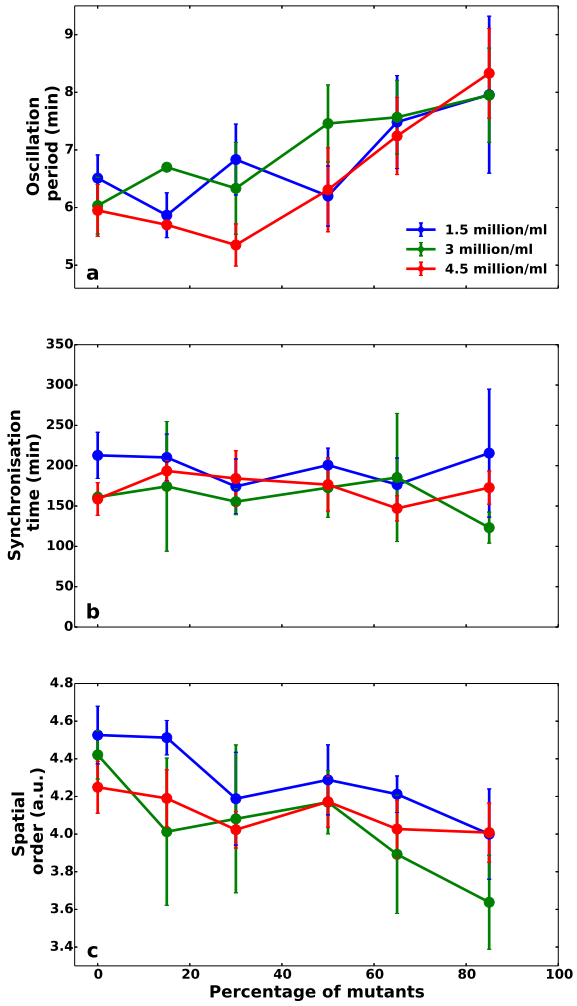

Figure 5.3: Parameters measured from the patterns of populations of varying ratios of mutants for three fixed cell densities : a. Oscillation period b. Synchronization time c. Spatial order

and the aggregates are well mixed.

So far, we have seen evidence that cAMP is not critical for synchronization, but something else is. There are two possible sources - mechanical and chemical. A recent study [1] showed that mechanical stimuli can activate signal transduction pathways. As a first step, we replaced the mutants with beads to see if just mechanical collisions could synchronize the population. We performed experiments by mixing 1.5 million/ml beads and wild type cells each for two bead di-

ameters. Spirals were still formed for both bead sizes. The synchronization time was much higher than for a mixture of wild type cells and mutants of the same concentration. The time corresponded to the synchronization time for only 1.5 million/ml wild type cells. The data are indicated with a red circle in fig. 5.2b. This result proves that passive mechanical collisions alone cannot synchronize the cells; the mutants actively participate in synchronizing the population. This leaves chemical effects. Although the mutants do not synthesize cAMP, they do produce the other chemicals like PDE, inhibitors, CMF etc. We propose that it is one of these that plays a more important role in the synchronization of the cells.

5.4.2 Simulations

We use the model first proposed by [11] and later modified by [16]. This is a part cellular automata and part continuous model - rules govern each grid point, while diffusion of cAMP is treated continuously, as described in equations 5.6, 5.7 and 5.8. All cells are excitable. If the concentration of cAMP, C, exceeds a threshold C^{thresh}, the cells emit cAMP, C_{rel} (350/min). Immediately after emission, they enter an absolute refractory state where they are incapable of emitting cAMP for a fixed time, T_{ARP} (2 min). Next, they go into a relative refractory state, which has a high threshold for emission of cAMP. This state also lasts for a fixed time, T_{RRP} (7 min). The threshold required for cAMP decreases throughout this state (as τ, the time spent in the relative refractory phase, increases from 0 to T_{RRP}) and reaches a minimum at the end of this state, after which the cells are excitable again and the cycle continues. The cAMP is degraded by an enzyme at a rate γ (8/min). The excitability of the cells, E, can increases autonomously,

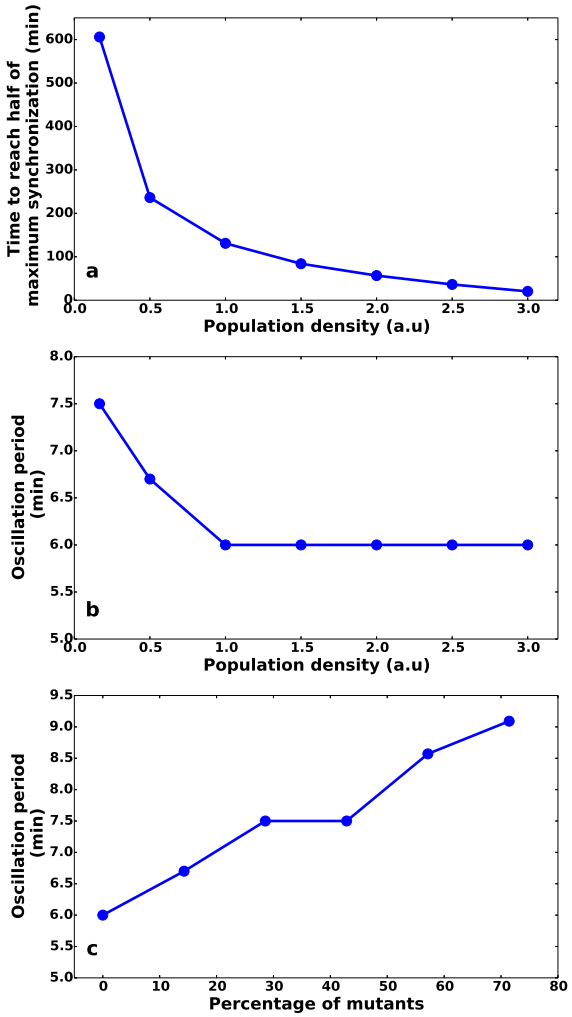

Figure 5.4: Parameters measured from the simulations: a. Synchronization time and b. Oscillation period for different population densities c. Oscillation period for different ratios of mutants. The error bars for all three parameters are so small that the data points obscure their visibility.

η (0.0001) and through coupling (β, 0.005) to the cAMP concentration, C, and saturates at a fixed value E_{max} (0.93).

$$\dot{C}_{i,j} = D \cdot L(C_{i,j}) - \gamma \cdot C_{i,j} + \theta \cdot C_{rel} \tag{5.6}$$

$$\dot{E}_{i,j} = \eta + \beta \cdot C_{i,j} \tag{5.7}$$

$$C_{i,j}^{thresh} = \left[C_{max} - A\frac{\tau}{\tau + T_{ARP}} \right](1 - E_{i,j}), 0 < \tau < T_{RRP} \tag{5.8}$$

L is the discrete Laplacian operator and θ is a step function - it is 1 if $C_{i,j} \geq C_{i,j}^{thresh}$ and 0 otherwise. C_{max} (100) is a constant related to the maximum value of the threshold required for emission of cAMP, D (0.00138 mm^2/min) is the diffusion coefficient and the constant A is a combination of the above constants chosen so that the threshold is maximum when the cells enter the relative refractory state and minimum when they leave it. The rules of the fixed durations of the refractory phases and the saturation of the excitability are implemented separately from these equations. Cells fire randomly with a probability of 10^{-5} per grid point. In experiments, the cells eventually stream after a few hours, which causes the amplitude of the power spectrum to decrease. But in the simulations, there is no change in the amplitude of the power spectrum because cell streaming is not included. So, to compare the trends in synchronization, we find the time taken by the system to reach half of it's maximum power spectrum amplitude, whereas the oscillation period is found after the system has reached maximum synchronization.

To simulate this model to incorporate mutants, we scaled C_{rel} by the ratio of the wild type cells in the population. As ratio of mutants increases, the amount of cAMP released decreases by the same ratio, while the degradation rate remains the same. For example, a population with 60% mutants will have $0.4C_{rel}$, and no change in γ. The random firing rate was also multiplied by this factor. Not only were spirals observed for all the cases simulated, the oscillation period of the spiral waves increased with increasing mutant ratios, as in experiments (compare Fig. 5.4c to Fig. 5.3a). However, this model failed to reproduce the constant synchronization time observed in experiments. We hypothesize that this could be because the model has an incorrect dependence on cAMP and PDE.

To simulate this model to incorporate effects of density, we scaled both C_{rel} and γ by the density, because more cells implies more C_{rel} and γ in the system. We set the population density of 3 million cells/ml to be 1 and scaled the other densities with 3 million /ml. However, with this scaling no spiral patterns were produced for the high and low cell densities. The only way spirals could be generated was by scaling C_{rel} by the ratio mentioned before, but by scaling γ by the square root of that ratio. (Scaling γ by the ratio raised to any power less than or equal to 0.4 and greater than 0.7 did not reproduce spirals for the range of cell densities considered.) With this scaling, we observed spirals for all the densities, and found that the synchronization time decreased with increasing cell density with the same trend as in the experiments (compare trends of Fig. 5.4a and Fig. 5.2b). The oscillation period also remained constant as in the experiments (compare Fig. 5.4b to Fig. 5.2a). However, this model did not reproduce the spiral densities of the experiments. The requirement that cAMP and γ scale differently with cell density further strengthens our hypothesis that the model's dependence on these two quantities is incorrect.

5.5 Conclusions

To conclude, by systematically analyzing patterns, we have shown that although cAMP is essential for synchronization, small amounts are sufficient for synchronization and aggregation. We have shown that some proteins like PDE, or CMF could play a more important role than was thought. Our experimental results provide insights into the robustness of the synchronization to the natural variability of individuals in a population. We have also shown that though the model reproduces some experimental quantities, it is incomplete until the

effects of other important proteins are incorporated. We have also introduced the measure of spatial order for the first time in this field to analyze patterns. On a more general note, this work is a proof of method that a study of patterns provides useful insights into the mechanisms involved.

BIBLIOGRAPHY

[1] Yulia Artemenko et al. "Chemical and mechanical stimuli act on common signal transduction and cytoskeletal networks". In: *Proceedings of the National Academy of Sciences* 113.47 (2016), E7500–E7509. DOI: 10.1073/pnas.1608767113. eprint: http://www.pnas.org/content/113/47/E7500.full.pdf. URL: http://www.pnas.org/content/113/47/E7500.abstract.

[2] Mark-Anthony Bray et al. "Experimental and Theoretical Analysis of Phase Singularity Dynamics in Cardiac Tissue". In: *Journal of Cardiovascular Electrophysiology* 12.6 (2001), pp. 716–722. ISSN: 1540-8167. DOI: 10.1046/j.1540-8167.2001.00716.x. URL: http://dx.doi.org/10.1046/j.1540-8167.2001.00716.x.

[3] P Devreotes. "Dictyostelium discoideum: a model system for cell-cell interactions in development". In: *Science* 245.4922 (1989), pp. 1054–1058. ISSN: 0036-8075. DOI: 10.1126/science.2672337. eprint: http://science.sciencemag.org/content/245/4922/1054.full.pdf. URL: http://science.sciencemag.org/content/245/4922/1054.

[4] A.J. Durston. "Pacemaker activity during aggregation in Dictyostelium discoideum". In: *Developmental Biology* 37.2 (1974), pp. 225–235. ISSN: 0012-1606. DOI: http://dx.doi.org/10.1016/0012-1606(74)90144-4. URL: http://www.sciencedirect.com/science/article/pii/0012160674901444.

[5] Martin Falcke and Herbert Levine. "Pattern Selection by Gene Expression in Dictyostelium Discoideum". In: *Phys. Rev. Lett.* 80 (17 Apr. 1998),

pp. 3875–3878. DOI: 10.1103/PhysRevLett.80.3875. URL: https://link.aps.org/doi/10.1103/PhysRevLett.80.3875.

[6] Güunther Gerisch. "Chapter 6 Cell Aggregation and Differentiation in Dictyostelium". In: ed. by A.A. Moscona and Alberto Monroy. Vol. 3. Current Topics in Developmental Biology. Academic Press, 1968, pp. 157–197. DOI: http://dx.doi.org/10.1016/S0070-2153(08)60354-3. URL: http://www.sciencedirect.com/science/article/pii/S0070215308603543.

[7] Albert Goldbeter. "Oscillations and waves of cyclic AMP in Dictyostelium: A prototype for spatio-temporal organization and pulsatile intercellular communication". In: *Bulletin of Mathematical Biology* 68.5 (2006), pp. 1095–1109. ISSN: 1522-9602. DOI: 10.1007/s11538-006-9090-z. URL: http://dx.doi.org/10.1007/s11538-006-9090-z.

[8] Richard H. Gomer, Wonhee Jang, and Derrick Brazill. "Cell density sensing and size determination". In: *Development, Growth & Differentiation* 53.4 (2011), pp. 482–494. ISSN: 1440-169X. DOI: 10.1111/j.1440-169X.2010.01248.x. URL: http://dx.doi.org/10.1111/j.1440-169X.2010.01248.x.

[9] J Halloy, J Lauzeral, and A Goldbeter. "Modeling oscillations and waves of cAMP in Dictyostelium discoideum cells". In: *Biophysical Chemistry* 72.1–2 (1998), pp. 9–19. ISSN: 0301-4622. DOI: http://dx.doi.org/10.1016/S0301-4622(98)00119-7. URL: http://www.sciencedirect.com/science/article/pii/S0301462298001197.

[10] W F. Heinz, J L. Werbin, E. Lattman, et al. "Computing Spatial Information from Fourier Coefficient Distributions". In: *J Membrane Biol* 241.2 (2011),

pp. 59–68. DOI: http://dx.doi.org/10.1007/s00232-011-9362-x.

[11] David A. Kessler and Herbert Levine. "Pattern formation in Dictyostelium via the dynamics of cooperative biological entities". In: *Phys. Rev. E* 48 (6 Dec. 1993), pp. 4801–4804. DOI: 10.1103/PhysRevE.48.4801. URL: https://link.aps.org/doi/10.1103/PhysRevE.48.4801.

[12] J. Lauzeral, J. Halloy, and A. Goldbeter. "Desynchronization of cells on the developmental path triggers the formation of spiral waves of cAMP during Dictyostelium?aggregation". In: *Proceedings of the National Academy of Sciences* 94.17 (1997), pp. 9153–9158. eprint: http://www.pnas.org/content/94/17/9153.full.pdf. URL: http://www.pnas.org/content/94/17/9153.abstract.

[13] Kyoung J. Lee, Edward C. Cox, and Raymond E. Goldstein. "Competing Patterns of Signaling Activity in *Dictyostelium Discoideum*". In: *Phys. Rev. Lett.* 76 (7 Feb. 1996), pp. 1174–1177. DOI: 10.1103/PhysRevLett.76.1174. URL: http://link.aps.org/doi/10.1103/PhysRevLett.76.1174.

[14] William F. Loomis. "Cell signaling during development of Dictyostelium". In: *Developmental Biology* 391.1 (2014), pp. 1–16. ISSN: 0012-1606. DOI: http://dx.doi.org/10.1016/j.ydbio.2014.04.001. URL: http://www.sciencedirect.com/science/article/pii/S0012160614001924.

[15] E Pálsson et al. "Selection for spiral waves in the social amoebae Dictyostelium". In: *Proceedings of the National Academy of Sciences* 94.25 (1997), pp. 13719–13723. eprint: http://www.pnas.org/content/94/25/

13719.full.pdf. URL: http://www.pnas.org/content/94/25/13719.abstract.

[16] Satoshi Sawai, Peter A. Thomason, and Edward C. Cox. "An autoregulatory circuit for long-range self-organization in Dictyostelium cell populations". In: *Nature* 433.7023 (Jan. 2005), pp. 323–326. URL: http://dx.doi.org/10.1038/nature03228.

[17] Cornelis J Weijer. "Morphogenetic cell movement in Dictyostelium". In: *Seminars in Cell & Developmental Biology* 10.6 (1999), pp. 609–619. ISSN: 1084-9521. DOI: http://dx.doi.org/10.1006/scdb.1999.0344. URL: http://www.sciencedirect.com/science/article/pii/S1084952199903440.

CHAPTER 6

COOPERATION OF THE *HAVES* AND THE *HAVE-NOTS*

Kaumudi H Prabhakara, Albert J Bae, Eberhard Bodenschatz *To be submitted*

6.1 Abstract

Upon starvation, *Dictyostelium discoideum (D.d.)* exhibit social behavior by releasing a chemical messenger cyclic adenosine monophosphate (cAMP). Large scale waves of cAMP synchronize the population of starving cells and enable them to aggregate and form a multi-cellular organism. In this work, we explore the effect of cell-to-cell variability in the production of cAMP on aggregation. We create an extreme mixture of cell-to-cell variability by adding a few cells that can produce cAMP (*haves*) to mutant that cannot produce cAMP (*have-nots*). Surprisingly, such mixtures aggregate, even though each population on its own cannot aggregate. We show that (1) a lack of divalent ions kills the *haves* at low densities (2) the *have-nots* supply the cAMP degrading enzyme, phosphodiesterase, in addition to the divalent ions, which enables the mixture to aggregate. Our results suggest the existence of a range of degradation rates for optimum aggregation. We find that the *haves* and the *have-nots* cooperate by sharing complementary resources.

6.2 Introduction

Dictyostelium discoideum (D.d.) is a soil-dwelling amoeba, about 10 μm in size with a unique survival strategy. In nutrient rich environments, the cells feed, divide and lead a solitary life, but when food becomes scarce and the cells start to starve, they exhibit social behavior [22, 4]. *D.d.* signal each other by generating excitable waves of the chemical messenger cyclic adenosine monophosphate (cAMP)—when cells at one location sense that the external cAMP concentration is rising due to secretions from their neighbors to one side, these cells are in turn stimulated to secrete cAMP and relay the signal to their neighbors to the other side. To bring the concentrations back down after a wave passes, there is global degradation of cAMP by a phosphodiesterase (PDE) that is continuously secreted by the cells [13, 2]. Excitation centers emerge, and after about 6 hours of starvation, the cells become chemotactic, migrating towards these centers. Approximately 10^5 cells come together to form a multi-cellular organism which culminates into a fruiting body composed of a ball of spores atop a stalk. The spores will germinate into amoebae once food is available This unique ability of *D.d.* to transform from solitary cells to a multi-cellular organism has made it a much studied model system for morphogenesis [8, 25, 20, 10]

Essential to the survival of *D.d.* is its ability to self-organize by chemical signaling. However, in a population, there is significant cell-to-cell variability in the cAMP production [26, 27, 9]. How then is the signaling mechanism so robust? We intensified the cell-to-cell variability by mixing two kinds of cells, those that can produce cAMP, which we call the *haves*, and the *have-nots*, which are mutants that cannot produce cAMP and thus cannot aggregate. Puzzlingly, when we add a small number of *haves* to a high density of *have-nots*, the mixture

aggregates, whereas neither population aggregates on its own. In this paper we solve this puzzle.

6.3 Results

The self-organization of *D.d.* under starvation is typically studied at densities of $\approx 10^5$ cells/cm^2 on agar [25, 24]. In our experiments, we worked with similar densities of cells, albeit on a Petri dish under a layer of buffer solution instead of agar, because this gave us the greatest uniformity in cell plating density. At these densities, cells initially form a confluent layer on the surface and later aggregate under starvation. When we decreased the density below $\approx 10^4$ cells/cm^2, the population no longer aggregated. However, when we added about 10^5 cells/cm^2 of the acaA$^-$ mutants (*have-nots*) to these low densities of wild-type cells (*haves*) aggregation was rescued (figure 6.1). This is surprising because a population of only 10^5 cells/cm^2 of *have-nots* didn't aggregate on their own, as they were unable to produce cAMP. Since neither the low density population of *haves* nor the high density of *have-nots* were capable of aggregating on their own, there must be a synergy between the two populations that rescued aggregation.

How do these *haves* and *have-nots* cooperate? The cooperation between the two populations can only be chemical or mechanical in nature. Let's first hypothesize that the presence of *have-nots* is sensed by *haves* through mechanical interactions because the *have-nots* don't produce cAMP, and therefore shouldn't directly affect the cAMP relay. This mechanical hypothesis is supported by recent work showing that mechanical stresses play a role in signal transduction

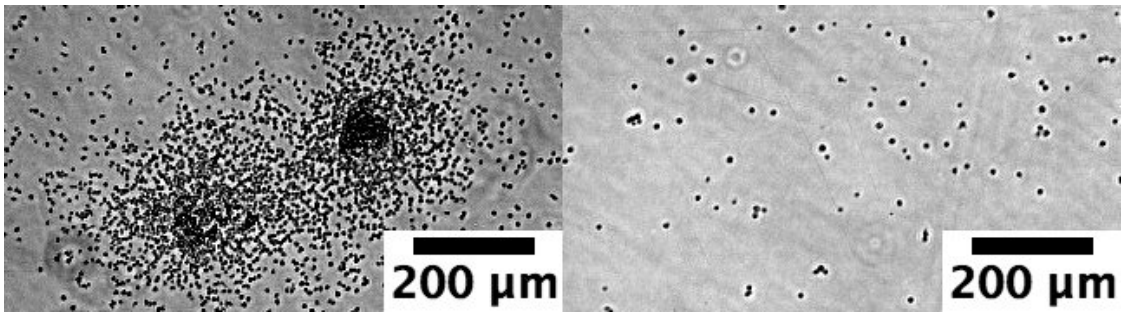

Figure 6.1: (a) A mixture of the the high density *have-nots* and a low density *haves* can aggregate, whereas (b) a low density population of *haves* cannot aggregate on its own. Images were taken about 12 h after start of starvation.

[28, 7]. To first approximation, we replaced the mutants with 10 μm polystyrene beads. If the interactions were due to simple mechanical contacts, beads might play the role of the *have-nots*. This, however, we did not observe. The beads did not rescue aggregation. As a positive control, to ensure the beads are not harmful to the cells, we added the beads to a high density of *haves*, where we know the cells do aggregate. We found that the cells not only aggregated, but also actively transported the beads as they moved and incorporated them into their aggregates. (figure 6.2, Supplementary movie S1)

Other more subtle contact-dependent interactions could be in play. To completely rule these out, we placed a Millipore filter between the populations of the *haves* and the *have-nots*. This filter allows the exchange of chemicals, but does not allow the cells to come into mechanical contact. The populations aggregated. Thus we have disproved our mechanical hypothesis. The effect must be chemical in origin.

What is this chemical interaction? Could the aggregation be caused by some yet-to-be-identified chemical factors secreted by high density cell populations into the buffer? We obtained supernatants from three sources: a high density

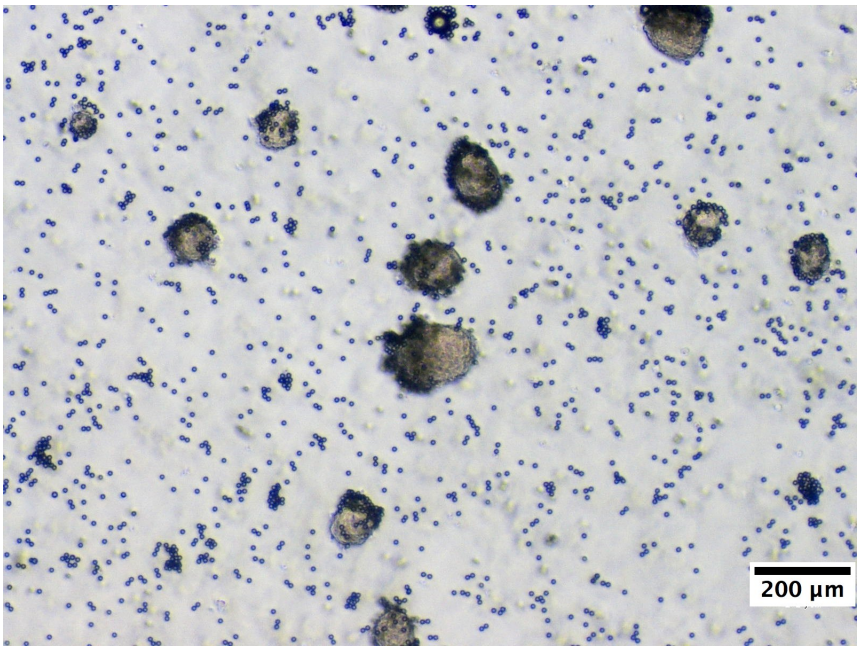

Figure 6.2: Beads added to a high density population of *haves* are incorporated into the aggregates.

population (2 x 10^5 cells/cm^2) of *haves*, a high density population of *have-nots* (2 x 10^5 cells/cm^2), and the mixture described above (9 x 10^3 cells/cm^2 of wild type cells and 2 x 10^5 cells/cm^2 of acaA- mutants). We starved these populations for six hours and then carefully collected the supernatants and added each of these supernatants to low density populations of *haves*. Aggregation was rescued in all three cases, showing that the factors responsible for aggregation are secreted by both *haves* and *have-nots*.

What in the supernatants causes the aggregation? To narrow down the list of chemical factors that could potentially be responsible, we separated the supernatant into two fractions, one containing chemicals $> 30kDa$ and a fraction $< 30kDa$, containing small proteins, ions, and other low molecular weight chemicals (see Methods). We denote these fractions as the high molecular weight fraction (HMWF) and low molecular weight fraction (LMWF) respectively. To

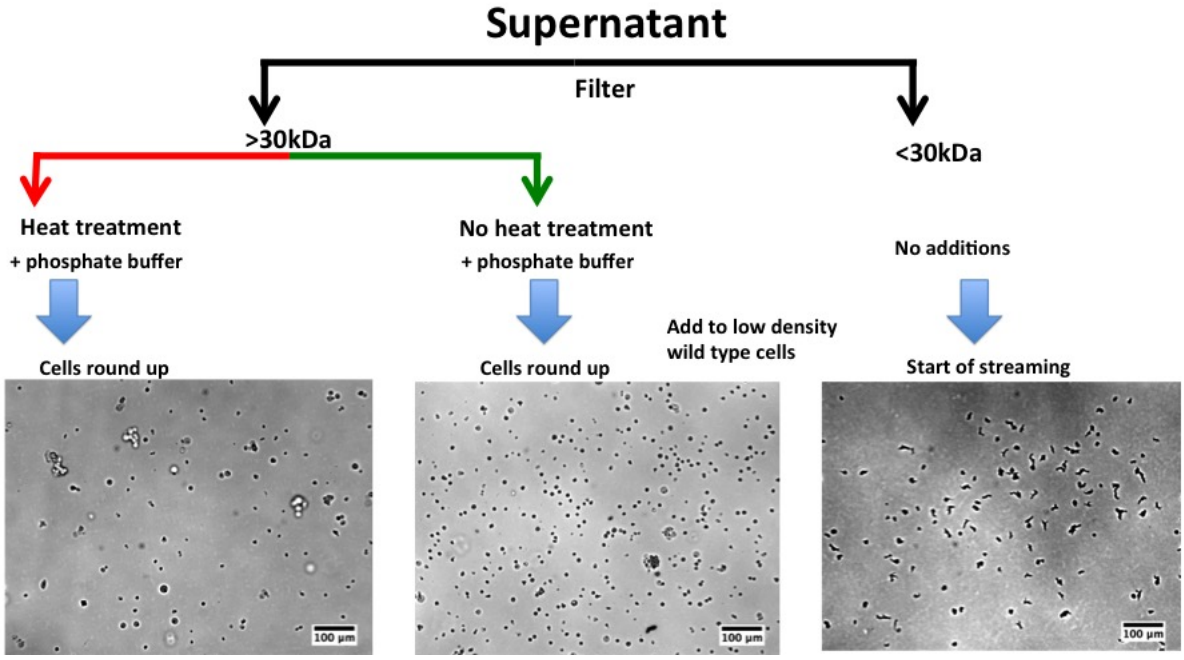

Figure 6.3: We performed a series of experiments with different components of the supernatant. Adding just the HMWF of the supernatant, both heat-treated and non-heat treated, to the low density *haves* caused the cells to round up. When the LMWF of the supernatant was added to the low density haves, the cells were healthy and beginning to stream.

further fractionate the large fraction, we subjected a part of it to heat treatment to deactivate heat sensitive enzymes, and left the rest untreated.

Low densities of *haves* were starved in these fractions. After about **20h**, we found:

- Cells + LMWF: The low density *haves* were viable and appeared polarized, but no tight aggregates were observed. (figure 6.3)
- Cells + heat-treated, HMWF: The low density *haves* rounded up and did not appear viable. Furthermore, many cells had de-adhered from the substrate (figure 6.3).
- Cells + non-heat-treated, HMWF: The low density *haves* also rounded up

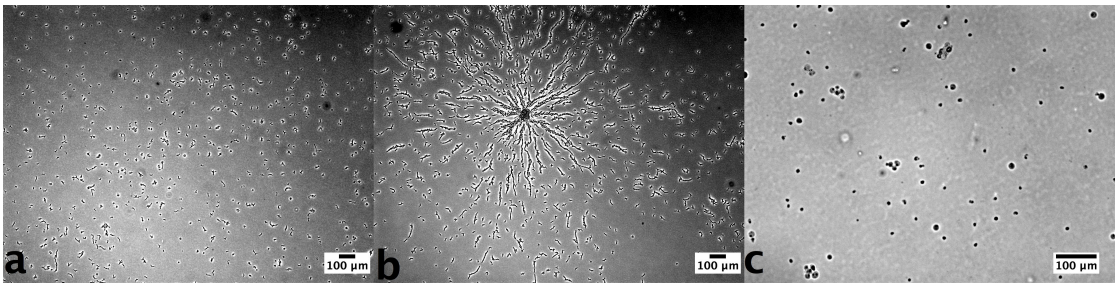

Figure 6.4: (a) Positive control - heat-treated, HMWF of the supernatant mixed with the LMWF of the supernatant was used to condition the low density *haves*. (b) Positive control - non-heat treated, HMWF of the supernatant mixed with the LMWF of the supernatant was used to condition the low density *haves*. (c) Negative control - buffer was added to the low density *haves*.

and did not appear viable (figure 6.3).

- Cells + LMWF + heat-treated, HMWF: In this positive control, the low density *haves* looked polarized (figure 6.4a).
- Cells + LMWF + non-heat-treated, HMWF: In this second positive control, the low density *haves* showed clear large scale streaming (figure 6.4b).

We also conducted a negative control, in which the low density *haves* were unconditioned. These cells rounded up and did not appear viable (figure 6.4c). Clearly, something smaller than 30kDa is essential for viability. This chemical is secreted by both *haves* and *have-nots*, and is not present in our buffer. Additionally, a heat-sensitive factor larger than 30kDa enables the cells to signal effectively over long distances.

What could be in the smaller fraction that keeps the cells viable? We hypothesize that cells carry over essential ions into our low ionic strength buffer. At low densities the ionic strength might not be sufficient for the cells to remain viable. [12, 18, 19] To test this hypothesis, we supplemented our buffer

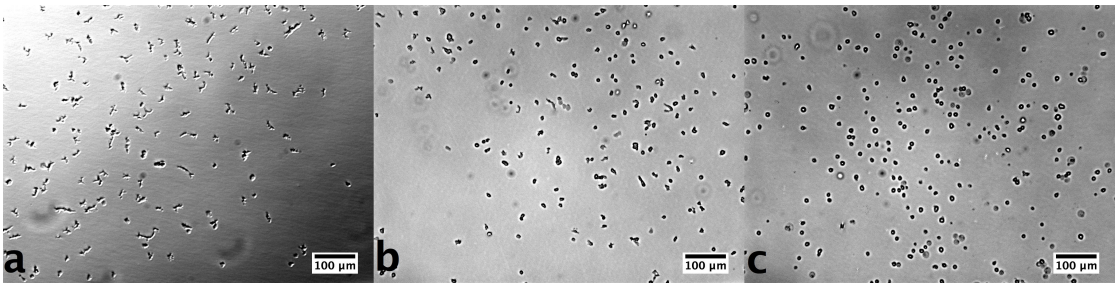

Figure 6.5: Low density *haves* in (a) calcium enriched buffer were polarized and beginning to stream, (b) magnesium enriched buffer were polarized and beginning to stream, (c) sodium enriched buffer rounded up and were therefore unhealthy. Images were taken a day after start of starvation.

with either 50μM $CaCl_2$, 50μM $MgCl_2$ or 150μM NaCl. For the latter, we used a higher concentration to match the ionic strengths of the other two buffers. In the calcium and magnesium enriched buffers, (figures 6.5a,b) after 20 h, the low density *haves* were viable and polarized, but did not form clear aggregates. The low density *haves* in the sodium enriched buffer (figure 6.5c) rounded up, indicating that they were not viable. We can conclude that divalent ions, Ca^{2+} or Mg^{2+}, which are secreted by *have-nots* as well, are responsible to keep the cells viable.

Although the addition of calcium and magnesium kept the cells viable, it did not fully rescue aggregation. This is consistent with the experiment where we added the LMWF of the supernatant to the low density *haves*. Above, we showed that factors in the heat-sensitive large fraction were necessary to rescue aggregation (figure 6.4a,b). In the HMWF, we expect to find Conditioned Medium Factor (CMF) and PDE, both of which were shown to be important for aggregation [15, 30, 16, 1]. PDE is heat sensitive [23, 14, 17] (see supplementary note S1 for the experimental verification) whereas CMF is not [15]. Could PDE be the missing factor? To resolve this, we added exogenous PDE (PDE4A)

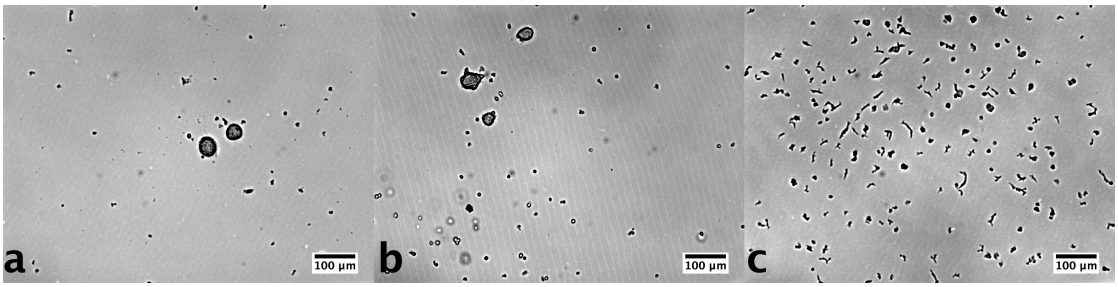

Figure 6.6: Addition of PDE in different amounts to calcium enriched buffers to condition the low density WT cell populations. (a) 20 μg/ml (b) 0.8 μg/ml (c) 0.032 μg/ml. Images were taken a day after start of starvation.

at various concentrations to the low density *haves* conditioned by the calcium enriched buffer. We found that at concentrations of PDE above 2 units/ml (see Methods), normal aggregation behavior was recovered (figure 6.6).

6.4 Discussion

We started this manuscript with a riddle: when a low density population of *haves* were added to a high density population of *have-nots*, the mixture aggregated, whereas each population on its own dies.

We found that the lack of divalent ions kills the low density *haves*. Ions like Ca^{2+} and Mg^{2+} are necessary to keep the cells viable, but they alone cannot enable the low density *haves* to form tight aggregates. Addition of external PDE is necessary to enable these low density *haves* to aggregate. We found that the addition of calcium induces the cells to secrete more PDE (see Supplementary note S1). This effect of increase in PDE with the addition of calcium has been observed before [6, 5, 11, 29]. However, in the low density *haves*, the increase in PDE due to the addition of calcium is not sufficient to cause aggregation.

We found that the addition of external PDE to the low density *haves* in buffers enriched with divalent ions, enabled them to form tight aggregates. Previous experiments have shown that pdsa$^-$ cells, in which the gene responsible of PDE production has been knocked out, displayed decreased cAMP activity and aberrant development and chemotaxis.

The importance of PDE can be understood by considering wave propagation in populations of *D.d*. The propagation of more than one wavefront requires degradation of cAMP within one wave period, i.e., within about 6 - 8 min, most of the cAMP should be degraded. As an estimate, if the cells communicate over a length scale corresponding to about 10 cell lengths, which is about 130 μm at high cell densities, the required degradation rate is about 1.4/ min, which corresponds to 0.7 min. (See Appendix A1 for more details.) Being much smaller than the wave period, this degradation time allows wave propagation, which we observe in the mixture of *haves* and *have-nots* (see supplementary movie S2). If we assume that degradation rate scales linearly with density, at the low cell density we consider, the degradation rate is 70 times smaller, i.e., the degradation time is 70 time larger and is about 50 min. This is much higher than the wave period. Therefore well developed spirals cannot exist here, which we observe in the low density population of *haves* in a calcium enriched buffer (see supplementary movie S3).

Addition of exogenous PDE supplements the degradation of cAMP. In the experiments with PDE4A, we estimate the degradation time due to the exogenous PDE to range from 0.2 min to 130 min. (See Appendix A2 for details.) In accordance with our requirements, we observe tight aggregates only in cases where the degradation rate is smaller than or comparable to the wave period,

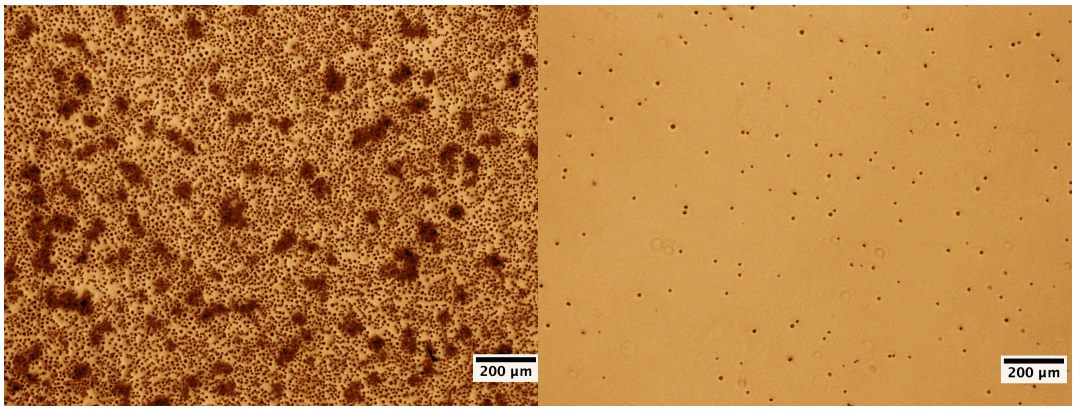

Figure 6.7: The right panel shows the the formation of aggregates in a mixture of 200 cells/cm^2 of *haves* and 1 x 10^6 cells/cm^2 of *have-nots*. The left panel shows 9000 cells/cm^2 of *haves* after the same starvation time. As expected, the cells round up. The *haves* act as centers of activity and the have-not around them aggregated. Due to the high degradation of cAMP by the PDE produced by the *have-nots*, the cAMP waves did not reach all the cells, due to which many cells were not included in any aggregate.

as seen in figure 6.6.

Having gained these insights, we return to the cooperation between the *haves* and the *have-nots*. The *have-nots* supply divalent ions and PDE (see supplementary note S1), both of which are vital for aggregation. In fact, in a mixture of a 200 cells/cm^2 of *haves* and 1 x 10^6 cells/cm^2 of *have-nots*, so much PDE is produced that waves cannot propagate for long distances – cAMP is completely degraded at short distances (see supplementary movie S4), resulting in small aggregates. In figure 6.7, the right panel shows the small aggregates formed by the mixture, whereas the left panel shows the low density *haves*. Although aggregates were formed in the mixture, due to the absence of large scale waves, many cells were unable to aggregate. Thus, we see that the degradation rate is an important parameter for aggregation – both at very low and very high degradation rates, aggregation is not efficient.

We naïvely called the wild-type cells the *haves* and the acaA$^-$ cells the *have-nots*, simply because the latter group is incapable of producing cAMP. But we found that the mutants provide other components that are vital for survival. While investigating their cooperation, we found that (1) a critical amount of divalent ions is necessary to keep the cells viable, and (2) PDE in a certain range is necessary for optimum aggregation. Further, we see when these two criteria are satisfied, even a small fraction of cAMP producing cells can synchronize the population and cause aggregation, explaining the robustness of the mechanism. The cooperation occurs by the sharing of complementary resources. It remains to be seen if other species display such cooperation.

6.5 Methods

6.5.1 Preparation of the cells

AX2 WT cells and acaA$^-$ cells were grown in HL5 medium (35.5g of Formedium powder from Formedium Ltd., England, per liter of double distilled water, autoclaved and filtered) at 22^0C. The acaA$^-$ cells were obtained from the Kortholt lab. They are derived from AX3 strain. The cells were harvested when they became confluent and were washed in phosphate buffer (2g of KH_2PO_4, 0.36g of $Na_2HPO_4.2H_2O$ per liter at pH 6, autoclaved) and centrifuged three times. The cells were then counted using a hemocytometer and diluted to the appropriate density with fresh phosphate buffer. They were then plated on a 8.6 cm diameter plastic Petri dish with 10 ml phosphate buffer – this corresponds to a buffer thickness of 2 mm. Sometimes, we used plastic Petri dishes divided into

quadrants, or smaller diameter Petri dishes. In all these cases, we maintained a constant areal and volume density of the cells. Parafilm was wrapped around the sides to prevent evaporation of the buffer. A re-structured hair dryer blew warm air above the dish to equilibrate the temperature. The entire room was dark during the experiment and maintained at 22^0C.

6.5.2 Supernatants

The supernatant was removed from the Petri dishes using pipettes and centrifuged to pellet any cells accidentally picked up. The clear supernatant was then filtered using 0.2μm filters. The heat treatment consists of heating the supernatant uniformly at 80^0C for about 20 min in a thermostat. The actual temperature was monitored using a thermometer. After 20 min, the supernatant was allowed to cool to room temperature before being used for experiments.

To fractionate the supernatant into the high and low molecular weight fractions, we used a a 30kDa ultrafiltration device from Centricon. The supernatant was added to the filter. Spinning it in the centrifuge at 3500 g for about 15 min left about 200μL of high molecular weight retentate. The efflux contains the rest of the supernatant which has substances smaller than 30kDa. To use the retentate as conditioning medium at the same concentration as in the supernatant, we reconstituted it in phosphate buffer of the same volume as the starting volume of the supernatant used.

6.5.3 Addition of external PDE

PDE4A were purchased from Enzo and Signal Chem. For each experiment, the enzyme was diluted based on the activity provided on sample and from the experimental value of the Michaelis-Menten constant for these enzymes. 1 unit = 1 nmol/min at 37^0C. For details of the calculations, see Appendix A2.

6.6 ACKNOWLEDGEMENTS

None of this work would have been possible without the help of Maren S Müller and Katharina Gunkel. The authors are grateful to their invaluable help in the preparation of the cells and in obtaining the necessary chemicals and enzymes. The authors gratefully acknowledge the help and support provided by Bastian Hüllsmann in the Gorlich lab at the Max-Planck Institute for Biophysical Chemistry for the use of the luminometer. The authors also thank J. P. Sethna, V. Vogt, I. Guido and G. Gerisch for useful discussions. Further, the authors thank C. Westendorf for help with the microscopes and discussions. This work has been supported by the Max Planck Society.

6.7 Supplementary Materials

6.7.1 Supplementary note S1: Measuring the extra-cellular PDE activity

To measure PDE activity, we used the PDELight kit from Lonza. The measurement works on the principle that PDE degrades cAMP to create AMP. The detection reagent provided in the kit converts AMP to ATP, Luciferin and oxygen. In the presence of luciferase, these combine to produce AMP and photons (among other products). The number of photons measured is thus an indicator of the amount of AMP present. We allowed the PDE from our cell populations to react with cAMP for 20 min and measured the resulting amount of AMP by counting photons with a luminometer. From the amount of AMP remaining, we estimated the degradation of the PDE in our sample.

We first collected the supernatant from the populations as described in Methods. We diluted the retentate of the filtration appropriately. For each sample, we created multiple dilutions of the retentate and added 30μL of each in a black 96 well plate. To each dilution, we added 10μL of 100μM cAMP. After 20 min of reaction time, we added the stop solution - a 1:1 mixture of the Lonza stop solution and 100 mM DTT. Then, we added the detection reagent, and allowed 10 min for the reaction to stabilize. For each dilution, we created a background sample by adding the just diluted retentates without cAMP to the wells in the 96 well plate. During each experiment, for calibration, we added 30μL of different concentrations of AMP to the same 96 well plate. To make the same volume, instead of cAMP, we added 10μL of phosphate buffer to these standards. We

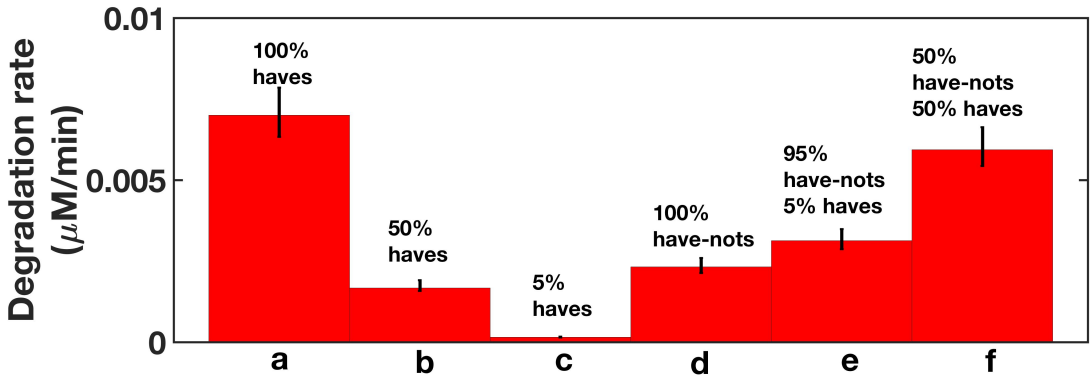

Figure 6.8: Comparison of the degradation rate of the extra cellular PDE produce by different cell populations. 100% corresponds to a cell density of about 2 x 10^5 cells/cm^2

added the same amounts of stop solution and detection reagent. An integration time of 0.1s was used. We recorded the luminosity every 10 min to account for the decay of AMP. We fit the time series of the intensities with a model (Appendix A3) to obtain the degradation rates.

We performed this assay to first find the degradation rate of cAMP in different cell populations. At high wild type cell densities, the degradation rate is about 0.007 /min (figure 6.8 column a). At half this density, the degradation rate decreases to 0.0018 /min (figure 6.8 column b) and at the low density, it is 0.0002 /min (figure 6.8 column c). The mutants also produce a significant amount of PDE, although it is not as much as that produced by the same number of wild type cells (compare figure 6.8 columns a and d). Further, keeping the total cell density fixed, as the ratio of mutants to wild type cells is decreased, the population mixture produces more PDE (figure 6.8 columns d -f). From these measurements it was clear that the mutants contribute PDE in addition to the divalent ions in the mixture of low density wild types and high density mutants.

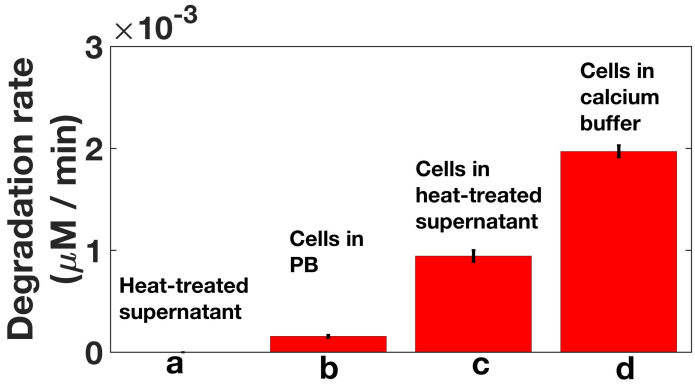

Figure 6.9: Comparison of the degradation rate of the extra cellular PDE produced by the low density populations in different conditions. PB is phosphate buffer. Low density *haves* are used in columns b, c, and d.

Next, to observe the effect of the heat-treated supernatant, we conditioned the low density WT cells with the heat treated supernatant, starved them for about six hours and then measured the PDE activity in the supernatant. We found that this activity (figure 6.9 column c) was much higher than the activity of the low density WT cells in phosphate buffer (figure 6.9 column b). As a check, we verified that our heat treatment denatures PDE, column a in figure 6.9. Finally, the degradation rate was even higher in low density populations conditioned by the calcium enriched buffer (figure 6.9 column d) than in just phosphate buffer. This suggested that the addition of calcium, which keeps the cells viable, induces them to produce more PDE.

Our measurement of the reaction rates of the high density of *haves* is consistent with measurements by other groups [3]. However, both these rates correspond to a degradation time of about 100 min. Theoretically, wave propagation is not possible at these rates. But we do observe waves. So there must be additional sources of degradation of cAMP that these measurements missed. What these could be, is an open question.

6.7.2 Appendix

A1: The importance of PDE in long range signaling

Consider the typical wild type cell density used in experiments i.e. cell density ρ is 6 x 10^5 cells/ml^2. The typical cell separation d_{sep} is given by

$$d_{sep} = \frac{1}{\sqrt{\rho}}. \tag{6.1}$$

For the typical cell density mentioned above, this gives a d_{sep} of about 13μm. The typical wavelength of the cAMP waves is about 1 - 2 mm. The dynamics of *D.d.* forms a reaction - diffusion system. If we assume that the degradation follows first order kinetics, the length scale L for diffusion is set by the diffusion constant D and the degradation rate of cAMP γ.

$$L = \sqrt{\frac{D}{\gamma}} \tag{6.2}$$

This gives,

$$\gamma = \frac{D}{L^2} \tag{6.3}$$

If we assume a diffusive length of about 130 μm, which corresponds to the distance between 10 cells (10 x d_{sep}), and use D = 0.024 mm^2/min, we get γ = 1.4 min^{-1}, which corresponds to a degradation time of 0.7 min. The diffusion length scale L cannot be shorter than the typical separation between two cell, d_{sep}, because if it were, the signal would diffuse before it reached the neighboring cell, and there would be no excitation waves. Similarly, the characteristic decay time given by $1/\gamma$ has to be shorter than the period of the waves (6 - 8 min), so that cAMP can be degraded before the next wave begins. Therefore, the value of the degradation rate at high cell densities allows wave propagation because it is shorter than the period of the wave.

Now, the density of our low density population is about 70 times smaller than the value considered above. If we assume that the degradation scales linearly with density, the degradation rate of the low density population will be 70 times smaller, and the degradation time will be 70 times larger, or about 49 min. This number is much higher than the period of the waves. This larger degradation time will not allow wave propagation. As we have seen in figure 6.8, the extra cellular PDE decreases more rapidly with density than a linear fit would predict. Therefore, for aggregation, more PDE is necessary in the low density *haves*.

A2: Activity of exogenous PDE

To illustrate the calculation of activity, let us start with the activity stated on the vial of PDE. For example, in one experiment, the activity of PDE4A was 2429 units/mg. 1 unit = 1 nmol/min at 37^0C. Since our experiments are at 22^0C, we used 1 unit = 0.5 nmol/min.

$$V_{max} = \frac{0.5nmol}{min \quad unit} \quad \frac{2429units}{mg} = \frac{1.21\mu mol}{min \quad mg}$$

Let us assume that we dilute the sample to $\frac{X\mu g}{ml}$. Then,

$$V_{max} = \frac{X\mu g}{ml} \quad \frac{1.21\mu mol}{min \quad mg} = X1.21\mu M/min$$

We know that the Michaelis-Menten constant for PDE4A is about $K_M = 5\mu M$ [21]. At high substrate concentration, the degradation rate is given by $\gamma = \frac{V_{max}}{K_M} = \frac{1.21X\mu M}{5\mu Mmin}$. The degradation time is given by $1/\gamma$. As a particular case, when X = 0.0032, the degradation time is 129 min, whereas when X = 20, the degradation time is 0.2 min. We don't expect tight aggregates in the former case, whereas we do expect them in the latter case, as is shown in figure 6.6.

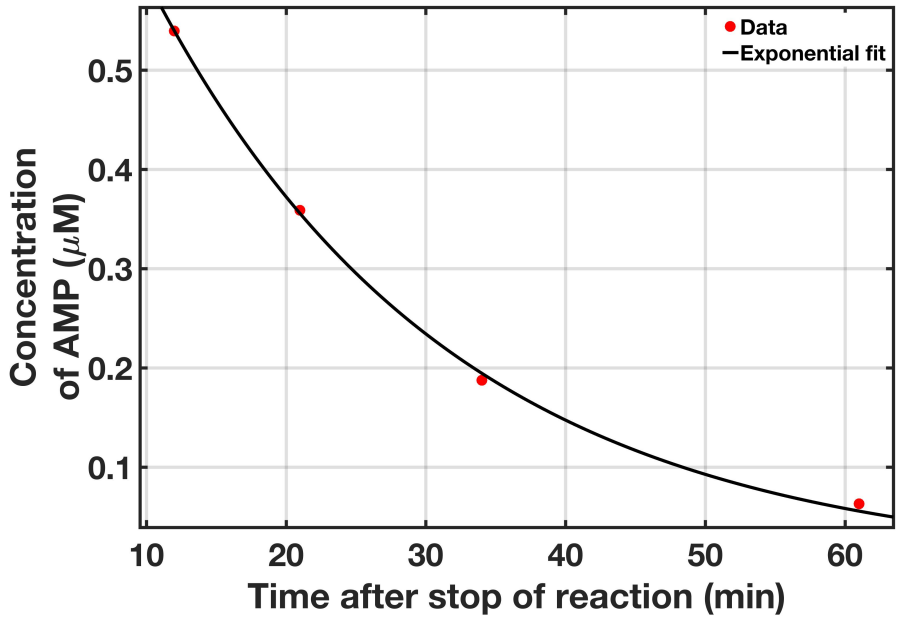

Figure 6.10: Sample fit of the decay of the concentration of AMP as a function of time.

A3: Obtaining the degradation rate

We modeled the system in the following way. AMP is produced through the action of PDE, and there is a decay rate. For PDE produced by *D.d..*, it is known that the value of the Michaelis-Menten constant is 0.75μM [3]. In our experiments, we add a much higher concentration of cAMP. So the rate of the reaction can be assumed to be independent of the substrate concentration. This rate is also V_{max}, the maximum rate of the reaction. We observe that AMP concentration decays after the reaction is stopped by adding the stop solution. Accounting for the production and decay of AMP, we can write

$$\frac{dC}{dt} = k_1 - k_2 C. \tag{6.4}$$

Here C is the concentration of AMP, k_1 is the degradation rate of PDE which creates AMP (this is the rate we are interested in finding) and k_2 is the decay

rate of AMP. The solution to the equation is

$$C(t) = \frac{k_1}{k_2}(1 - exp(-k_2 t)). \tag{6.5}$$

We stop the reaction after 20 min, the concentration of AMP after 20 min is C(20).

$$C(20) = \frac{k_1}{k_2}(1 - exp(-20k_2)). \tag{6.6}$$

After these 20 min, there is only decay of AMP because PDE doesn't act anymore. The equation for the concentration of AMP after these 20 min is therefore the decaying exponential

$$C(t) = C(20)exp(-k_2 t). \tag{6.7}$$

Here t is time after stopping the PDE action. We measure C(t) at different times after stopping. We first subtracted the background AMP and then converted the luminosities to concentrations using the AMP standards. Then we fit an exponential to the decaying concentration of AMP to get C(20) and k_2. We plug these values back into equation 6.6 to get the decay rate k_1. The error in k_1 is calculated by propagating the errors in $C(20)$ and k_2 from the confidence intervals provided by the fit. a sample fit is shown in the figure.

BIBLIOGRAPHY

[1] F Alcantara and G W Brazill. "Extracellular Cyclic AMP-Phosphodiesterase Accelerates Differentiation in Dictyostelium discoideum". In: *Journal of general microbiology* 92 (1976), pp. 351–68.

[2] FERNANDA ALCANTARA and MARILYN MONK. "Signal Propagation during Aggregation in the Slime Mould Dictyostelium discoideum". In: *Microbiology* 85.2 (1974), pp. 321–334. URL: http://mic.microbiologyresearch.org/content/journal/micro/10.1099/00221287-85-2-321.

[3] Sonya Bader, Arjan Kortholt, and Peter J M Van Haastert. "Seven Dictyostelium discoideum phosphodiesterases degrade three pools of cAMP and cGMP". In: *Biochemical Journal* 402.Pt 1 (Feb. 2007), pp. 153–161. DOI: 10.1042/BJ20061153. URL: http://www.ncbi.nlm.nih.gov/pmc/articles/PMC1783984/.

[4] John T. Bonner. "A Descriptive Study of the Development of the Slime Mold Dictyostelium discoideum". In: *American Journal of Botany* 31.3 (1944), pp. 175–182. ISSN: 00029122, 15372197. URL: http://www.jstor.org/stable/2437641.

[5] M. B. COUKELL and A. M. CAMERON. "Calcium depletion of Dictyostelium cells selectively inhibits cyclic nucleotide phosphodiesterase synthesis at a post-transcriptional step". In: *Journal of Cell Science* 97.4 (1990), pp. 649–657. ISSN: 0021-9533. eprint: http://jcs.biologists.org/content/97/4/649.full.pdf. URL: http://jcs.biologists.org/content/97/4/649.

[6] M.B. Coukell and A.M. Cameron. “Effects of suboptimal levels of extracellular calcium on the regulation of the cyclic AMP phosphodiesterase-inhibitor system and membrane differentiation in Dictyostelium discoideum”. In: *Journal of Cell Science* 90.4 (1988), pp. 691–700. ISSN: 0021-9533. eprint: http://jcs.biologists.org/content/90/4/691.full.pdf. URL: http://jcs.biologists.org/content/90/4/691.

[7] Emmanuel Décavé et al. “Shear flow-induced motility of Dictyostelium discoideum cells on solid substrate”. In: *Journal of Cell Science* 116.21 (2003), pp. 4331–4343. ISSN: 0021-9533. DOI: 10.1242/jcs.00726. eprint: http://jcs.biologists.org/content/116/21/4331.full.pdf. URL: http://jcs.biologists.org/content/116/21/4331.

[8] Peter N. Devreotes, Michael J. Potel, and Stephen A. MacKay. “Quantitative analysis of cyclic AMP waves mediating aggregation in Dictyostelium discoideum”. In: *Developmental Biology* 96.2 (1983), pp. 405–415. ISSN: 0012-1606. DOI: http://dx.doi.org/10.1016/0012-1606(83)90178-1. URL: http://www.sciencedirect.com/science/article/pii/0012160683901781.

[9] Soheila Dolatabadi et al. “Cell Cycle and Cell Size Dependent Gene Expression Reveals Distinct Subpopulations at Single-Cell Level”. In: *Frontiers in Genetics* 8 (2017), p. 1. ISSN: 1664-8021. DOI: 10.3389/fgene.2017.00001. URL: https://www.frontiersin.org/article/10.3389/fgene.2017.00001.

[10] Dirk Dormann and Cornelis J. Weijer. “Propagating chemoattractant waves coordinate periodic cell movement in Dictyostelium slugs”. In: *De-*

velopment 128.22 (2001), pp. 4535–4543. ISSN: 0950-1991. eprint: http://dev.biologists.org/content/128/22/4535.full.pdf. URL: http://dev.biologists.org/content/128/22/4535.

[11] G.N. Europe-Finner, S.J. McClue, and P.C. Newell. "Inhibition of aggregation in Dictyostelium by EGTA-induced depletion of calcium". In: *FEMS Microbiology Letters* 21.1 (1984), pp. 21–25. ISSN: 0378-1097. URL: http://www.sciencedirect.com/science/article/pii/0378109784901721.

[12] Paul R. Fisher and Zofia Wilczynska. "Contribution of endoplasmic reticulum to Ca2+ signals in Dictyostelium depends on extracellular Ca2+". In: *FEMS Microbiology Letters* 257.2 (2006), pp. 268–277. ISSN: 1574-6968. DOI: 10.1111/j.1574-6968.2006.00180.x. URL: http://dx.doi.org/10.1111/j.1574-6968.2006.00180.x.

[13] G Gerisch. "Chapter 6 Cell Aggregation and Differentiation in Dictyostelium". In: *Current Topics in Developmental Biology* 3 (1968), pp. 157–197. ISSN: 0070-2153. DOI: http://dx.doi.org/10.1016/S0070-2153(08)60354-3. URL: http://www.sciencedirect.com/science/article/pii/S0070215308603543.

[14] G. Gerisch et al. "Cyclic AMP Phosphodiesterase and its Inhibitor in Slime Mould Development". In: *Nature* 235 (1972), pp. 90–92.

[15] R.H. Gomer, I.S. Yuen, and R.A. Firtel. "A secreted 80 x 10(3) Mr protein mediates sensing of cell density and the onset of development in Dictyostelium". In: *Development* 112.1 (1991), pp. 269–278. ISSN: 0950-1991. eprint: http://dev.biologists.org/content/112/1/269.full.pdf. URL: http://dev.biologists.org/content/112/1/269.

[16] R Jain et al. “A density-sensing factor controls development in Dictyostelium.” In: *Genes & Development* 6.3 (1992), pp. 390–400. DOI: 10.1101/gad.6.3.390. URL: http://genesdev.cshlp.org/content/6/3/390.abstract.

[17] R H Kessin et al. “Binding of inhibitor alters kinetic and physical properties of extracellular cyclic AMP phosphodiesterase from Dictyostelium discoideum.” In: *Proceedings of the National Academy of Sciences of the United States of America* 76.11 (Nov. 1979), pp. 5450–5454. URL: http://www.ncbi.nlm.nih.gov/pmc/articles/PMC411666/.

[18] Daniel F. Lusche, Deborah Wessels, and David R. Soll. “The effects of extracellular calcium on motility, pseudopod and uropod formation, chemotaxis, and the cortical localization of myosin II in Dictyostelium discoideum”. In: *Cell Motility and the Cytoskeleton* 66.8 (2009), pp. 567–587. ISSN: 1097-0169. DOI: 10.1002/cm.20367. URL: http://dx.doi.org/10.1002/cm.20367.

[19] F T Marin and F G Rothman. “Regulation of development in Dictyostelium discoideum. IV. Effects of ions on the rate of differentiation and cellular response to cyclic AMP.” In: *The Journal of Cell Biology* 87.3 (1980), pp. 823–827. ISSN: 0021-9525. DOI: 10.1083/jcb.87.3.823. eprint: http://jcb.rupress.org/content/87/3/823.full.pdf. URL: http://jcb.rupress.org/content/87/3/823.

[20] Peter C. Newell. “Aggregation and Cell Surface Receptors in Cellular Slime Molds”. In: *Microbial Interactions*. Ed. by J. L. Reissig. Boston, MA: Springer US, 1977, pp. 1–57. ISBN: 978-1-4615-9698-1. DOI: 10.1007/978-1-4615-9698-1_1. URL: http://dx.doi.org/10.1007/978-1-4615-9698-1_1.

[21] Kenji Omori and Jun Kotera. “Overview of PDEs and Their Regulation”. In: *Circulation Research* 100.3 (2007), pp. 309–327. ISSN: 0009-7330. DOI: 10.1161/01.RES.0000256354.95791.f1. eprint: http://circres.ahajournals.org/content/100/3/309.full.pdf. URL: http://circres.ahajournals.org/content/100/3/309.

[22] Kenneth B Raper. “Dictyostelium discoideum, a new species of slime mold from decaying forest leaves”. In: *Journal of Agricultural Research* 50.2 (1935), pp. 135–148.

[23] Volkhard Riedel et al. “Cyclic AMP phosphodiesterase interaction with its inhibitor of the slime mold, Dictyostelium discoideum”. In: *Biochemical and Biophysical Research Communications* 46 (1972), pp. 279–287.

[24] FLORIAN SIEGERT and CORNELIS WEIJER. “Digital image processing of optical density wave propagation in Dictyostelium discoideum and analysis of the effects of caffeine and ammonia”. In: *Journal of Cell Science* 93.2 (1989), pp. 325–335. ISSN: 0021-9533. URL: http://jcs.biologists.org/content/93/2/325.

[25] KJ Tomchik and PN Devreotes. “Adenosine 3′,5′-monophosphate waves in Dictyostelium discoideum: a demonstration by isotope dilution–fluorography”. In: *Science* 212.4493 (1981), pp. 443–446. ISSN: 0036-8075. DOI: 10.1126/science.6259734. eprint: http://science.sciencemag.org/content/212/4493/443.full.pdf. URL: http://science.sciencemag.org/content/212/4493/443.

[26] Douwe M. Veltman, Ineke Keizer-Gunnik, and Peter J.M. Van Haastert. “Four key signaling pathways mediating chemotaxis in Dictyostelium discoideum”. In: *The Journal of Cell Biology* 180.4 (2008), pp. 747–753. ISSN: 0021-9525. DOI: 10.1083/jcb.200709180. eprint: http://jcb.

rupress.org/content/180/4/747.full.pdf. URL: http://jcb.rupress.org/content/180/4/747.

[27] Bin Wang and Adam Kuspa. "Dictyostelium Development in the Absence of cAMP". In: *Science (New York, N.Y.)* 277 (Aug. 1997), pp. 251–4.

[28] Chenlu Wang et al. "The interplay of cell–cell and cell–substrate adhesion in collective cell migration". In: *Journal of The Royal Society Interface* 11.100 (2014). ISSN: 1742-5689. DOI: 10.1098/rsif.2014.0684. eprint: http://rsif.royalsocietypublishing.org/content/11/100/20140684.full.pdf. URL: http://rsif.royalsocietypublishing.org/content/11/100/20140684.

[29] Fumie YAMASAKI and Hidenori HAYASHI. "Participation of Calcium in the Induction of Phosphodiesterase by Cyclic Adenosine 3′, 5′-Monophosphate in Dictyostelium discoideum". In: *The Journal of Biochemistry* 92.6 (1982), pp. 1911–1917.

[30] I S Yuen et al. "A density-sensing factor regulates signal transduction in Dictyostelium." In: *The Journal of Cell Biology* 129.5 (1995), pp. 1251–1262. ISSN: 0021-9525. DOI: 10.1083/jcb.129.5.1251. eprint: http://jcb.rupress.org/content/129/5/1251.full.pdf. URL: http://jcb.rupress.org/content/129/5/1251.

CHAPTER 7

EFFECT OF SUBSTRATE ON PATTERN FORMATION

7.1 Introduction

In nature, *D.d.* live in the soil. Different soils have different properties, like texture, porosity, stiffness etc. Do these properties affect pattern formation and aggregation in cell populations? In this chapter, I will address this question of how substrates affect pattern formation in *D.d.* The importance of the role of cell-substrate interactions on the locomotion of cells has been well studied [3]. In *D.d.*, the cell-substrate interactions are mediated through the focal adhesions, which link the cytoskeleton to the extracellular matrix [1]. Filamentous actin is primarily responsible for these focal adhesions. In their study, Schindl et al. [3] found that mutants lacking in proteins involved in cross-linking and fragmenting filamentous actin behave very differently, with respect to properties like contact area and pseudopod protrusion, from wild type cells, and this behavior depends on the substrate. The role of adhesion in cell migration has also been investigated [2]. However, there has been no research on the dependence of pattern formation on the properties of the substrate.

7.2 Methods

7.2.1 Substrate preparation

Continuing the work of a pervious post doctoral researcher, N. Oikawa, I used agar, polysaccharide derived from algae, as the substrate for these experiments. Agar is not soluble in water or buffer at room temperature. But, if the water or buffer is heated, agar dissolves in it and forms a viscous solution depending on the amount of agar added. These solutions can be stored in refrigerators at 4C and re-heated before the next use. But, long term storage causes evaporation, changing the composition of the mixture. Further, if the agar is stored for short durations in the refrigerator for later use, it should be done in a large container. This is because, when re-heated in a microwave, sometimes, the upper portions of the solid melts first and oozes out of the container, while the lower portions is still solidified. This can also change the composition. So, for these experiments, I prepared fresh agar solutions before each experiment.

The lowest agar density used had 0.4% agar and the highest agar density had 2% agar. Agar gel was made by weight to volume percentages. For example, to make 1% agar, I weighed 0.5 g of agar and mixed it with 50 ml of phosphate buffer. I stirred this mixture and sterilize it by autoclaving. During the autoclaving procedure, which takes about 45 min, I prepare the cells as described in the Methods section. After autoclaving, I allowed the mixture to slightly cool down and then using a pipette, poured 10 ml of the warm mixture into a Petri-dish and allowed it to solidify in the dish. Extra care has to be taken for higher percentages of agar, because they solidify rapidly.

Once the plates were ready, I added the cell solution to it. The cell solution is concentrated to one ml of buffer with 35 million cells. One ml of cell solution cannot easily cover the entire dish, especially for high agar densities – the layer has to be spread manually. After this spreading, I left the Petri-dish open under a running hood for about 20 min. In this duration, the cells settle down on the agar, and due to the continuous air flow in the hood, the excess buffer evaporates leaving behind a thin layer of buffer. In a different set of experiments, I added a larger amount - 10 ml - of buffer with the same cell number. In these experiments, the buffer layer was about 2 ml thick.

7.2.2 AFM measurements

An AFM from JPK Instruments was used. A cantilever with a pyramidal tip was used to probe the substrates. The cantilever tip is mounted on the AFM head, and the laser beam is adjusted so that it reflects from the top of the tip of the cantilever. The deflection of the cantilever causes a displacement in the reflected spot in the laser beam. This displacement is detected by a photodiode and converted to the displacement of the cantilever tip. In order to fit the sample holder, smaller Petri-dishes (about 2 cm in diameter) have to be used. For calibration, I used a dish with buffer in it. The position of the tip is changed by using a piezo-controller. First the position of the surface of the buffer is noted. An approach speed and distance is set making sure to stay away form the surface of the dish. The cantilever is calibrated by measuring its free oscillations. For the experiments, the small Petri-dish with agar in it is placed under the cantilever that has been calibrated. Using the piezo-controller, the cantilever is made to approach the surface at a constant speed and retract. The displacement

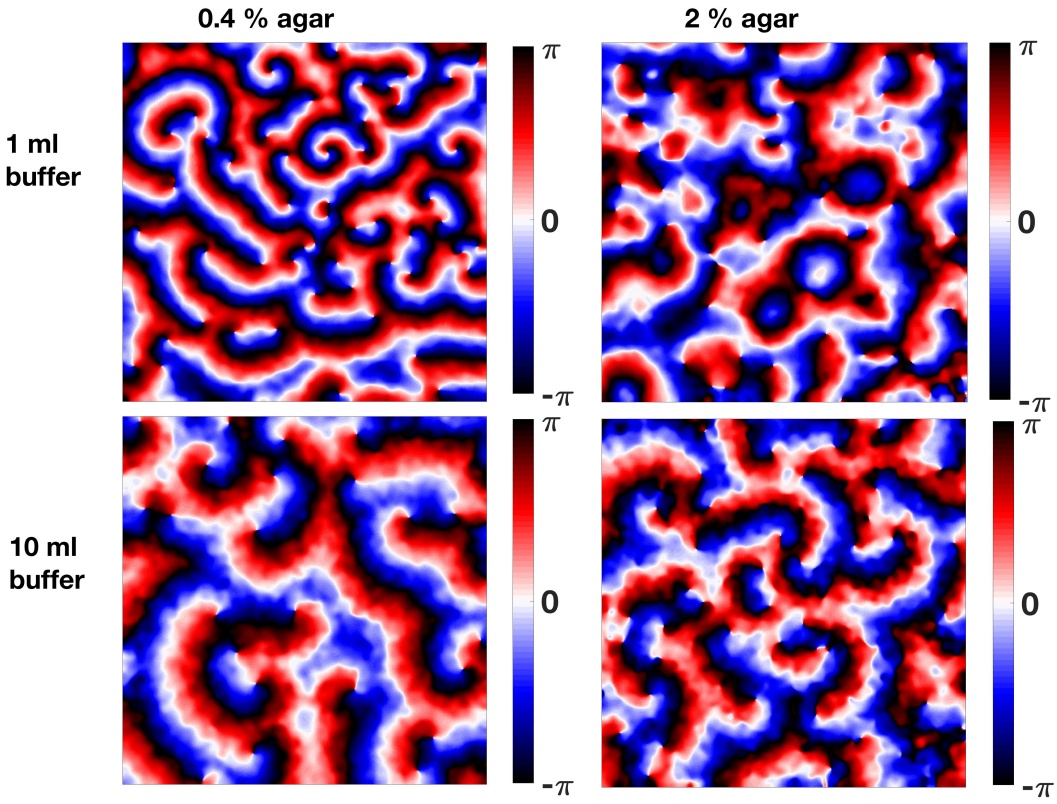

Figure 7.1: Exemplary patterns formed by populations of *D.d.* on different substrates. The top row shows the patterns with 1ml buffer, while the bottom row shows the patterns with 10 ml buffer. Each side is of length 1.3 cm.

of the tip is converted to a force - separation curve. The built-in software uses the standard Hertz model for a pyramidal tip to obtain the elastic modulus from this curve. The measurements are repeated over many positions and samples to get good statistics.

7.3 Results and Discussion

As the agar density increased, the patterns changed drastically. For low agar densities, many spirals were formed, whereas for higher agar densities, well de-

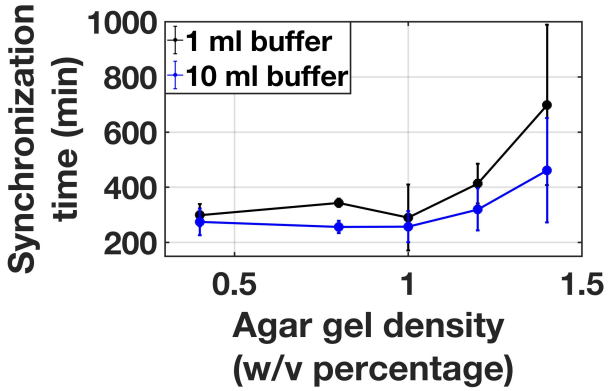

Figure 7.2: The variation of synchronization time as a function of agar density.

veloped spirals failed to form. Patterns at high agar densities were dominated by target patterns were formed. Some exemplary patterns are shown in the top row of fig. 7.1. Further, the time needed for these patterns to synchronize with each other increased, almost linearly with increasing gel density. This is shown by the black curve in fig. 7.2. How does the changing gel density cause a change in the patterns? The first hypothesis was diffusion. It is possible that increasing the gel density increases diffusion co-efficient. And if diffusion takes longer, it would affect the long range signaling of cAMP. Previously, in our group by N. Oikawa had shown that the diffusion co-efficient indeed increases with increasing agar gel density, by measuring the diffusion of fluorescein. However, on analyzing the theoretical models, I found that while the diffusion coefficient indeed affects the length scales of the pattern, it does *not* affect the kind of patterns produced. In simulations, changing diffusion coefficient only changed the size of the spirals. Smaller spirals were formed for higher diffusion coefficients, as is shown in figure. But there was no transition form spirals to target patterns. Of course, it is possible that the model is inaccurate – other parameters of the system could depend on the diffusion coefficient, but not incorporated in the model.

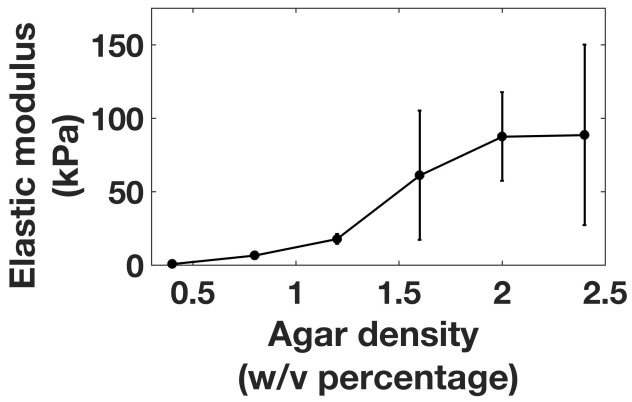

Figure 7.3: The elastic modulus of the substrate as a function of agar density.

The next hypothesis was that elastic modulus of the substrate could play a role. I measured the elastic modulus of agar substrates for different densities using an AFM. The results are shown in fig. 7.3. Indeed, as the gel density increases, the agar substrate becomes stiffer. However, none of the models consider the effect of substrate in pattern formation.

In both the hypotheses proposed, we observe a correlation. But correlation is not causality. I performed another set of experiments to confirm if the substrates' elasticity and diffusion played a role. In these experiments, instead of having a very thin layer of buffer, I used an excess amount of buffer, with the same number of cells as before. In particular, I used 10 ml buffer instead of the 1 ml used before. If the cause of the changing patterns was indeed diffusion through the substrate of the substrate elasticity, then increasing the amount of buffer on top of the cells should have no effect. However, surprisingly, addition of an excess amount of buffer washed the effect away – well developed spirals were the dominant patterns on high density agar substrates too. These patterns are shown in the bottom row of fig. 7.1. The time needed for the cells to synchronize did increase, but at a slower rate, as depicted in the blue line in fig.

7.2.

This means that the thin layer over the cells plays an important role in determining the patterns. Further, the patterns also depend on some property of the substrate which causes the transition with increasing density. Whether this property is diffusion, substrate elasticity, or an entirely different property, or a combination of one or more of these properties is yet to be ascertained. It is also important to note that in these experiments, the image quality was rather poor. More experiments are needed to understand this phenomenon.

BIBLIOGRAPHY

[1] Keith Burridge and Magdalena Chrzanowska-Wodnicka. "FOCAL ADHESIONS, CONTRACTILITY, AND SIGNALING". In: *Annual Review of Cell and Developmental Biology* 12.1 (1996). PMID: 8970735, pp. 463–519. DOI: 10.1146/annurev.cellbio.12.1.463. URL: https://doi.org/10.1146/annurev.cellbio.12.1.463.

[2] Anna Huttenlocher, Rebecca R Sandborg, and Alan F Horwitz. "Adhesion in cell migration". In: *Current Opinion in Cell Biology* 7.5 (1995), pp. 697–706. ISSN: 0955-0674. DOI: https://doi.org/10.1016/0955-0674(95)80112-X. URL: http://www.sciencedirect.com/science/article/pii/095506749580112X.

[3] M. Schindl et al. "Cell-substrate interactions and locomotion of Dictyostelium wild-type and mutants defective in three cytoskeletal proteins: a study using quantitative reflection interference contrast microscopy". In: *Biophysical Journal* 68.3 (1995), pp. 1177–1190. ISSN: 0006-3495. DOI: https://doi.org/10.1016/S0006-3495(95)80294-8. URL: http://www.sciencedirect.com/science/article/pii/S0006349595802948.

CHAPTER 8

PARAMETER ESTIMATION

In the previous section, to explain experimental results with simulations, I varied the model parameters, by introducing spatiotemporal variations. However, all these changes were done manually, by trial and error. Given that the models have numerous parameters, which can vary in time and space, searching for optimal combinations of these parameters by trial and error is a daunting task. It is impossible to explore the entire parameter space by hand. A mathematical approach is most suitable for this task.

I used the method proposed by Berg et al. [1]. To explain this method, consider a system modeled by differential equations for three variables and with N parameters. Let's say, experimentally, only one of the variables can be measured, and only some of the N variables are known *a priori*. The two variables of the model that are not measured experimentally are called hidden variables. The goal is to obtain these hidden variables and unknown parameters by using the information from the experiments in the model.

The experimental data is coupled to the model in the following way. A term equal to the difference between the data and the model variable corresponding to this data is added to the equation. The strength of the coupling is tuned by a coupling parameter that is multiplied to this difference. As the responding model, the slave, evolves, the the coupling term either pulls the observed variable back or pushes it forward to force the model to follow the experiment. In some cases, this will automatically force the hidden variables to their "true" values. Additionally, to estimate the unknown parameters, the error, i.e. the square of the difference between the experimentally measured variable and the model

variable, is minimized using standard optimization algorithms, by searching for the optimal set of parameters. In many cases, the experimental variable is not measured directly, e.g., in experiments involving imaging, the variable is in the form of images, i.e., a scaled version of the variable is measured. This adds further complexity to the estimation technique described above. In this chapter, I will describe the application of this technique to the models of pattern formation in *D.d.*

Rather than coupling the models to experimental data, which are usually noisy, I will use the method described above to study the models proposed to explain pattern formation in *D.d.* One of the major models proposed was by Goldbeter and co-workers [4]. This model has been modified in many ways [3, 5, 2]. In this chapter, I will present the results of analyzing two of these models.

8.1 Lauzeral-Halloy-Goldbeter (LHG) model

In this model, the authors [3] introduced a temporal variation in two parameters of the model originally proposed in [4]. As mentioned in the Introduction, the model equations are described by the following equations.

$$\frac{d\rho}{dt} = -f_1(\gamma)\rho + f_2(\gamma)(1-\rho) \tag{8.1}$$

$$\frac{d\beta}{dt} = q\sigma\phi(\rho,\gamma) - (k_i + k_t)\beta \tag{8.2}$$

$$\frac{d\gamma}{dt} = (k_t\beta/h) - k_e\gamma + D\nabla^2\gamma \tag{8.3}$$

The two parameters σ and k_e, corresponding to the rate of production and degradation of cAMP respectively, are varied in time according to the equations:

$$\sigma(t) = 0.3 + 0.25tanh[(t-200)/50] \tag{8.4}$$

$$k_e(t) = 6.5 + 3tanh[(t - 260)/30] \tag{8.5}$$

Further, the model assumes that the values of these two parameters at different points on the simulation grid are not the same. The different values follow an exponential distribution. The simulations begin with each of these variables in steady state, with a perturbation in γ applied to some of the grid points.

In experiments, some function of the variable γ is measured through the images. Therefore γ is the coupling variable and β and ρ are the hidden variables. First, I checked if the method proposed by Berg et al. [1] worked for this system. I did this, by first generating "data" using the above equations. The values of γ obtained are the data, γ_{data}. Next, I added a term that coupled the data to the model variable γ through a coupling constant k:

$$\frac{d\gamma}{dt} = (k_t\beta/h) - k_e\gamma + D\nabla^2\gamma + k(\gamma_{data} - \gamma) \tag{8.6}$$

The starting values for all three variables are zero. I found that this coupling method works very well for this system. Well-developed spiral patterns form after about 300 min. The coupling forces, not only the coupled variable to follow the data, but also the hidden variables. Since the data is generated by simulations, these can be easily checked. Fig. 8.1 shows the patterns formed by the master, the slave and the difference in values between the two. The difference between the true values and the estimated values is at least two orders of magnitude lower than the values of the variables themselves, for all three variables. Next, I assumed that the slave has information of only one of the two parameters σ and k_e. The goal was to check if minimizing the error enabled the slave to converge to the correct value of the unknown parameter, reproducing the temporal variation. To achieve this, I assumed that the unknown parameter is constant for about 5 min. I allowed the simulation to start with a guess

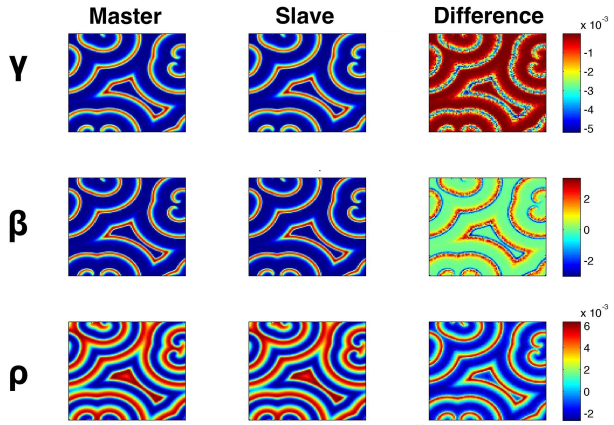

Figure 8.1: The patterns formed by the master, the slave and their difference after 300 minutes. Only γ is coupled, β and ρ are the hidden variables. Each side is 100 pixels, which corresponds to 1cm.

value, run for 500 time steps (corresponding to 5 min), find the error between γ_{data} and γ, and then performed a search to find the value of the parameter that minimizes the cost function, defined by $(\gamma_{data} - \gamma)^2$. The optimization procedure uses the Nelder-Mead algorithm. Once it's found, the simulation moves to the next block of 500 time steps and repeats this procedure. The result of this procedure produces reasonably good estimates of the parameters. To better see this convergence, fig. 8.2 shows the optimized values of the parameter as a function of time. Since the master system that produces the data has a spatial variation in the parameters, it is to be expected that the parameters optimized by the slave will not be perfect. By setting the parameters to be homogenous in space, the convergence is better. For example, fig. 8.3 shows the optimized value of k_e as a function of time, when both the parameters are assumed to be homogenous in space. For the next step, I assumed that the slave has no information on either of the two parameters and optimize both parameters simultaneously. However, this method did not work. Neither parameter was correctly optimized as seen

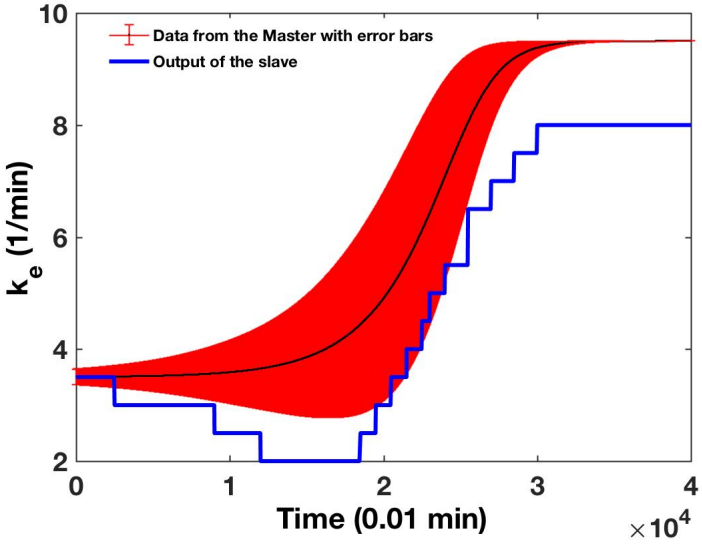

Figure 8.2: The value of the parameter k_e as a function of time. The spatial variance of the parameter in the Master at each time point, is represented by the red error bars.

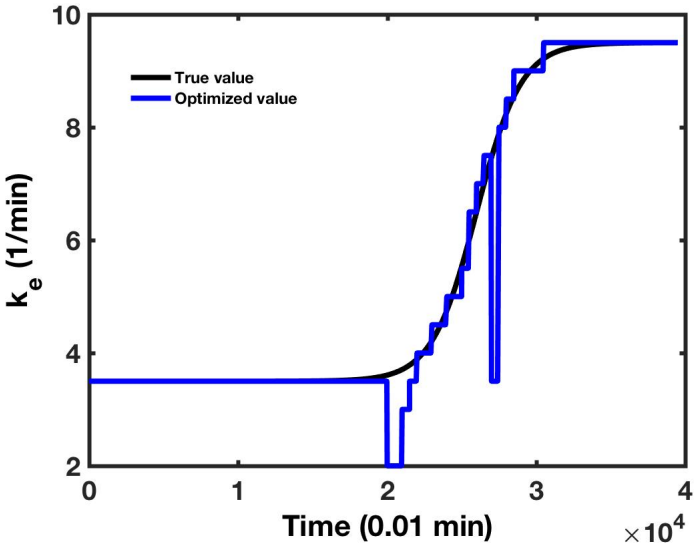

Figure 8.3: The value of the parameter k_e as a function of time.

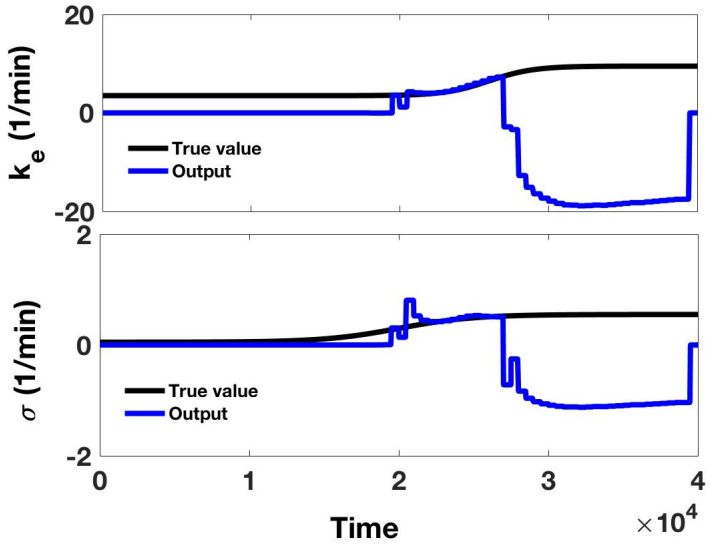

Figure 8.4: The values of the parameters k_e and σ as a function of time.The optimized values do not match the true values even though there is no spatial variation.

in fig. 8.4.

8.2 Pálsson-Cox (PC) model

Another modification of the model proposed by [4] was proposed by [5]. In this version, the authors assumed that k_e has a small spatial variation and decreases linearly with time. The equations for the model are:

$$\frac{d\rho}{dt} = -f_1(\gamma)\rho + f_2(\gamma)(1-\rho) \tag{8.7}$$

$$\frac{d\beta}{dt} = s\phi(\rho,\gamma) - (k_i + k_t)\beta \tag{8.8}$$

$$\frac{d\gamma}{dt} = (k_t\beta/h) - k_e(t)\gamma + D\nabla^2\gamma \tag{8.9}$$

In this version, the parameter s in eq. 8.8 corresponds to σ in eq. 8.2 and is held constant. As before, I first checked if the method works on this system, by

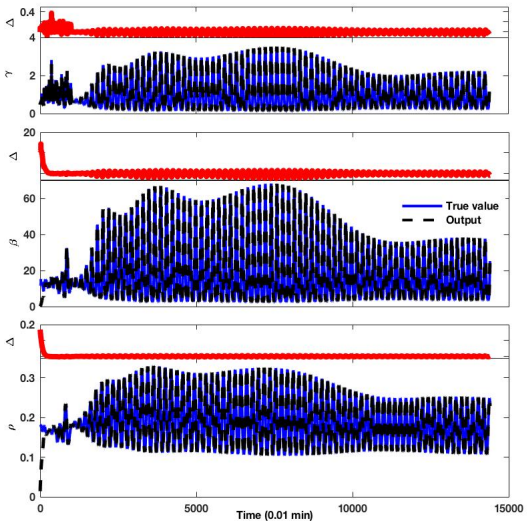

Figure 8.5: The values of the variables γ, β and ρ as a function of time. Only γ is coupled. The red curves above each variable represents the error. As can be seen, the errors are not as small as in fig. 8.1, where the errors were about two orders of magnitude lower than the values of the variables.

assuming that the slave has information on all the parameters of the model. The method proposed by Berg et a. [1] does work for this model too, as is shown in fig. 8.5 However, one can observe that the three variables are not perfectly reproduced, the errors are high. So far, I had been using k=1, for coupling. The coupling parameter k can itself be optimized. I found the value of the cost function for different values of k, assuming that it was constant in time. It is important to note here that, when the parameter directly multiplies to the error terms, the cost function has to be modified to prevent the trivial solution - zero. The cost function is therefore, $|\gamma_{data} - \gamma| + k$. Fig. 8.6 shows the values of the cost function for different k. Surprisingly, the trend is non-linear and non-monotonic. The global minimum occurred at k = 0.05. Using this value for the coupling, I found that the hidden variables indeed match very well with their true values.

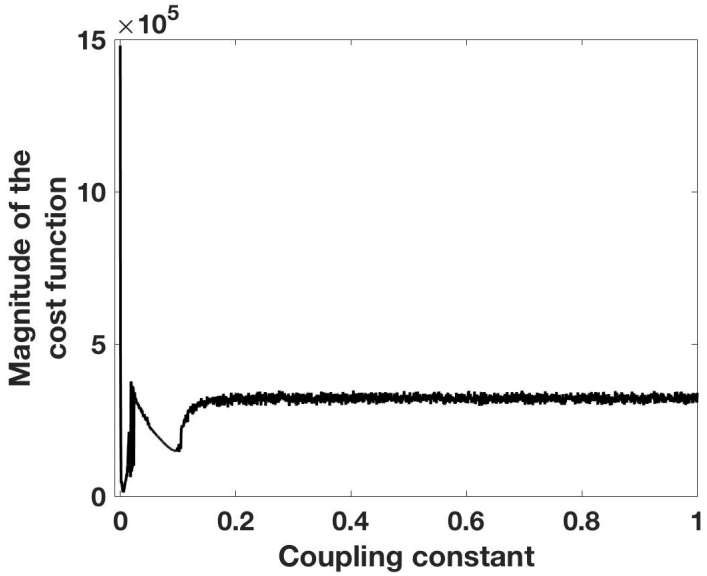

Figure 8.6: The variation of the cost function for different values of the coupling constant.

Next, I assumed that the slave has no information about only the parameter $k_e(t)$, and checked if its temporal variation in could be reproduced by the optimization. I did this in two ways. The first way was, as described above, by optimizing the parameter k_e in blocks of 500 time steps. The result of this optimization is shown in fig.

In the second method, rather then optimizing the parameter directly, I optimized the two parameters of the linearly decreasing trend. This method doesn't require blocks of 500 time steps. Rather, the two parameters are optimized for the entire simulation time. The resulting values of the two parameters were very close to the true values: optimized slope = -1 x $10^{-}4$; true slope = 6 x $10^{-}5$; optimized intercept = 3.7298; true intercept = 3.73.

So far, the inputs to the coupling were the actual values of γ_{data}. As mentioned before, in experiments, we cannot measure these values directly. The intensities of the experimental images will be some function of the γ. The na-

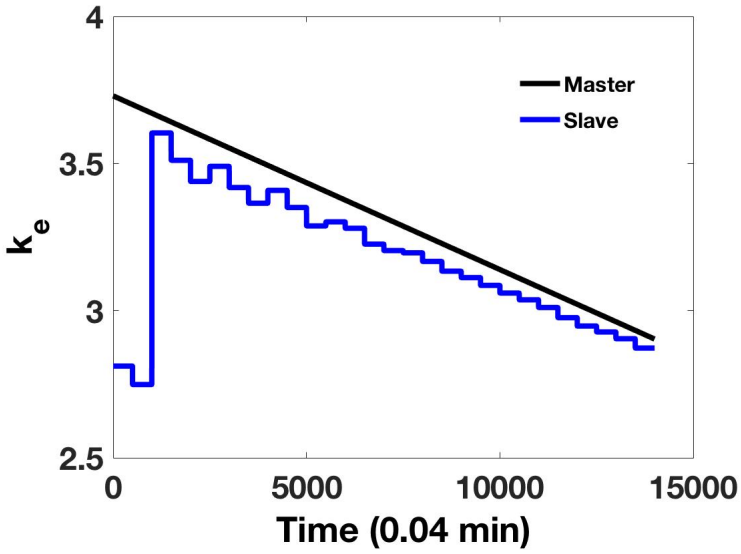

Figure 8.7: A comparison of the temporal variation of k_e as a function of time for the Master and the Slave.

ture of this function is unknown. As a first assumption, the function could be linear: $f(\gamma) = x(1)\gamma + x(2)$. I created this scaling for γ_{data} to check if the optimization can find the scaling parameters. The cost function had to be scaled by x(1), to be $|\gamma_{data} - \gamma|^2/k$ to avoid the trivial solution of zero. However, I found that the optimization failed to synchronize the master and the slave. To understand why, I searched the space of one parameter keeping the other at its true value. From the results in fig. 8.8, it is seen that while x(1) has a well-defined global minimum, x(2) has many local minima. It is easily conceivable that the optimization algorithm gets "stuck" in one of these local minima and is unable to find the global minimum.

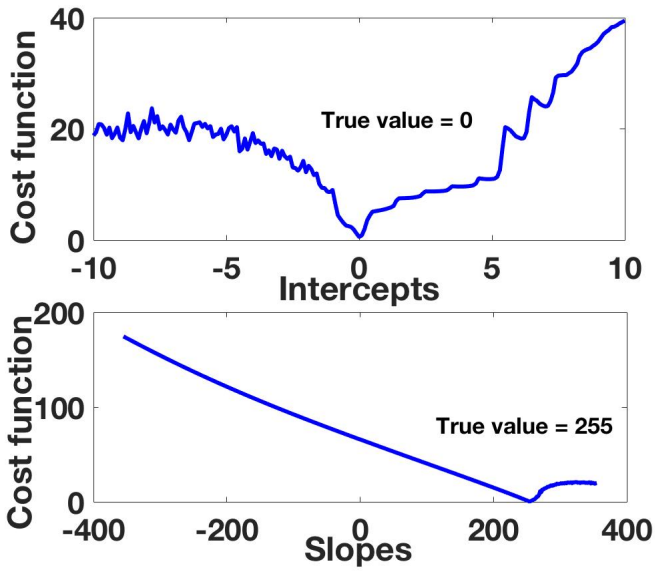

Figure 8.8: A comparison of the cost function for different values of the linear scaling function.

8.3 Comparison of the two models

The two models considered here are very similar to each other. Is it possible that the two models are equivalent? In other words, could the patterns generated by one model be reproduced in the framework of the other? To answer this question, I used the data generated by the LHG model [3] as the input to the PC version [5]. The idea behind this was to check if the sigmoidal variation of the two parameters in the LHG model are equivalent to the linear trend of one and constancy of the other in the PC model.

I optimized for three parameters: two corresponding to the linear trend in $k_e(t)$ and one parameter s in eq. 8.8. However, I found that this method of optimization produces nonsensical results in this case. For all guess values, the parameter s is optimized to be zero, and the two hidden variables do not converge to the true values. This is not realistic, because β in eq 8.8 corresponding

to intracellular cAMP, is the source for the extracellular cAMP γ in eq 8.9. When it goes to zero, by setting s to zero, there is no intracellular cAMP, and therefore there can be no extracellular cAMP. The fact that γ matches very well with the data implies that γ is blindly following the data without going through the model.

To overcome this issue, instead of coupling the data to the model, I assumed that $\gamma_{data} = \gamma$ and optimized for the the three parameters as before. However, this method failed too, assigning a value of zero to the parameter s.

Although this method was not successful, I believe that the basic idea of comparing the two models can still be achieved. Many studies have dealt with the question of whether parameters and hidden variables can be uniquely identified for coupled systems of differential equations [7]. Other studies provide insights into estimating the size of the basin of he global minimum [8]. Other methods to estimate parameters and hidden variables have been found [6]. By analyzing the models of *D.d.* based on these works, it should be possible to understand them better. Further, estimating hidden variables and unknown parameters is an important tool, which is applied to experimental data can increase our knowledge of these systems by leaps and bounds.

BIBLIOGRAPHY

[1] S. Berg, S. Luther, and U. Parlitz. "Synchronization based system identification of an extended excitable system". In: *Chaos: An Interdisciplinary Journal of Nonlinear Science* 21.3 (2011), p. 033104. DOI: 10.1063/1.3613921. eprint: https://doi.org/10.1063/1.3613921. URL: https://doi.org/10.1063/1.3613921.

[2] Martin Falcke and Herbert Levine. "Pattern Selection by Gene Expression in Dictyostelium Discoideum". In: *Phys. Rev. Lett.* 80 (17 Apr. 1998), pp. 3875–3878. DOI: 10.1103/PhysRevLett.80.3875. URL: https://link.aps.org/doi/10.1103/PhysRevLett.80.3875.

[3] Jacques Lauzeral, José Halloy, and Albert Goldbeter. "Desynchronization of cells on the developmental path triggers the formation of spiral waves of cAMP during Dictyostelium aggregation". In: *Proceedings of the National Academy of Sciences of the United States of America* 94.17 (Aug. 1997), pp. 9153–9158. URL: http://www.ncbi.nlm.nih.gov/pmc/articles/PMC23083/.

[4] Jean-Louis Martiel and Albert Goldbeter. "A Model Based on Receptor Desensitization for Cyclic AMP Signaling in Dictyostelium Cells". In: *Biophysical Journal* 52.5 (1987), pp. 807–828. ISSN: 0006-3495. DOI: http://dx.doi.org/10.1016/S0006-3495(87)83275-7. URL: http://www.sciencedirect.com/science/article/pii/S0006349587832757.

[5] E Pálsson and E C Cox. "Origin and evolution of circular waves and spirals in Dictyostelium discoideum territories". In: *Proceedings of the National*

Academy of Sciences 93.3 (1996), pp. 1151–1155. eprint: http://www.pnas.org/content/93/3/1151.full.pdf.

[6] Daniel Rey et al. "Accurate state and parameter estimation in nonlinear systems with sparse observations". In: *Physics Letters A* 378.11 (2014), pp. 869–873. ISSN: 0375-9601. DOI: https://doi.org/10.1016/j.physleta.2014.01.027. URL: http://www.sciencedirect.com/science/article/pii/S0375960114000735.

[7] J. Schumann-Bischoff, S. Luther, and U. Parlitz. "Estimability and dependency analysis of model parameters based on delay coordinates". In: *Phys. Rev. E* 94 (3 Sept. 2016), p. 032221. DOI: 10.1103/PhysRevE.94.032221. URL: https://link.aps.org/doi/10.1103/PhysRevE.94.032221.

[8] Jan Schumann-Bischoff et al. "Basin structure of optimization based state and parameter estimation". In: *Chaos: An Interdisciplinary Journal of Nonlinear Science* 25.5 (2015), p. 053108. DOI: 10.1063/1.4920942. eprint: https://doi.org/10.1063/1.4920942. URL: https://doi.org/10.1063/1.4920942.

CHAPTER 9

OUTLOOK

Although *D.d.* and it's patterns have been studied for many years, a lot can still be learnt through a systematic analysis. In this chapter I will present some projects that I did not have sufficient time to work on, but which I think, will be of interest.

9.1 Unifying mechanisms for pattern selection

In this work, I've shown that the patterns formed by starving populations of *D.d.* depend on various conditions. Is there a fundamental way to compare these different conditions? For example, I have shown that at high initial starvation times, at high agar densities and at extremely low cell densities well-developed spirals fail to form. How are these different conditions connected? Despite their outward dissimilarities, do they affect the systems in the same way fundamentally? This would not only be interesting because it would enable us to compare different environmental conditions, but also because it can reveal the fundamental nature of pattern formation.

9.2 Patterns in confined space

While it is known that populations of *D.d.* form waves, what happens when the populations are spatially confined? This is a pertinent question for many reasons. First, in a confined space, at high densities, the cells no longer forms

a monolayer. Confining the populations to such small areas allows the study of pattern formation in layers of cells. Second, it allows the determination of whether it is the total number of cells that is important to pattern formation or the number of cells per unit volume. Third, such experiments allow the study of spiral wave dynamics in confined environments.

I performed some experiments where the *D.d.* populations were confined to small areas. I created high cell density solutions and using pipettes, created drops of different sizes on a Petri-dish. The total number of cells in these small regions was high enough to form patterns. As the spatial extent decreased, fewer number of spirals were formed. At a certain area, only one spiral was observed. At even smaller regions, spirals were no longer observed. Instead, the entire population showed bulk oscillations. However, it is important to repeat these experiments, ensuring that the buffer in the drops does not evaporate.

To perform controlled experiments, I propose using multi-well plates. Since these are available in many different sizes and volumes, better control of size and volume can be achieved. For example, one can look for patterns in a 48 well plate by adding cells of a particular density to each row. Next, the same cell densities can be added to wells of a 96 well plate, a 384 well plate and a 1536 well plate. The surface area of a well ranges two orders of magnitude from about $1cm^2$ to about $0.01cm^2$. Such an experiment can provide information about the critical size of a population where the transition from spirals to bulk oscillations occur. Further, as stated above, at certain densities only one spiral is obtained. In experiments of the BZ reaction, many perturbation experiments were performed. This has been difficult to do in *D.d.* population because of the numerous spirals formed. Now, if we can produce only one spirals, various

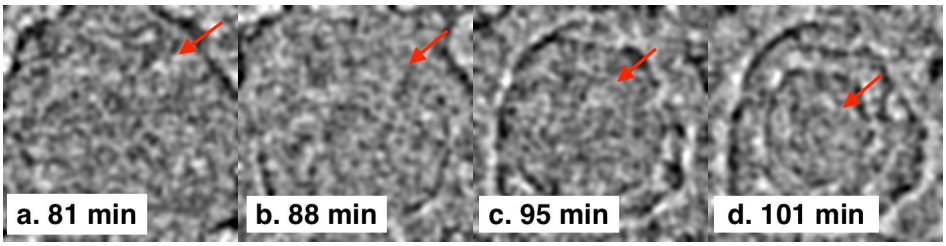

Figure 9.1: When a drop of cAMP is added to a pattern forming region, it wipes out the patterns. The waves from outside propagate into the region, making it appear like anti-target patterns.

perturbation experiments and spatial experiments can be carried out in *D.d.* populations as well.

9.3 Perturbation experiments

When a pulse of cAMP is added to a population of *D.d.* cells that are forming patterns, the patterns in that region are wiped out. The waves from the surrounding regions move inwards into this region giving the appearance of inward propagating waves. I observed this phenomenon by adding a pulse of cAMP through a syringe pump to a population that was initially starved for about 6 h, just when the patterns begin to form. At this point the patterns are dominated by target pattern (which are then taken over by spirals). The inward waves are shown in fig. 9.1.

It will be interesting to systematically check the response of the patterns on addition of a pulse of cAMP. As reported in an earlier chapter, populations initially starved for different durations show different patterns. One could measure the time required for the patterns to recover (which could be defined as the time after which the apparent inward propagation of waves stops) as a function

of the initial starvation time. Such an experiment could provide information about the refractory period of the cells for the production of cAMP.

Further, instead of a single pulse of cAMP, a series of pulses could be used as a perturbation. This resembles forced oscillations. So it would be interesting to see how the response of the patterns depends on the periodicity of the added pulses. Since the period of oscillation in these cases decreases with time, it is possible that the response of the patterns also changes depending on when the pulses are added.

9.4 Spatially structured populations

Previously, patterns formed by well mixed populations of different initial starvation time was discussed. It will be interesting to see how the patterns behave if such populations are spatially separated. For instance, a populations initially starved for 5 h starts forming patterns within 20 min of plating on a dish, whereas a population initially starved for 1h takes about 2 h to start forming patterns. If these two populations are spatially separated, it will be interesting to see what happens to the waves formed by the older population. Can they waves propagate into the younger population?

One way to achieve this is to divide the Petri-dish into two parts. I tried to do this by placing a thin metallic divider (1mm width) in the dish. I added the cells to one side of the dish and waited for them to settle down. Next, I added the other population to the other side of the divider and removed the divided after about 20 min to make sure there was no mixing. However, this created problems because there was a gap of about 1mm where there were no

cells. This artificial heterogeneity created waves. So it was difficult to analyze the interactions. Another way is to divide the Petri-dish by the ring divider. This way, there is more possibility for interaction - instead of the diameter, the interaction now happens along the circumference of a circle. Again, I had the similar problems - the divided was several orders of magnitude thicker than the typical cell width, which created artificial heterogeneities.

Very thin dividers are not stable. So, a possible solution is to have a wedge shaped divider that tapers down to a sharpness of a few microns. At the broader edge, clamps can be designed which can fix the divider securely to the Petri-dish to ensure that there is no leakage. It has been shown theoretically, that waves cannot propagate form a highly excitable medium into a medium with lower excitability. Such predictions can be checked in *D.d.* populations.

9.5 Interaction of D.d with micron-sized particles

In one of the previous chapters, it was mentioned that *D.d.* interact with the polystyrene beads. It was shown that the $10\mu m$ sized beads are dragged by the cells into the mounds. However, if the beads are larger than cell size, e.g. about $20/mum$ in diameter, the cells cannot drag them anymore. But they do get pushed around as the cells form aggregates. Fig. 9.2 shows some images of the cells and the larger beads. It would be interesting to analyze the ordering of the beads with time to check for emergence of order.

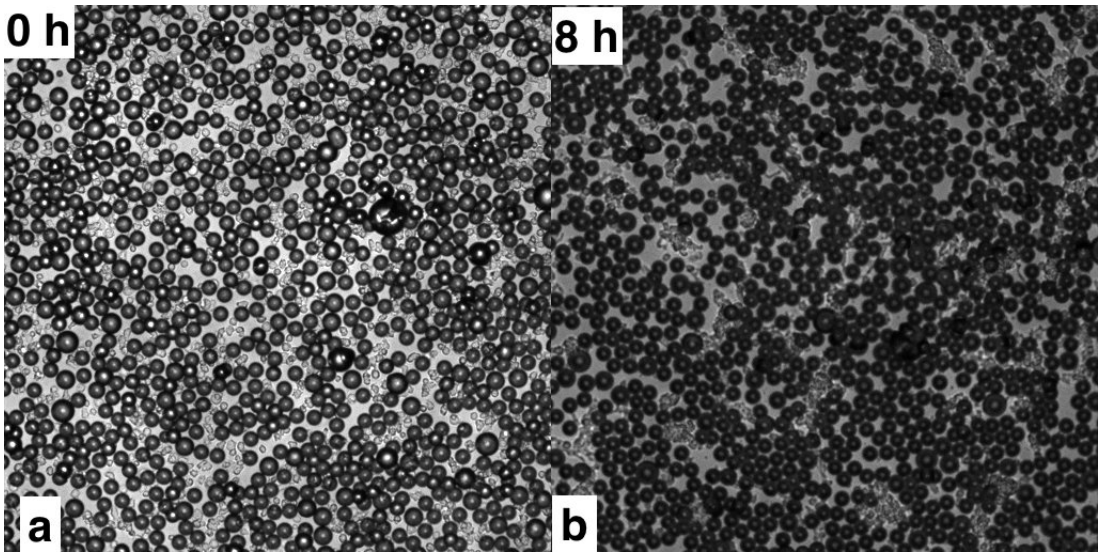

Figure 9.2: The interaction of beads and *D.d.* The density of beads and cells is equal here.

9.6 Further effects of heterogeneity

One of the previous chapter dealt with mixtures of populations. There both populations were in equal amounts. It will be interesting to see how the ratio of the two populations determine the patterns. For example, a population starved for 8 h shows target patterns where as when mixed with a population starved for 1h there is a coexistence of targets and spirals. However, what if the 1 h population constituted a smaller fraction of the total population, say 1/10th? Such experiments can be performed systematically and a third dimension to the phase map could be added. This could reveal the importance of outliers of a population on the pattern selection. In fact, this is a realistic scenario because in nature it is very likely that not all the cells began starving at the same time. Figure shows some pattern for different ratio of a 10 h and 1 h population mixture.

9.7 Further implications of memory

In a previous section, we have shown that cells "remember" being starved for about 1 h. An interesting question is what if a part of the population was starved whereas the rest of the population was not. Is there a "communication" about the starved state between the two populations? It was hypothesized that the cells de-regulate their parameters at different rates, resulting in the patterns observed. Keeping this in mind, will a mixture of non-starved cells and starved cells just resemble a heterogenous population with different biochemical parameters? Or is there some "communication" between the cells that relays the message of previous starvation? It remains to be seen.

Another interesting project involving memory is to test if this memory can be used for adaptation. In particular, if a population goes through repeated cycles of nutrient availability and starvation, will the population expect nutrients after starvation? If so how many such cycles of feeding and starving does it take to adapt a population? Is the ratio of feeding time to starvation time important?

9.8 Dynamics of pulsed cells

As has been shown in previous works, externally pulsed cells have very different biochemical parameters compared to non-pulsed cells. It will be interesting to repeat the experiments and parameter estimation of the models to learn the dynamics of the pulsed cells. From the few experiments that I have performed, it is very clear that the patterns shown by cells that were externally pulsed during the initial starvation phase, are very different from patterns of non-pulsed

cells. One can check if pulsing merely accelerates the time variation of the biochemical parameters or if it drastically changes the dynamics of the cells.

9.9 Rigorous estimation of parameters

In this work, the parameter estimation was done by means of trial and error. It was long, tedious and error prone process. A more efficient method to do it would be to use optimization algorithms to find the parameters of the model that best fit the experiments. Regularization algorithms developed by numerical mathematician could be very important for this problem. However, it has to be noted that such a project is likely to take an enormous amount of time and computational resources. This is because, a typical experimental movie has about 1000 x 1000 pixels and there are about a 1000 such images in each movie. Each pixel therefore has a time series of 1000 points. The regularization algorithm has to search for parameters at each time step and at each pixel, because we know that the parameters vary in space and time. As a conservative estimate, if the algorithm needs 20 runs of the simulation for each pixel, it will need 20 * 1000 * 1000 runs for each time step. And this has to be repeated for all 1000 time steps to obtain the parameter variation in time. And this is assuming that there is a global minimum that the optimizer can find. Unless the algorithm is very efficient, such estimations can be exceedingly troublesome. As an example, I tried to estimate two time varying parameters on the Taranis cluster at the MPIDS. However, the job was killed within minutes because the algorithm was overloading the clusters.

9.10 Spiral core dynamics

There have been many studies of the behavior of spiral waves. In many of the experiments described here, I have obtained clear spiral waves. Some of them have symmetric cores, while some have asymmetric cores. This in itself is interesting. What mechanisms cause the break in symmetry? Further, while some of the cores are fixed, in some spirals the cores tend to move away from their initial positions. It could be an interesting project to trace the path of the spiral cores and to relate them to theoretical explanations of the core dynamics.

9.11 Aggregation patterns

Towards the end of pattern formation, cells show distinctive aggregation domains, where they stream towards the spiral cores. At this stage it is easy to visualize the entrainment domains of the spirals. It may be interesting to check if the aggregation domains are Voronoi tessalations of the spiral core. This would tell us if a cell was entrained by the spiral nearest to it. If the entrainment domains are significantly different from Voronoi tesselation of the space, then an interesting question is how the cell can be entrained by a spiral farther away from it. However, a crucial point here is to develop a quantitative parameter that measure the difference between aggregation domain and the Voronoi tesselation of the space.

9.12 Role of Calcium

In a previous chapter, it was shown that a critical amount of Calcium is necessary for the cells to be healthy. In the presence of Calcium, the low density cells produce more external phosphodiesterase enzyme. However, what will happen if Ca ions are added to populations of different cell densities? Will they also produce more phosphodiesterase? Or is there a critical amount of Ca, after which additional Ca has no effect on the degradation rate of cAMP? To answer these questions, one can add different amounts of Ca to low density cell populations and measure their extracellular degradation rate. If there is indeed a critical concentration of Ca beyond which the degradation rate does not increase, then one way to check it is to add Ca to a high density cell population. At high cell densities, when cells are healthy, presumably they have sufficient Ca. So adding more Ca should not affect the degradation rate. If the rate does increase, then we can infer that the population at that density had Ca concentration that was below the threshold. Such a project can tell us the importance of Ca in the aggregation of *D.d.*

CHAPTER 10

SUMMARY

I have presented my work on various aspects of pattern formation in *D.d*. I began by exploring the effects of the cells's developmental pathway on pattern formation, and found a strong dependence. Further, I found, by mixing populations at different developmental stages, that heterogeneity plays an important role in pattern selection. I characterized these patterns using order parameters. These order parameters showed clear trends with respect to the developmental stage. To enable a model to reproduce these results, I had to include a developmental path, i.e., a temporal variation of the parameters. The requirement that the model reproduce the patterns formed for single populations, population mixtures and the trends in the order parameters allowed only a specific temporal variation in its biochemical parameters. Further, it was essential to include the spatial heterogeneity of the cell distribution in the model. With a realistic temporal variation and spatial heterogeneity, the modified model was able to semi-quantitatively reproduce my experimental results. Further, this modified model also reproduced the experimental results of a group carried out about 20 years ago. Based on the experiments and the model, I concluded that the system becomes oscillatory towards the end of the signaling phase.

Next, using the knowledge gained so far, I probed the system to look for memory. By subjecting a starving population to varying durations of feeding, I found that *D.d*. indeed "remember" starvation. In my experiments, this starvation memory lasted for about an hour. I provided a possible mechanism through the de-regulation of parameters to explain the phenomenon of memory.

There is cell–cell variability in the production of cAMP in a population. My

next project was aimed at understanding the robustness of the signaling mechanism to this variability. I created mixtures of extreme cell–cell variability by replacing some of the wild type cells with mutants incapable of producing cAMP. Surprisingly, I found that although the mutants do not produce cAMP, they were somehow involved in synchronizing the populations, because the populations in which the mutants had replaced a fraction of the wild type cells synchronized at the same time as the populations with no mutants. To find the effects of the mutants, I used a very low cell density. At this low density, the wild type cells cannot aggregate. However, when mutants were added, the mixture aggregated. Clearly, the mutants were helping aggregation. I tested for mechanical coupling and found that the effect was not mechanical. After a series of chemical tests and assays, I found that the low density wild types cells were unable to aggregate because of a lack of divalent ions. In the presence of additional ions, the cells were viable, but did not aggregate. I found that it was an insufficient amount of the enzyme PDE that was causing the lack of aggregation. The mutants provided PDE, restoring aggregation capability. These results showed that the signaling mechanism requires very little amount of cAMP, providing insights into its robustness.

In nature, *D.d* have to survive on various kinds of substrates. Does the substrate have an effect on the pattern formation and aggregation processes? To test this, I performed a series of experiments to study patterns formation on different densities of agar substrates. As the density of agar in the substrate increased, well developed spirals failed to form. The populations needed more time to synchronize. However, I found that on adding an excess amount of buffer on top of the cell layer, well developed spirals were formed even at high agar densities. The time taken to synchronize did increase, but not as rapidly as

before. This led to the hypothesis that the thin layer of buffer was important in causing the transition, in addition to change in substrate density. However, the nature of the effect is still unknown.

Finally, I tried to develop a rigorous method to estimate model parameters using experimental data. To start with, I used simulated data and coupled it back to the model and optimized it to obtain the best fit parameters. I applied this method to two models to explain pattern formation in *D.d.*, which differ only in their temporal variation of parameters. This technique was able to reproduce the temporal variation of the parameters proposed in the models. Since these models were similar, I tried to compare them, by using data from one model and coupling it to another. However, this technique only provided a trivial estimate of the parameters. Other techniques could provide sensible results.

To conclude, I have shown that analyzing patterns can provide information about the temporal variation of the system's parameters, its dynamical state, memory and robustness. Analyzing patterns can therefore be a powerful technique to understand the dynamics of systems. In the Outlook chapter, I have suggested various possible ways to extend these experiments to further understand the system.